Geological Survey of Norway
NO-7491 Trondheim, Norway
Tel.: 47 73 90 40 00
Telefax 47 73 92 16 20

REPORT

Report no.: 2005.075 | ISSN 0800-3416 | Grading: Open

Title:
Potential resources of quartz and feldspar raw material in Sørland IV: Relationships between quartz, feldspar and mica chemistry and pegmatite type

Authors:
Axel Müller, Peter M. Ihlen, Andreas Kronz

Client:
NGU - NTNU - NFR

County:
Aust - Agder

Commune:
Froland, Birkenes

Map-sheet name (M=1:250.000)
Arendal

Map-sheet no. and -name (M=1:50.000)
Mykland, Nelaug, Lillesand

Deposit name and grid-reference:
See text

Number of pages: 94 Price (NOK): 565,00
Map enclosures: 0

Fieldwork carried out: 15.09.-03.10.2004
Date of report: 01.05.2006
Project no.: 286100
Person responsible: Peter M. Ihlen

Summary:

The Sveconorwegian pegmatite fields of Froland and Herefoss is located at the western edge of the Bamble terrane in southern Norway. The field comprises different pegmatite types which can be roughly classified as follows: (1) PGr - pegmatitic granites, (2) GP - granite pegmatites, (3) NaP - Plagioclase-dominant granitic pegmatites, (4) ZoP - zoned granitic pegmatites, (5) KP - K-feldspar-dominant granitic pegmatites, (6) PD - muscovite pegmatite/granite dykes and (7) HP - zoned pegmatites related to the Herefoss pluton. Types (1) to (5) and (7) represent relative primitve pegmatites in respect to granitic differentiation containing predominantly Fe phlogopite and Mg siderophyllite. Type (6) has an more evolved chemistry reflected by zinnwaldite.

79 quartz, 38 K-feldspar, 41 plagioclase, 34 biotite and 6 muscovite samples were collected and analysed. Trace elements in quartz were analysed with laser ablation inductively coupled mass spectrometry (LA-ICP-MS). Scanning electron microscope cathodoluminescence (SEM-CL) has been applied to quartz in order to reveal different quartz generations (primary and secondary quartz) at micro-scale (0.001 to 10 mm). Feldspar and mica were analysed by XRF.

Trace elements (Li, B, Be, Na, Al, P, K, Ti, Fe, Ge) of pegmatite quartz were determined in order to classify the quartz into low-, medium- and high-purity quality raw material. Quartz of type (1) to (5) has relative similar chemistry of medium quality. Concentrations vary between 2.0 to 14.3 ppm for Li, 0.7 to 2.2 ppm for Ge, 21 to 65 ppm for Al and 0.7 to 10.7 ppm for Ti. Pegmatites of type (1) to (6) located inside gneiss enclaves of the Herefoss pluton (e.g. Vaselona and Fossheia, vest) comprise non-predictible variation of the quartz and feldspar chemistry. Concentrations in quartz from PD fall in the range 1.6 - 9.5 ppm Li, 2.0 - 2.5 ppm Ge, 17 - 164 ppm Al and 3.0 - 17.7 ppm Ti. PDs are divided into two subtypes based on the differences in Li, Al, Ti, K and Fe content. Quartz of the PD at Haukemyrliene is of low quality (average of 122 ppm Al), whereas quartz of the PD at Skåremyr and Hellheia is of medium quality. However, the PD dykes are to small (<1 m in thickness) and fine-grained to be of economic relevance. Quartz in pegmatites related to the Herefoss pluton (HP) contains high Ti (15.1 to 30.8 ppm) and Al (18 to 105 ppm) and is of low quality. Secondary fluid-driven overprint of quartz from all pegmatite types result in the refinement of quartz on micro-scale (<100µm). The processes caused crystallisation of secondary quartz which has lower trace element contents than the primary magmatic pegmatite quartz.

K-feldspar in type (1) to (6) is commonly of good chemical quality (K_2O >13 wt.%), whereas K-feldpar in HP is not suitable as raw material for glass and ceramics. Plagioclase chemistry of all pegmatite types is of low quality due to CaO concentrations >2 wt.%.

Keywords: scientific report	industrial minerals	Froland
pegmatite	quartz	feldspar
mica	LA-ICP-MS	SEM-CL

CONTENTS

FIGURES

TABLES

APPENDIX

1. Introduction

In this study 14 representative pegmatite localities of the Froland and Herefoss pegmatite field in southern Norway were mapped and sampled (Figs. 1 and 2). The 14 pegmatites represent different chemical (e.g., Na- rich or K-rich) and structural types (e.g., zoned, unzoned, lens-shaped, dykes) of different emplacement age. Five of the larger pegmatites (Løvland, Hellheia midtre, Skåremyr, Sønnristjern, Lille Kleivmyr) were multiple sampled along traverses crossing the different zones of the pegmatite. Beside quartz, one sample of K-feldspar, plagioclase, biotite and muscovite was taken per sample point if the mineral occurs less than 0.5 m away from the sampled quartz. Additional importance was attached to the collection of quartz of different structure (massive quartz, interstitial quartz, graphic intergrowth with K-feldspar and plagioclase, quartz segregation) and colour (clear, milky, smoky).

The field work was carried out by Axel Müller and Peter M. Ihlen between 15.09. and 03.10. 2004. All together 79 quartz, 38 K-feldspar, 41 plagioclase, 34 biotite and 6 muscovite samples were taken and analysed. Trace elements in quartz (Li, Be, B, Mn, Ge, Na, Mg, Al, P, K, Ca, Ti, Fe) were analysed with laser ablation inductively coupled mass spectrometry (LA-ICP-MS). Quartz was investigated by scanning electron microscope cathodoluminescence (SEM-CL) in order to reveal different quartz generations (primary and secondary quartz) at micro-scale (0.001 to 10 mm). Primary quartz crystallised during pegmatite emplacement and secondary quartz resulted from subsequent tectonic and/or fluid-driven overprint and recrystallisation of primary quartz. The Al, Ti, K and Fe concentration of secondary quartz revealed by CL has been analysed by electron probe micro analysis (EPMA) by Andreas Kronz at the Geowissenschaftliches Zentrum Göttingen, Germany, in the frame of the NGU network collaboration 2005. Chemistry of feldspars and micas were determined with X-ray fluorescence spectrometer (XRF) at NGU.

The general aim is to find relationships between quartz, feldspar and mica chemistry and the granitic pegmatite types. The specific aims of study are:

1. to detect if the trace element concentration of quartz depends on the morphological type (massive quartz, interstitial quartz, graphic intergrowth with K-feldspar and plagioclase, quartz segregation) and colour (white, smoky) and transparency (clear, milky).
2. to compare the chemistry of quartz with the composition of neighbouring feldspar and mica
3. to reveal variations of quartz, feldspar and mica chemistry across pegmatites
4. to work out the sequence of the emplacement of the different pegmatite types, dyke populations and Herefoss pluton
5. to elaborate more criteria for classification of pegmatites in Froland
6. to conclude which pegmatite types are of economic importance

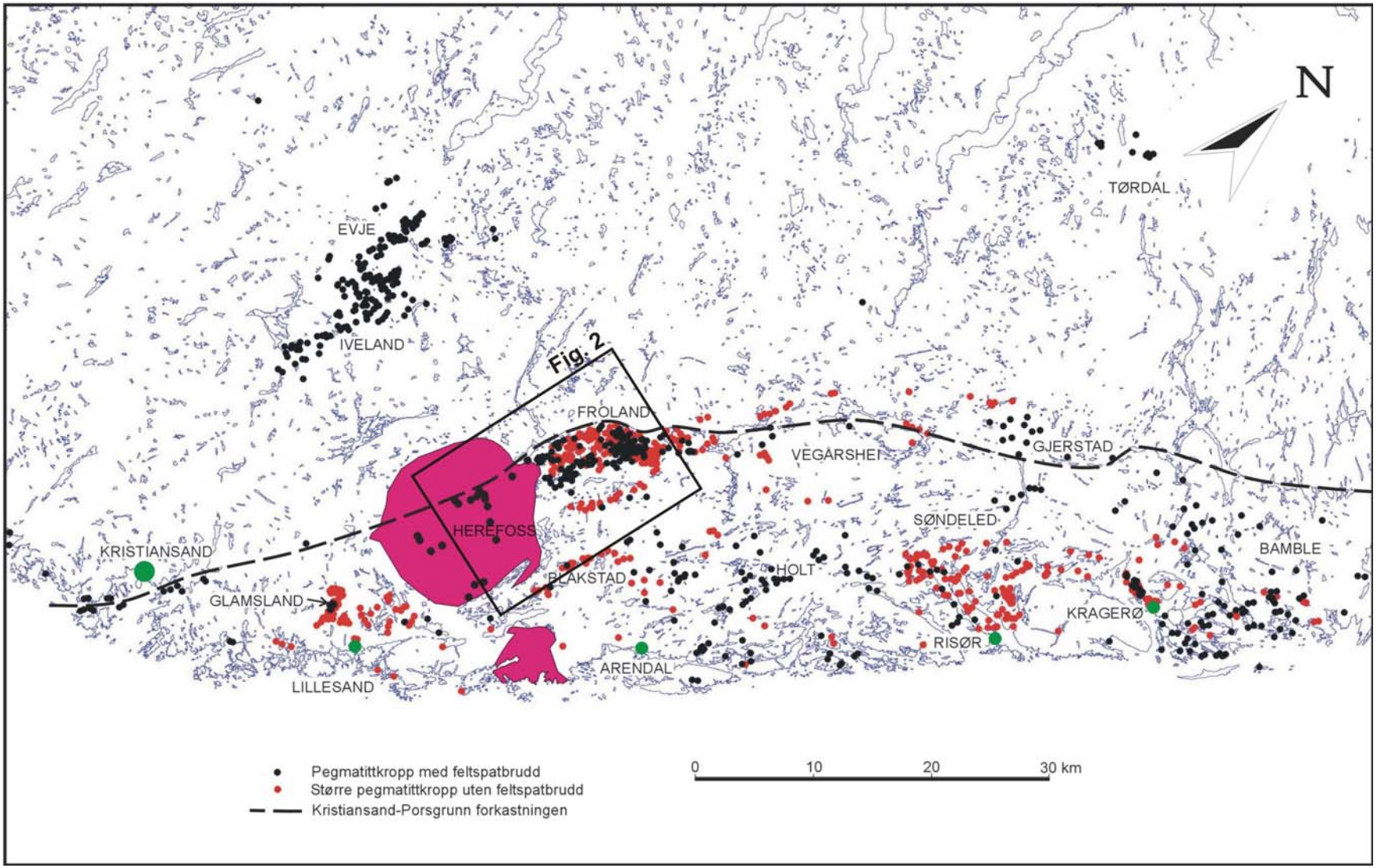

Fig. 1. *Localition of the Froland and Herefoss pegmatite fields in southern Norway.*

2. Geologic setting

The Froland pegmatite field occurs parallel along the western boundary fault of the Bamble terrane, i.e. Porsgrunn-Kristiansand Fault Zone (PKFZ; Fig. 2). The field extends ca. 20 km in NE-SW direction, is 5 km wide and comprises about 105 known major pegmatite occurrences (e.g., Ihlen et al. 2002). 76 of these granitic pegmatites were mined for feldspar and/or quartz since the end of the 18th century. The pegmatites form large tabular bodies and dykes emplaced in an isoclinally folded sequence of steeply dipping and NNE-SSW striking banded biotite-hornblende gneisses of volcano-sedimentary origin (Alirezaei 2000). The gneisses are affected by amphibolite facies metamorphism, possibly transitional to granulite facies as indicated by orthopyroxene-bearing felsic gneisses (Elders 1963) during the Sveconorwegian deformation (Falkum and Petersen 1980) in the period 1.14 to ca. 0.9 Ga (e.g., Bingen et al. 1998).

The Froland pegmatite field forms together with the Glamsland-Lillesand pegmatite a common pegmatite belt with similar quartz composition (Ihlen et al. 2002, 2003; Fig. 1). The circular Herefoss pluton intruded at 0.93 Ga (Andersen, 1997) into the central part of the pegmatite belt. The Herefoss pluton contains mainly pegmatites inside this belt, at least, all the former quarries occur inside this belt. The extension of the Herefoss pegmatite field corresponds to the circular intrusion of the Herefoss pluton which has a diameter of about 18 km. The density of pegmatite occurrences is much lower than in the Froland pegmatite field and pegmatites are much smaller and different in structure. However, mega enclaves of gneisses (several km in length) occur in the northern and central part of the Herefoss pluton which comprise a similar density and style of pegmatite occurrences as in the Froland pegmatite field.

For more information see Ihlen et al. (2002, 2003) and Henderson and Ihlen (2004).

3. Classification of Froland pegmatites

The granitic pegmatites in the Froland field comprise simple abyssal pegmatites with variable contents of quartz, alkali feldspar, plagioclase and biotite, as well as, locally minor garnet and muscovite (Černy 1991). Some of them appear transitional to muscovite pegmatites and NYF-type pegmatites with rare-metal minerals (Nilssen 1970). Ihlen et al. (2003) subdivided the simple pegmatites into several groups according to their mineralogy and presence of mineral zoning. The following groups were distinguished:

PGr - Pegmatitic granite
GP - Granite pegmatites
NaP - Plagioclase-dominant granitic pegmatites including types with quartz core
ZoP - Zoned granitic pegmatites
KP - K-feldspar-dominant granitic pegmatites

All these types emplaced pre- and/or syntectonically and their injection is most likely not separate so much in time. The distinction of these pegmatite types is not always obvious, because transitional pegmatites also occur exhibiting features of different types. This group of pegmatites is named the old pegmatite group.

This study includes also two pegmatite types, which are younger than the types described above revealed by the field relationships:

PD - muscovite pegmatite/granite dykes
HP - zoned pegmatites related to the Herefoss pluton emplacement

Pegmatitic granites (PGr), which occur preferentially in the northern Froland pegmatite field, form relative thin, folded sheets which can cover larger areas (Ihlen et al. 2002). They consist of 20 to 50 cm large K-feldspar crystals embedded in quartz monzonitic to granitic, medium- to coarse-grained groundmass (1 to 10 mm) of quartz and plagioclase with variable concentrations of K-feldspar, biotite and muscovite. The medium- to coarse-grained groundmass containing large K-feldspar phenocrysts is the main textural feature of the PGrs. The outcrop at Våtåskammen represents a typical example of PGr. 0.1 to 1 m K-feldspar phenocrysts in a coarse-grained granite matrix.

Granite pegmatites (GP) consist of roughly equal amounts of quartz, K-feldspar and plagioclase. Plagioclase and quartz form mainly the megacrystic groundmass (3 to 20 cm) in which larger K-feldspar crystals are embedded. These pegmatites have commonly a complex structure without distinct zoning. Occasionally, mono- or bi-mineralic domains are developed. Lille Kleivmyr is a typical example of a granite pegmatite.

Plagioclase-dominant granitic pegmatites (NaP) represented by Hellheia midtre and nordre, consist mainly of plagioclase and quartz and some of them do not contain K-feldspar (Hellheia midtre). The lack of K-feldspar is compensated by high biotite content and to some extent by muscovite. The plagioclase (oligoclase) occurs preferentially at the pegmatite margin and envelops massive quartz cores. Na-pegmatites occur in the SE part of the Froland pegmatite field.

Zoned granitic pegmatites (ZoP) comprise pegmatites with complex, asymmetric zoning. A marginal zone of massive plagioclase intergrown with quartz is commonly developed. Inwards the contact zone changes gradually to an intermediate zone with increasing K-feldspar which grades into the blocky core zone with abundant quartz and/or K-feldspar (blocky zone). Examples of ZoP are Skåremyr and Sønnristjern. The distinction between ZoP and NaP is not always clear because some pegmatites exhibit macro-structural features which are typically for both types (e.g., Skåremyr).

K-feldspar-dominant granitic pegmatites (KP) are composed dominantly of microcline and quartz. Plagioclase forms commonly less than 10 vol.% of the pegmatite body and, sporadically, KPs contain muscovite. K-feldspar occurs both as megacrysts up to 2 m and as groundmass mineral. Plagioclase-rich contact zones or quartz-rich cores are not developed. Quartz is preferentially graphically intergrown with K-feldspar.

A number of the pegmatites described above are crosscut by fine- to medium-grained *biotite granite dykes*.

Muscovite pegmatite and granite dykes (PD) form horizontal or flat dipping muscovite-bearing pegmatite and granite dykes which are rich in K-feldspar. The straight borders of the dykes indicate a brittle behaviour of the rock during emplacement and, thus, they are considered as post-tectonic. The dykes are less than 1 m in thickness. The dykes crosscut GP, KP, ZoP, NaP, PGr and the biotite granite dykes but they were not observed in the Herefoss pluton and in pegmatites hosted by the Herefoss pluton (HP). It is assumed that the muscovitisation observed in some NaP (Hellheia midtre, Bjortjørn), GP, KP and ZoP is related to the emplacement of PD.

Zoned pegmatites related to the Herefoss pluton emplacement (HP) are relative small (<400 m^2) pegmatite dykes and segregations related to the different granite facies of the Herefoss pluton. The pegmatites are zoned consisting of a feldspar-rich margin and quartz-rich core. At least four different pegmatite generations can be distinguished within this group. The Herefoss pluton itself consists of four major granite facies: 1) early megacrystic leucogranite, (2) coarse-grained biotite quartz monzonite, 3) medium-grained grey leucogranite, and 4) red fine- to medium-grained aplogranite. (1) and (2) show the development of pegmatite segregations, e.g., the pegmatite at Heimdal is related to (1) and the pegmatite at Fossheia øst to (2). All granites are cut by simple and zoned pegmatite dykes (Metveit). Their genetic relationship to the individual sub-intrusions is difficult to assess.

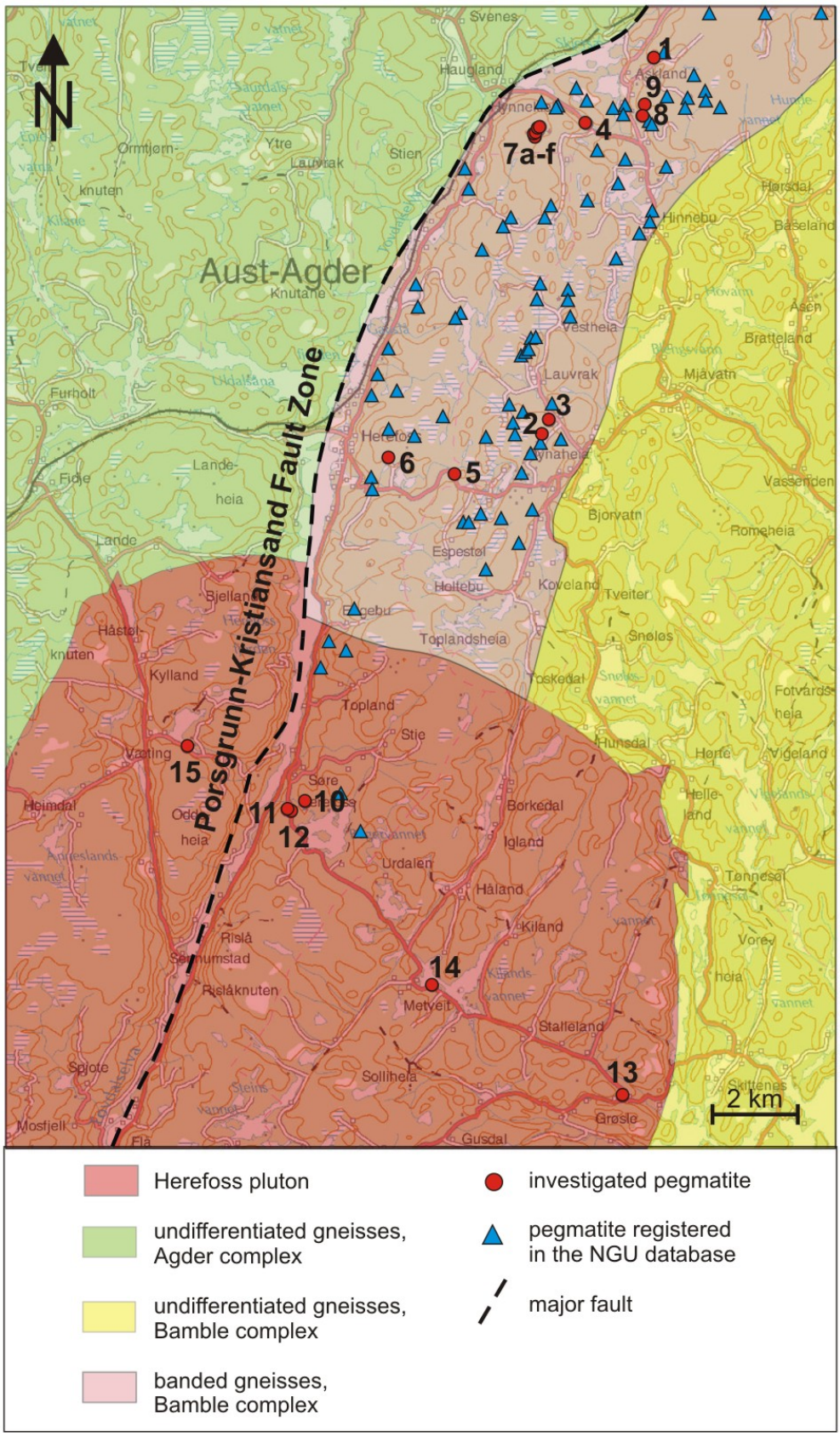

Fig. 2. *Simplified geologic map of the Froland area and the distribution of major and by NGU registered pegmatite occurrences. Localities: 1 – Løvland, 2 – Hellheia, midtre, 3 – Hellheia, nordre, 4 – Bjortjørn, 5 – Haukemyrlien, 6 – Skåremyr, 7 – Sønnristjern, 8 – Lille Kleivmyr, 9 – Våtåskammen, 10 – Vaselona, 11 – Fossheia, vest, 12 – Fossheia, øst, 13 – Husefjell, 14 – Metveit, 15 – Heimdal.*

4. Locality descriptions

The structure and mineralogy of sampled pegmatites are given below. For UTM coordinates and topographic description of the localities we refer to Appendix A.

4.1 Locality 1: Løvland

The quarry at Løvland (Fig. 3) exposes an unzoned, K-feldspar-rich granitic pegmatite (KP) along a E-W striking wall (Fig. 4). The pegmatite has an exposed extension of about 50 m x 100 m. It cuts at a low angle banded mylonitic gneisses with small lenses of sheared pegmatites, possibly representing fragments of dismembered dykes. The quarry is situated along the southern contact of the pegmatite. The pegmatite forms a flat-laying, openly folded lens dipping ca. 20º northward. Its maximal thickness is ca. 12 m in the quarry. Enclaves of granitic gneiss lenses with a length of up to 5 m occur near the upper contact of the pegmatite. The pegmatite consists of 40 to 50 vol.% K-feldspar (5 to 50 cm), plagioclase and quartz. Plagioclase and quartz are intensively intergrown and fill the intersticies between K-feldspar crystals. Ductilly deformed and boudinaged sub-horizontal quartz bands traverse the pegmatite (Figs. 4 and 5a). Figs. 5a and b show the typical macro texture of the Løvland pegmatite. The crystals are ductilly and brittlely deformed along their margins and are crosscut by micro-shearplanes (<1 mm wide; Fig. 5b). One large K-feldspar crystal (2 m) occurs in the central part of the quarry. The portion of plagioclase increases towards the eastern end of the lens. The main mafic mineral is magnetite 1 to 3 mm in size. It is heterogeneously distributed. Up to 2 cm large magnetite crystals occur in the western part of the quarry. Pegmatitic biotite is very rare and forms leaflets 2 to 20 cm in size. However, the micro-shearplanes are coated with bronze-coloured biotite flakes. The Løvland pegmatite is unique regarding its homogeneous macro-structure, the common occurrence of magnetite and the intense ductile and brittle deformation at micro-scale.

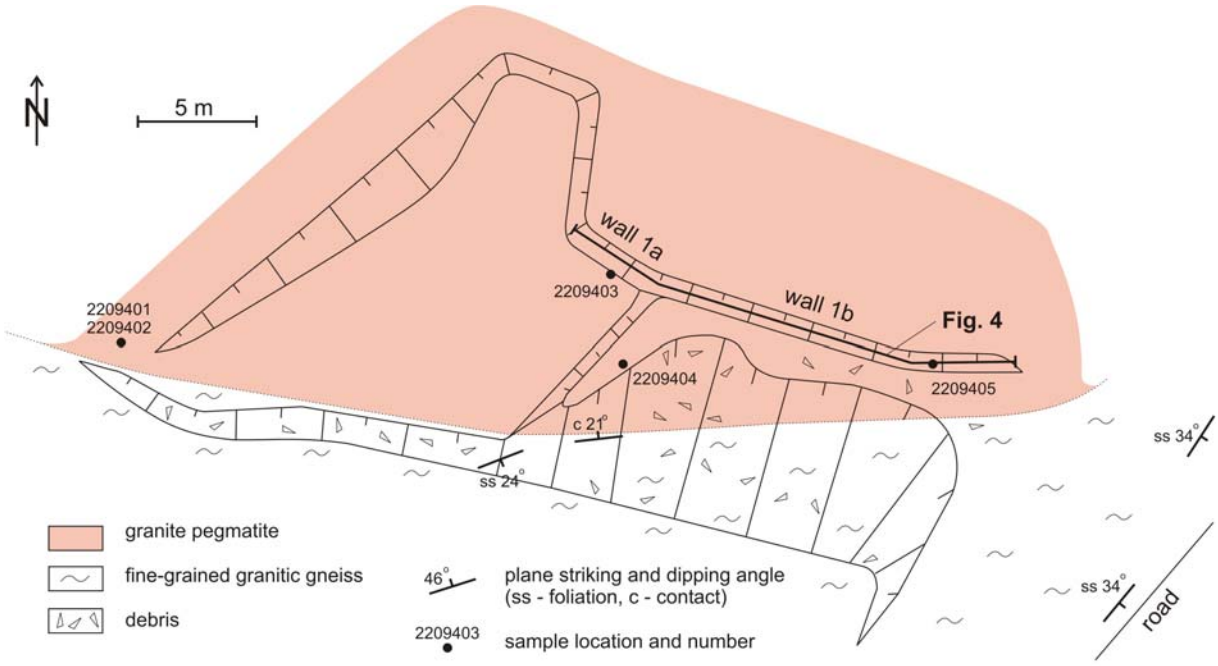

Fig. 3. *Outline of the Løvland quarry with sample localities. The walls shown in Fig. 4 are indicated with the bold line.*

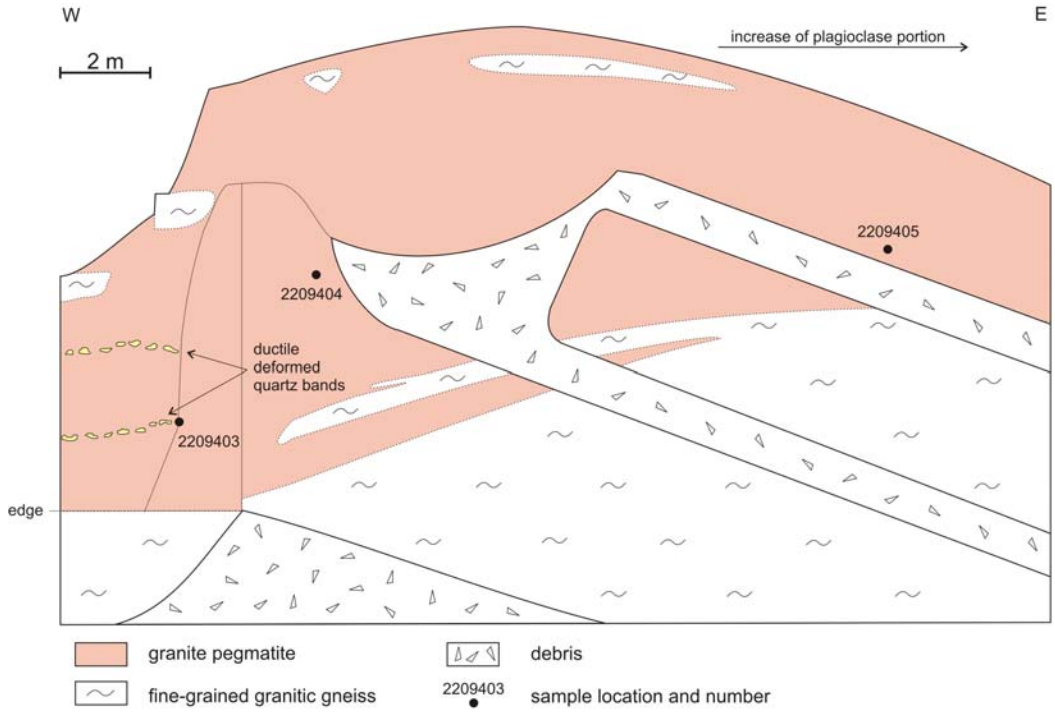

Fig. 4. *View of the E-W striking wall 1a and 1b of the Løvland quarry with sample localities.*

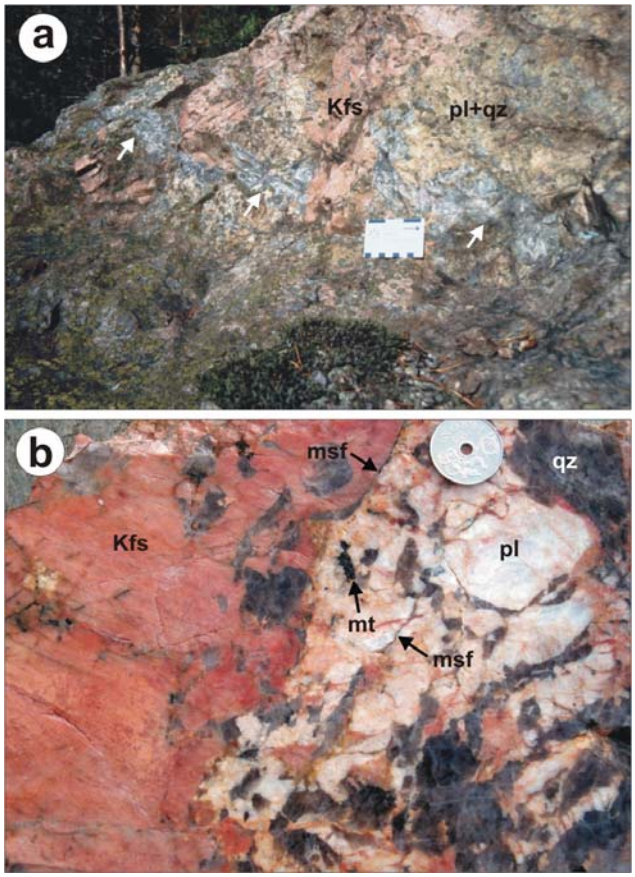

Fig. 5. *a - Macro texture of the Løvland pegmatite with pure, up to 50 cm long K-feldspar (Kfs)* crystals and massive plagioclase-quartz intergrowth (pl+qz). The section is crosscut by a flat, wormy and boudinaged quartz vein (arrows). b – Hand specimen showing the common pegmatite texture consisting of red K-feldspar (Kfs), white plagioclase (pl), smoky quartz (qz) and magnetite (mt). The sample is cut by offset micro-shearplanes (msf).

4.2 Locality 2: Hellheia, midtre

The quarry Helleheia midtre is situated in a 150 m long and 50 m wide Na-rich granitic pegmatite (NaP) which is hosted by amphibolitic leucogabbros. The pegmatite was mined for quartz. The pegmatite strikes NNE-SSW and dips 20º eastward in its western part and 75º eastward at its eastern flank. The quarry has a triangle outline. The deepest part of the quarry at the NE edge (~10 m below the surface) is filled with water (Fig. 6). The pegmatite is strongly deformed, particularly, along its contacts. Quartz forms massive lenses, usually 1 in thickness and to 5 m in length, enveloped by kinked, megacrystic biotite in massive plagioclase. The largest mined quartz lens, which was situated in the NE end of the quarry, had presumably a size of at least 15 x 8 x 6 m (720 m^3). The whole pegmatite is enveloped by a 1 to 5 m thick plagioclase zone along contacts (Fig. 7). Plagioclase is ductile deformed and penetrated by a dense network of wormy quartz veins (0.1 to 5 cm; Fig. 8b). Megacrystic, kinked biotite acted as lubricant for the large shear zones. Biotite sheaves are up to several meters in size. The steeply east-dipping shear zones occur throughout the quarry and become more frequent towards the eastern pegmatite contact.
The pegmatite is crosscut by a swarm of sub-parallel muscovite granite/pegmatite dykes which dip 15 to 60° NW. Pockets filled with thick booklets (20 cm) of euhedral muscovite megacrysts are common and occur preferentially above the large shear zones and next to muscovite granite dykes (Fig. 7). Common thin (1 to 5 mm) veinlets of quartz-muscovite in plagioclase are additional indicators for the secondary muscovitisation (Fig. 8b).

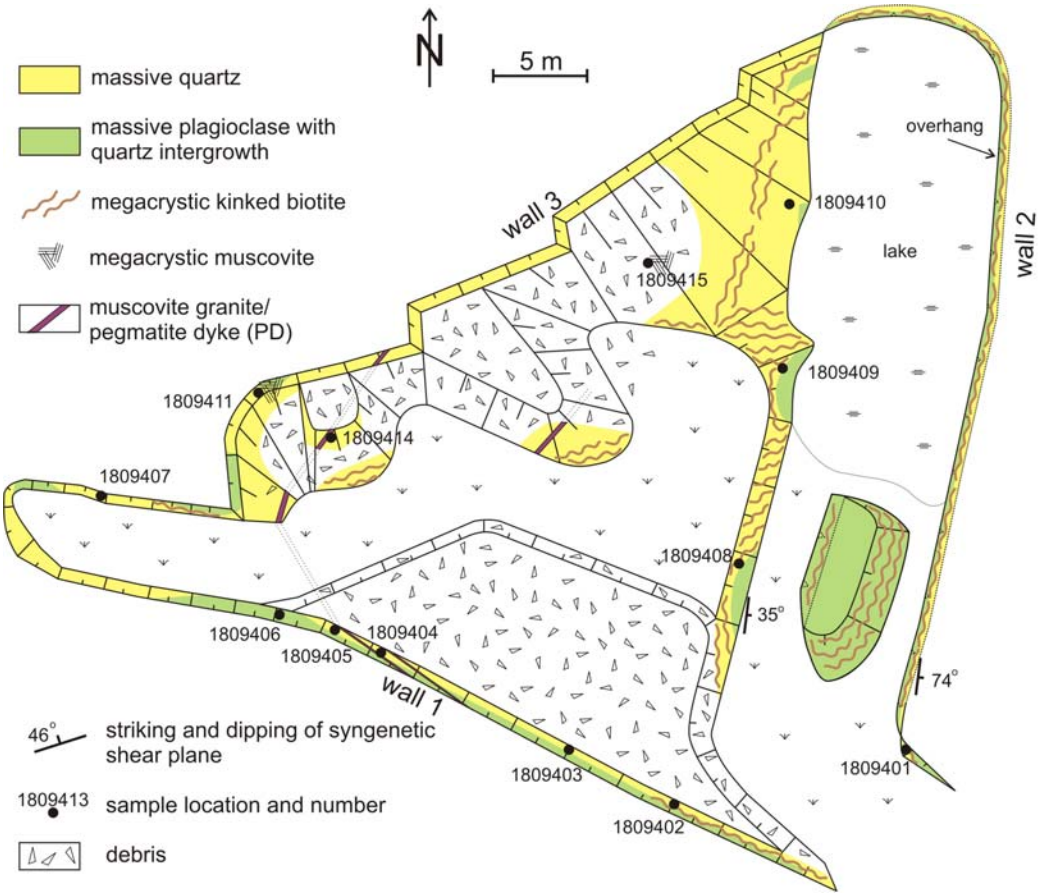

Fig. 6. *Outline of the Hellheia midtre quarry with sample locations.*

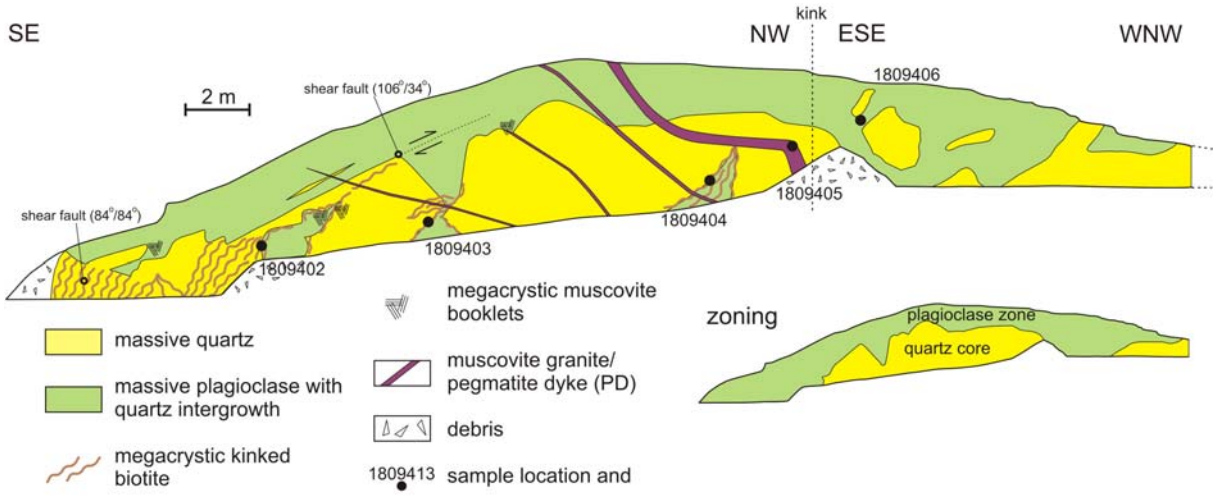

Fig. 7. *View of the SE-NW striking wall 1 of the Hellheia, midtre quarry with sample locations.*

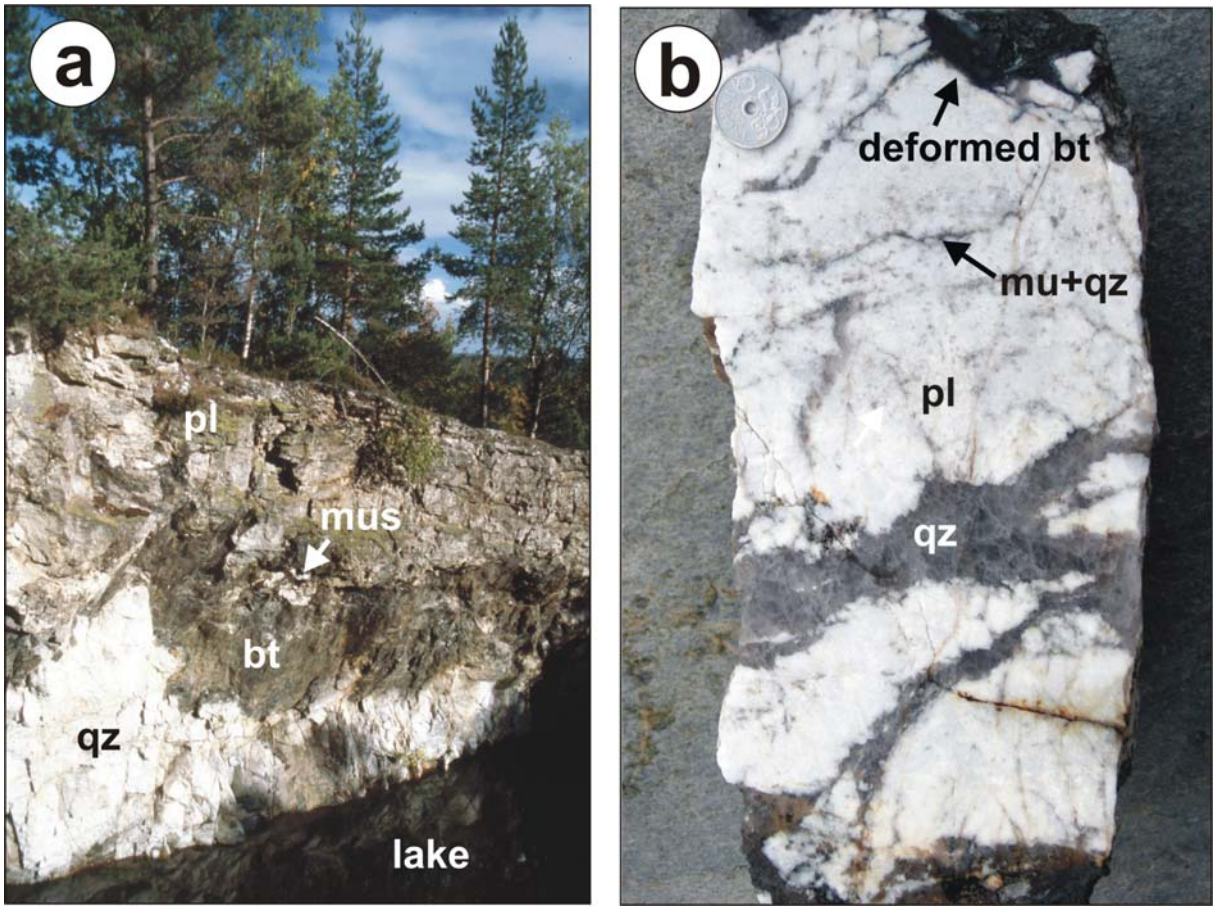

Fig. 8. *a - View towards SE showing the E wall (wall 2) of the Hellheia, midtre quarry. Relicts of the mined quartz core are preserved in the bottom part (qz). The quartz core is bordered by a biotite-coated, steeply eastward dipping shear zone, which is exposed in the middle of the wall (bt). Booklets of euhedral muscovite (mus) occur in the hanging wall of the shear zone. Massive, deformed plagioclase (pl) forms the 2 to 4 m thick pegmatite margin in the upper part of the wall. b – Hand specimen of a deformed plagioclase crystal bordered (top and bottom of the picture) by deformed biotite (bt) and penetrated by wormy quartz (qz) veins and muscovite-quartz veinlets (mus-qz).*

4.3 Locality 3: Hellheia, nordre

The Hellheia, nordre deposits belongs to the Na-rich granitic pegmatite type (NaP). The pegmatite crosscuts banded biotite-hornblende gneisses containing 1 to 5 cm thick amphibolite layers parallel to the foliation. The quarry exposes the pegmatite in a 35 m long and 8 m high wall at an eastward dipping hill slope. The strike of the quarry is parallel to the axis of the 55 m wide and at least 100 m long pegmatite which strikes NNE-SSW. The degree of deformation is lower than in the neighbouring pegmatite at Hellheia, midtre. Massive milky quartz up to 1 m in size occurs at the bottom and in the central part of the quarry. Euhedral muscovite booklets up to 20 cm are common. Towards the top of the quarry wall the plagioclase portion increases. Euhedral plagioclase megacrysts up to 1.5 m in size are intensively intergrown with quartz. Cores of the megacrystic plagioclases are partially altered to muscovite which is up to 2 cm in size. A few K-feldspar megacrysts up to 1 m occur at the upper edge of the quarry and become abundant towards the western contact. The pegmatite is crosscut by muscovite granite dykes.

4.4 Locality 4: Bjortjørn

The Bjortjørn mine is a 7 m wide, 4 m high and 10 m long underground working ending in a 20 m high, water-filled stope. The mine was worked on a NW-SE striking, 100 m long, 30 m thick lens of Na-rich granitic pegmatite (NaP). The NW edge of the pegmatite dips 30º south-eastward and the SE edge dips 70º westward. A massive quartz core containing booklets of muscovite megacrysts (50 cm) is exposed at the end of the stope (Fig. 9). The quartz core is surrounded by massive plagioclase intergrown with quartz. The pegmatite overprint resulted in an intensive muscovitisation (crystal size of 0.1 to 1 cm) and albitisation of plagioclase. The quartz core is crosscut by a sub-horizontal muscovite granite dyke. Uranium minerals and megacrystic muscovite were mined here during the Second World War. Accessory minerals are allanite $(Ca, Ce, La, Y)_2(Al, Fe)_3(SiO_4)_3(OH)$, samarskite $(Y, Ce, U, Fe)_3(Nb, Ta, Ti)_5O_{16}$ and other U- and Nb-Ta-bearing minerals (Nilssen 1970). Allanite forms up to 30 cm long crystals.

4.5 Locality 5: Haukemyrliene

At Haukemyrliene small granitic pegmatite dykes (GP; <2 m in thickness) of different age, composition and structure are exposed in a 80 m long road cut (Fig. 10). The outcrop, which can be considered as a type locality, is described in detail by Ihlen et al. (2002) and Henderson and Ihlen (2004). The pegmatites are hosted by banded gneisses and migmatitic amphibolites. Due to the small size of the pegmatites they are not of economic interest, but the outcrop reveals the relative timing and deformation history of two different pegmatite generations, separated in time by the intrusion of grey leucogranite dykes extending from the late phase (facies (3)) of the Herefoss pluton.

Steeply dipping, strongly folded GP dykes and veins represent the oldest pegmatite type of this locality. The pegmatites are composed of variable proportions of quartz, K-feldspar, plagioclase and biotite. Occasionally, the composition of the pegmatite dykes changes gradually from K-feldspar-rich to plagioclase-rich towards the end of the dykes (Fig. 10). The foliation in the gneisses has been ductile deformed after the intrusion of the first pegmatite generation (Henderson and Ihlen 2004). Most of the pegmatites have been affected by progressive deformation. Pegmatites in the eastern part of the road cut are chemical identically but less deformed.

Sub-horizontal, straight bordered dykes (0.5 m thick) of muscovite-garnet-bearing aplite/pegmatite (PD) crosscut the above described pegmatites as well as aplogranite dykes dissecting them (facies (4) of the Herefoss pluton). K-feldspar is the most abundant mineral in

PD followed by quartz, albite and muscovite. Accessory Fe-oxides are common. The dykes are composed of alternating pegmatitic and aplitic layers with comb quartz. The macro structure of the dykes is similar to layered pegmatites related to highly fractionated granites rich in Li, F and Mn (e.g., Morgan and London 1999).

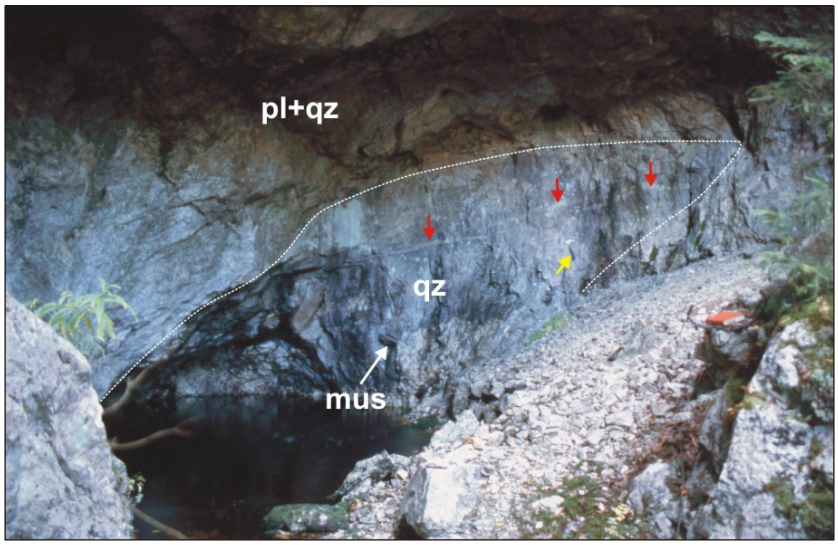

Fig. 9. *Complete view of the Bjortjørn mine. The white dashed line marks the border of the quartz core (qz) embedded in massive plagioclase intergrown with quartz (pl+qz). The core contains mecacrystic muscovite (mus). The quartz core is A sub-horizontal muscovite granite dyke (red arrows) crosscuts the pegmatite. For scale see hammer in the background (yellow arrow).*

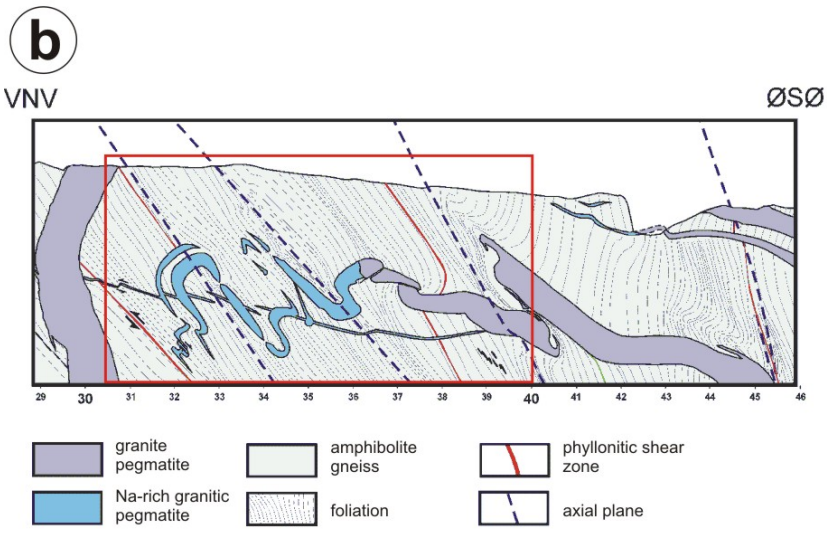

Fig. 10. *a – Detail of the road cut at Haukemyrliene with deformed pegmatite dykes of the oldest generation. b - Schematic detailed drawing of the road cut at Haukemyrliene by Ihlen et al. (2002) showing the deformation style of the granitic pegmatites and the gradual change from K-feldspar-rich to plagioclase-rich pegmatite towards the end of the dykes. The red quadrangle corresponds to the photograph shown in (a).*

4.6 Locality 6: Skåremyr

The pegmatite at Skåremyr is a zoned granitic pegmatite (ZoP) which is rich in plagioclase and biotite. Because of the high abundance of plagioclase it represents a transitional type between zoned granitic pegmatites and Na-rich pegmatites. The NW-SE striking pegmatite is 40 m long and 25 m wide and dips 50-70° north-westward. The quarry is 35 m long, 10 m wide and 5 to 12 m deep (Fig. 11). The pegmatite is hosted by amphibolites. On its western flank the pegmatite is truncated by a 50 m wide, NNW-SSE striking medium-grained biotite granite dyke (granite facies (3) of the Herefoss pluton). The dyke feeds several smaller dykes (0.1 to 2 m) crosscutting the pegmatite (Fig. 12). The biotite granite dykes themself are crosscut by muscovite-bearing aplite/pegmatite dykes (PD; 0.1 to 0.5 m wide), representing the youngest pegmatite stage (see Figs. 12a and b in Ihlen et al. 2002).

The pegmatite has a quartz-rich core zone (30 m long and 10 m wide) containing plagioclase (0.5 to 2 m; Fig. 13a), pink K-feldspar megacrysts (1 to 3 m) and biotite-zone of fan-like crystals (up to 2 m long) along the margin of the quartz-rich core. K-feldspar megacrysts crop out nowadays only in the western part of the quarry, but they occur previously in the entire area of quarry. Along the pegmatite contact a 1 to 5 m massive plagioclase zone is developed. The zone consists of pure euhedral plagioclase crystals (10 to 50 cm) embedded in massive plagioclase which is intensively graphically intergrown with quartz and biotite (3 to 10 cm; Fig. 13b).

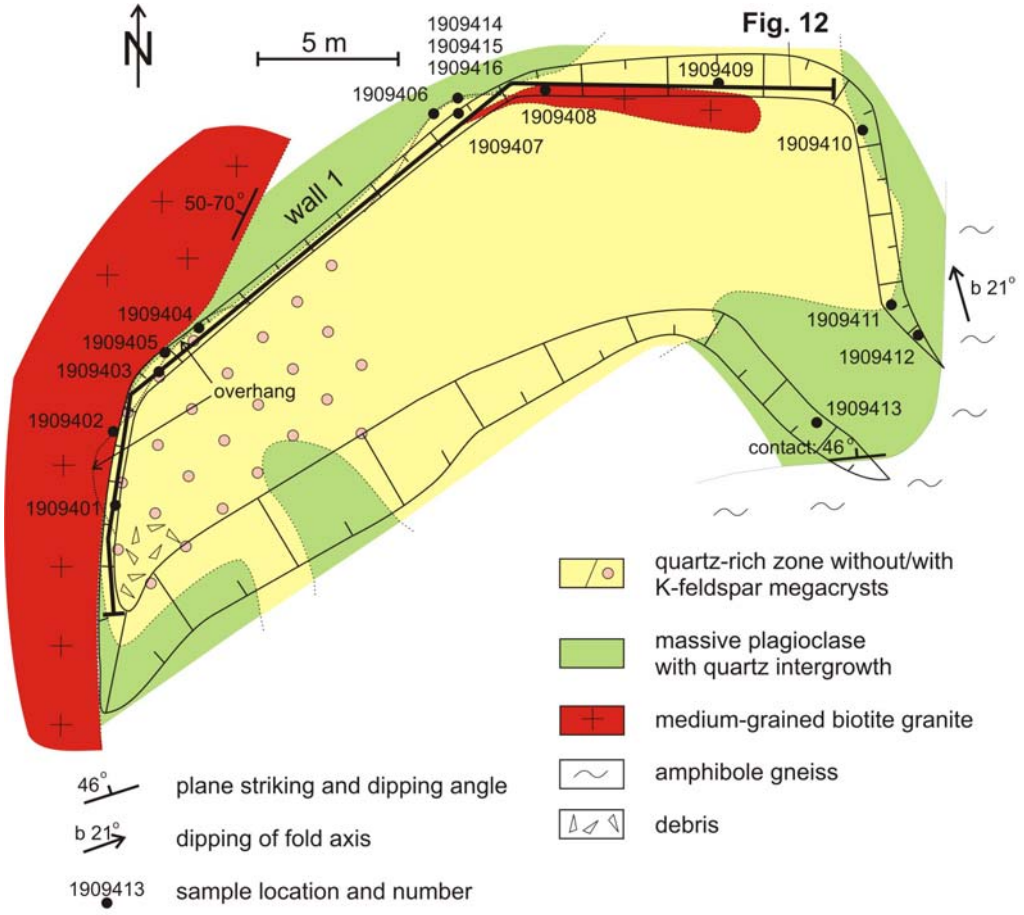

Fig. 11. *Outline of the Skåremyr quarry with sample locatities. The wall shown in Fig. 12 is indicated by the bold line.*

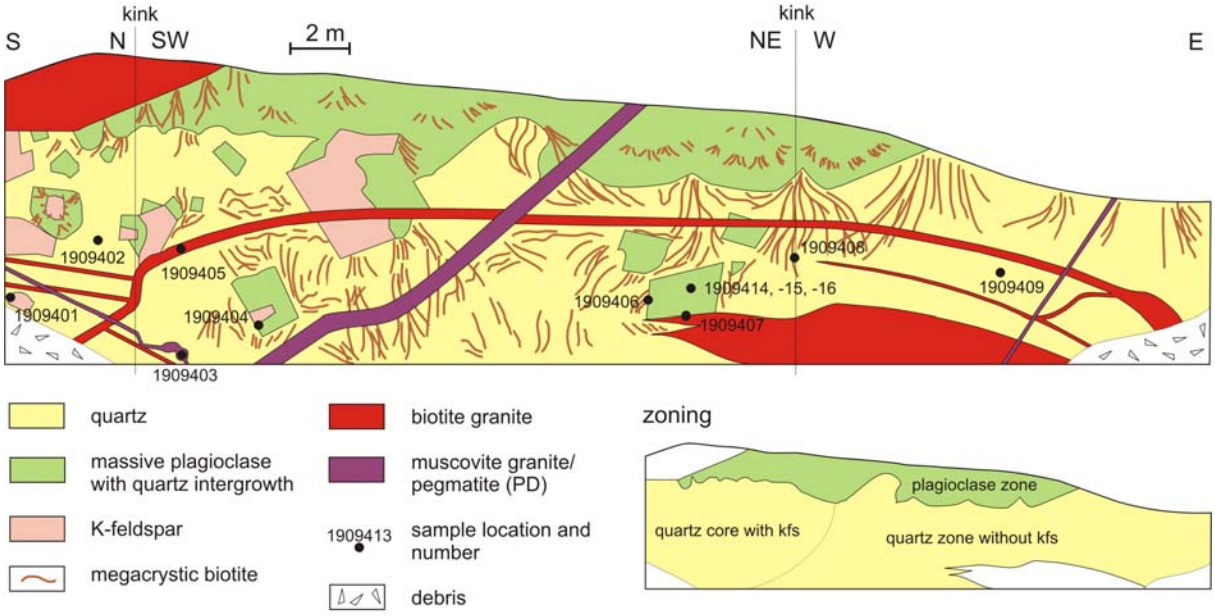

Fig. 12. *View of the SW-NE striking wall 1 of the Skåremyr quarry with sample localities.*

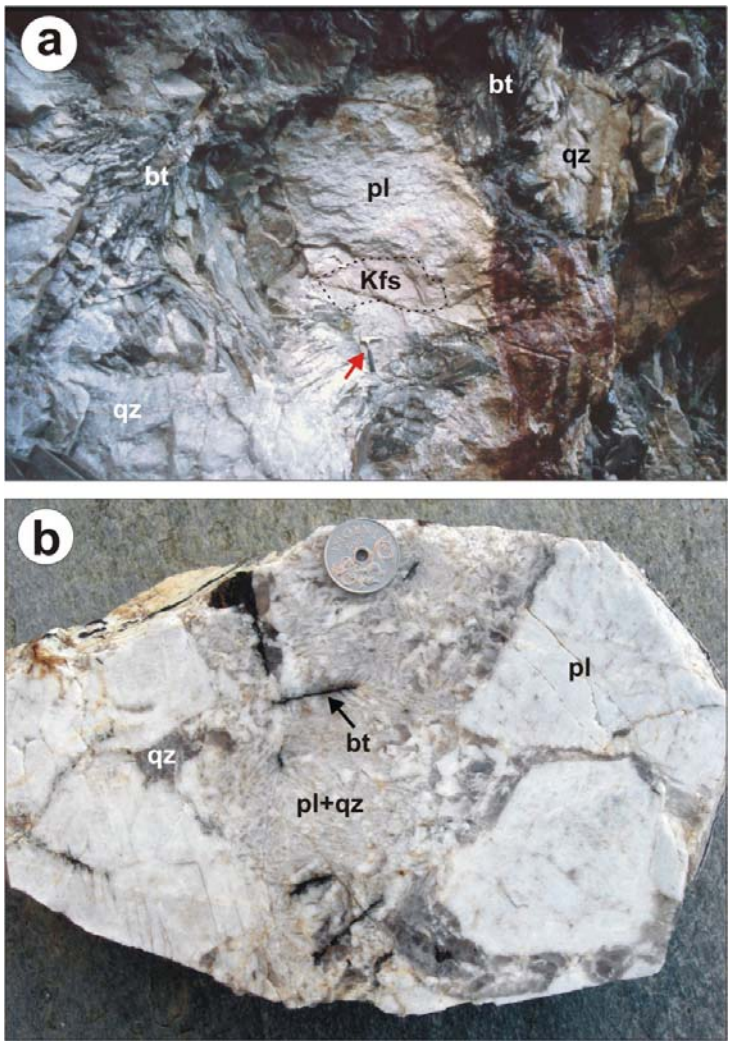

Fig. 13. *a – Plagioclase megacryst (pl) occurring in the quartz-rich core (qz) at the NW wall (wall 1) of the Skåremyr quarry. The megacryst encloses a smaller K-feldspar crystal (Kfs) and is surrounded by fan-like biotite (bt). For scale see hammer (red arrow). b – Hand specimen with pure plagioclase crystals (pl) and massive plagioclase intergrown with graphic quartz (pl+qz) and biotite (bt) from the wall zone of the pegmatite.*

4.7 Locality 7: Sønnristjern

Complexly zoned granitic pegmatite (ZoP) which forms steep-dipping lens on a ridge NE of Sønnristjern. The pegmatite which strikes NE-SW, is about 500 m long and 30 to 90 m wide (Søvegjarto 2001). It is hosted by amphibolites with foliation-parallel quartz-feldspar leucosomes. The pegmatite consists mainly of granite pegmatite with crystal sizes of 1 to 20 cm. Two separated zoned K-feldspar-rich cores occur in the SW and NE part of the pegmatite. Two large and several small quarries are situated in the pegmatite.

The Sønnristjern quarry occurs 60 m from the SW termination of the pegmatite and extends parallel to the axis of the asymmetric, zoned pegmatite core (Figs. 14, 15). The quarry is 30 m long, 8 m wide and 7 to 12 m deep. A 30 m long adit, 2 m x 4 m in cross-section, leads from the bottom of the quarry to the forest track. The contact between the pegmatite and amphibolites is exposed at the entrance of the adit. A 2 m wide wall zone of massive plagioclase intergrown with quartz and biotite occurs here at the amphibolite contact. The adit crosses through granite pegmatite consisting of plagioclase (2 to 10 cm), red K-feldspar (2 to 10 cm), smoky quartz (1 to 5 cm) and biotite stripes (5 cm to 1 m; Fig. 16a). Rarely, K-feldspar crystals of 0.5 to 2 m size are engulfed in the granite pegmatite. Where the adit enters the quarry, the granite pegmatite grades into massive red K-feldspar pegmatite with megacrystic biotite stripes. K-feldspar is commonly graphically intergrown with quartz. The K-feldspar zone is enveloped by a blocky plagioclase-dominated zones at its W and N side. The plagioclase zone consists of massive plagioclase (0.5 to 3 m in size) intergrown with smoky quartz and it contains a few K-feldspar megacrysts (0.5 to 2 m) and massive polycrystalline quartz batches up to 1 m in size. The plagioclase zone grades into a blocky quartz-rich zone capping the pegmatite core along its W, NW and NE borders with the granite pegmatite. The quartz-rich zone contains euhedral K-feldspar megacrysts (0,5 to 2 m) and plagioclase megacrysts (0.2 to 1 m; Figs. 16b, c). Plagioclase megacrysts are intensively intergrown with quartz (Fig. 16d). Megacrystic biotite flakes (up to 2 m long) grew from the granite pegmatite contact towards the pegmatite core (Fig. 15). Summarizing, the zoning of the Sønnristjern pegmatite is different from the classical zoned pegmatites which resembles the Skåremyr example. The zoning is complexly and asymmetrically. The blocky zone dominated by massive anhedral quartz crystals (0.1 to 0.5 m in size) grades into the blocky zoned dominated by anhedral plagioclase crystals (0.2 to 1 m in size). Both zones contain euhedral K-feldspar "blocky" megacrysts (0.5 to 2 m).

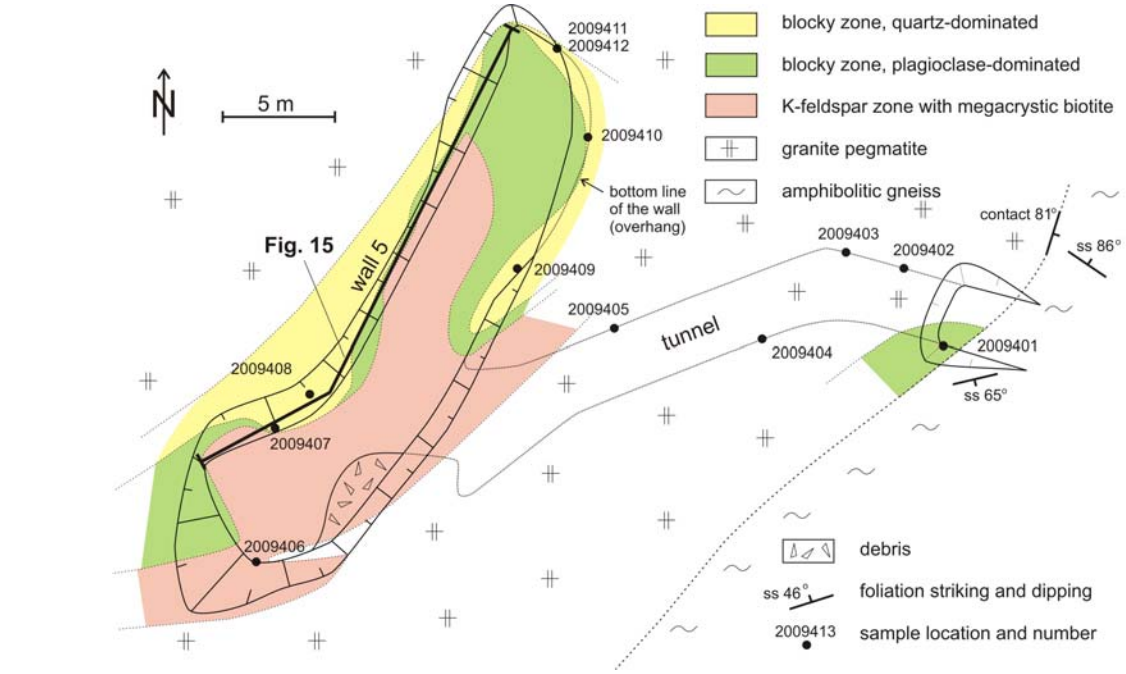

Fig. 14. *Outline of the Sønnristjern quarry with sample localities. The wall shown in Fig. 15 is indicated by the bold line.*

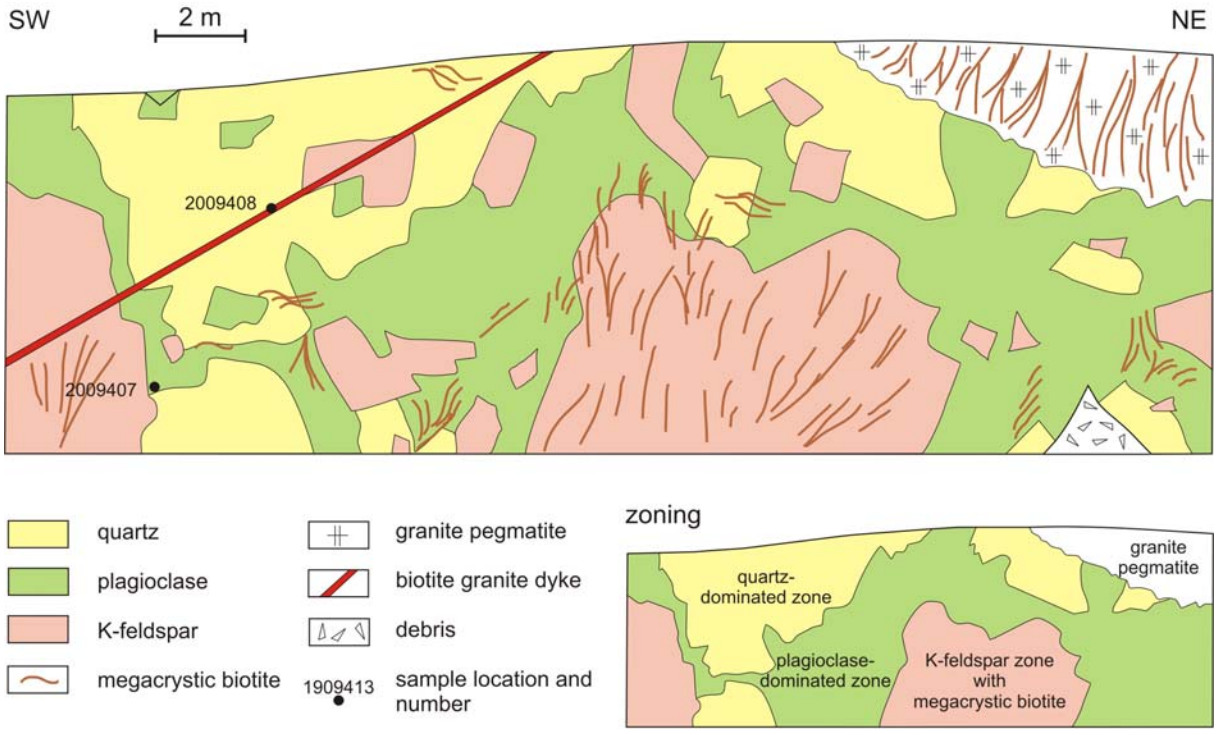

Fig. 15. *View of the SW-NE striking wall 5 of the Sønnristjern quarry with sample localities.*

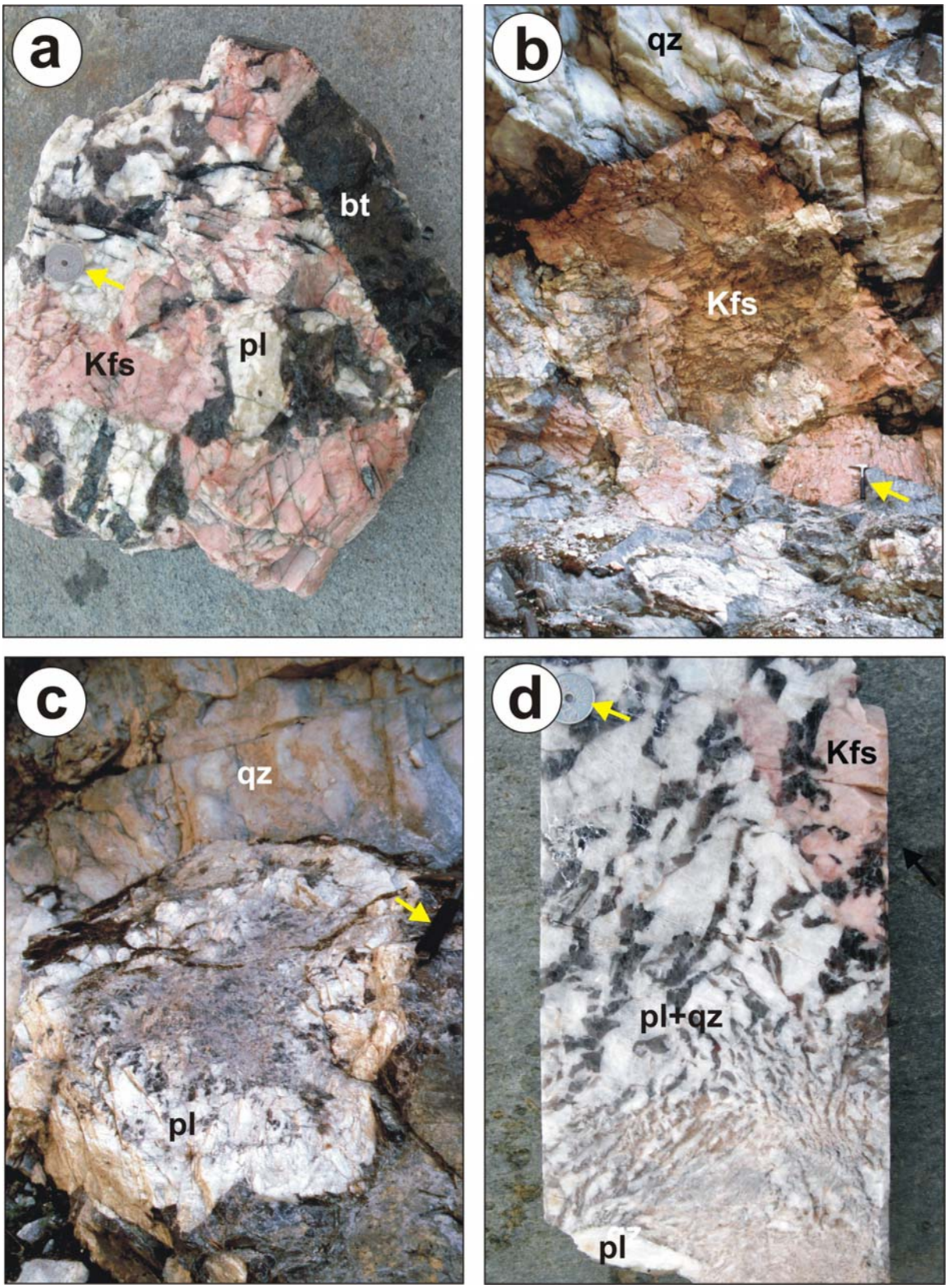

Fig. 16. a – Structure of the granite pegmatite hosting the Skåremyr pegmatite core. The One-Kroner-coin is for scale (yellow arrow). b – K-feldspar megacryst in the quartz-rich zone. The quartz at the megacryst contact is smoky. For scale see hammer (yellow arrow). c – Plagioclase megacryst (1 m) in the quartz-rich zone. d – Intergrowth of graphic quartz in plagioclase megacryst (pl+qz). A pure euhedral crystal (pl) forms the core (nuclei) of the former megacryst which was about 0.8 m in size . Kfs – K-feldspar.

4.8 Locality 8: Lille Kleivmyr

The GP at Lille Kleivmyr is about 150 m long and 50 m wide and comprises a variety of different pegmatite types. It forms a ENE-WSW striking lens which dips steeply NNW. The ca. 100 m long quarry along the axis of the pegmatite is one of the largest disused quarries in Froland. The host rocks of the GP are amphibolites and banded biotite-hornblende gneisses which contain foliation-parallel leucosoms of quartz and feldspar. Occasionally, enclaves of gneisses (up to 2 m) occur in the granite pegmatite. The quarry exposes two quartz-rich blocky zones containing commonly euhedral K-feldspar megacrysts (0.5 to 2 m in size) and several zones of massive plagioclase intergrown with quartz, containing occasionally K-feldspar megacrysts (Figs. 17, 18). These zones zones are embedded in granite pegmatite consisting of K-feldspar (10 to 20 cm), plagioclase (3 to 10 cm), quartz (1 to 5 cm) and biotite (up to 50 cm long). A ca. 1 to 3 m wide zone of plagioclase intergrown with quartz is developed along the northern contact of the pegmatite. The contacts between the blocky zones and the granite pegmatite are graditional.

The larger quartz-rich zone is exposed in the root of a water-filled stope at the E end of the quarry. The zone has a diameter of about 15 m and consists of massive smoky and milky quartz (10 to 50 cm) containing euhedral K-feldspar crystals (0.5 to 2 m). K-feldspar occupies 50 to 60 vol.%. Anhedral plagioclase crystals (0.2 to 1 m) fill the intersticies and is intergrown with quartz and biotite flakes (5 to 30 cm). Sporadically, large biotite plates occur (up to 1 m long). A smaller quartz-rich zone (ca. 6 m in diameter) occurs in the small, water-filled satellite quarry north of the main quarry.

Zones dominated by plagioclase intergrown with quartz occur in the western and central part of the quarry. They contain pink, euhedral K-feldspar megacrysts (0.5 to 2 m). The zones change gradually to pegmatitic granite with K-feldspar megacrysts (Fig. 18).

Characteristic for the Lille Kleivmyr deposit are irregular segregations and dykes of leucocratic, medium- to coarse-grained garnet-bearing granite which occur preferentially in the western and central part of the quarry. Garnets are commonly 1 to 3 mm in size but also 2-cm large crystals were found. The contacts between the garnet granite and the plagioclase zone and pegmatitic granite are diffuse. A ca. 3 m long enclave of biotite gneiss occurs in the small satellite quarry. It becomes progressively recrystallised towards the graditional contact with the garnet granite.

4.9 Locality 9: Våtåskammen

The pegmatitic granite (PGr) at Våtåskammen forms a E-W striking, 2000 m long and 70 to 80 m wide body. The granite contains of 10 to 80 cm long, red K-feldspar crystals which are embedded in coarse-grained (0.5 to 5 cm) granitic groundmass of quartz, plagioclase, K-feldspar and biotite. The K-feldspar crystals are aligned and weakly, presumably syn-genetically deformed (Fig. 19). Biotite crystals are slightly aligned. The sample was taken in order to trace relationships and/or differences between pegmatitic granite and granitic pegmatites.

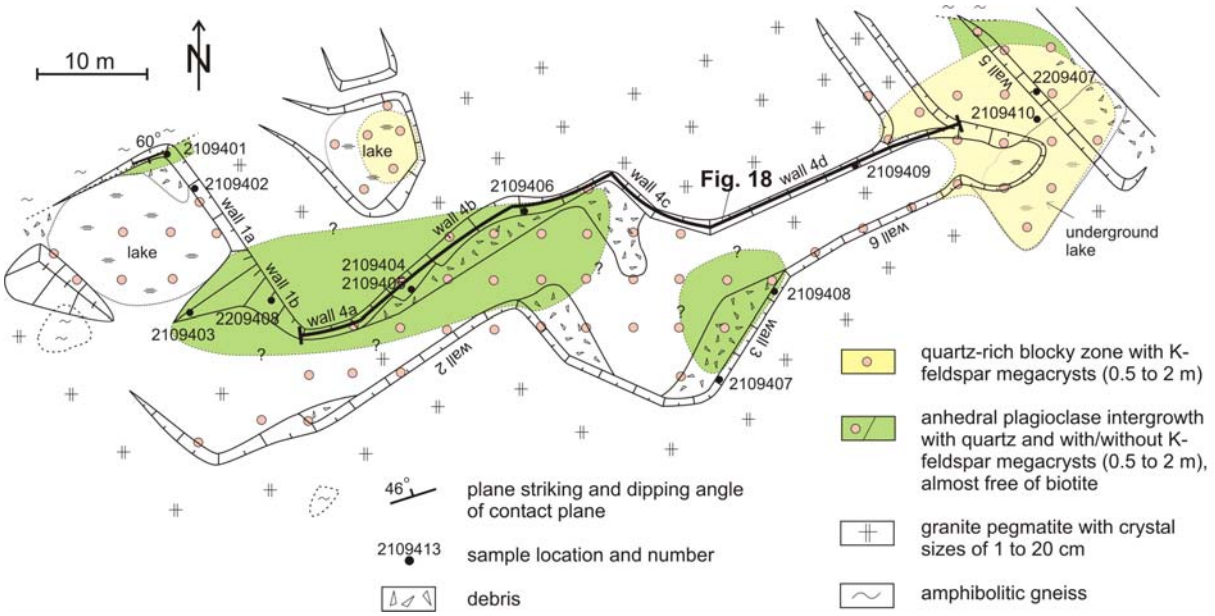

Fig. 17. *Outline of the Lille Kleivmyr quarry with sample localities. The wall shown in Fig. 18 is indicated by the bold line.*

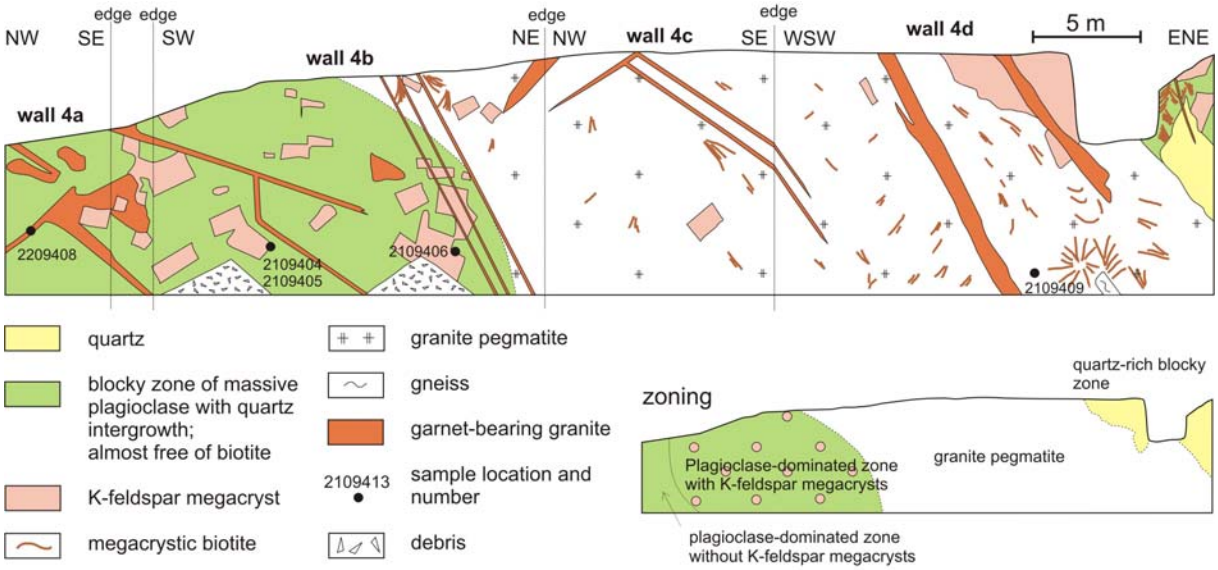

Fig. 18. *View of the WSW-ENE striking wall of the Lille Kleivmyr quarry with sample localities.*

Fig. 19. *Pegmatitic granite with aligned and weakly deformed K-feldspar megacrysts (Kfs) at Våtåskammen.*

4.10 Locality 10: Vaselona

The pegmatite is situated at the contact between metagabbro and amphibolitic gneisses and the coarse-grained granophyric granite of the Herefoss pluton. The metagabbro and amphibolitic gneisses form a mega-enclave within the Herefoss pluton. The Vaselona quarry exposes the core of a zoned pegmatite (ZoP) which is rich in palgioclase. The NW-SE striking pegmatite body is more than 80 m long and 25 m wide and dips steeply SW. The quarry striking along the axis of the pegmatite is 25 m long and 8 m wide with two water-filled inclined shafts. The mega-enclave consists of metagabbro and amphibolitic gneisses. The pegmatite has a quartz-rich core (8 m x 6 m) which contains K-feldspar crystals (0.5 to 1.5 m) and a few biotite laths (1 m). The quartz-rich core is enveloped by a zone (1 to 2 m) of pure plagioclase-quartz intergrowth which grades into a plagioclase-dominated zone with K-feldspar crystals (10 to 20 cm) towards the contacts of the pegmatite. Coarse-grained, K-feldspar-rich granophyric granite with sparse biotite (5 cm) occurs at the NE contact of the pegmatite. Secondary overprint of the NE part of the pegmatite resulted in the formation of megacrystic muscovite pockets (5 to 20 cm) along a NW-SE striking shear zone dipping 60º SW. Despite the macroscopic undeformed appearance of the pegmatite, its quartz is strongly mylonitised at micro-scale (see chapter 6.).

4.11 Locality 11: Fossheia, vest

The zoned granitic pegmatite (ZoP) at Fossheia, vest is strongly sheared resulting in complete recrystallisation of the pegmatite-forming minerals down to micro-scale. The ENE-WSW striking pegmatite is 60 m long and 20 m wide. The quarry is about 25 m long and 8 m wide and exposes a quartz-rich core with deformed K-feldspar megacrysts (2 to 3 m), plagioclase and kinked biotite. The smoky and dim microcrystalline quartz from the pegmatite core shows a fine, laminated foliation which gives it an unusual appearance.The pegmatite is bordered at its northern contact by a amphibolite mega-enclave occurring in the Herfefoss pluton. A medium-grained porphyritic, slightly deformed adamelite (dark biotite-bearing quartz monzonite) with red K-feldspar phenocrysts (up to 1.5 cm) occurs at its southern contact.

4.12 Locality 12: Fossheia, øst

The pegmatite at Fossheia, øst forms a tongue-like body which is 6 m long, 4 m wide and 3 m thick. It is hosted by coarse-grained porphyritic and biotite-bearing quartz monzonite belonging to the Herefoss pluton (Fig. 20). It represents a K-rich zoned granitic pegmatite of the granite facies (2) of the Herefoss pluton (HP). The pegmatite is 8 m E of the contact to the mega enclave which hosts the Fossheia øst and Vaselona pegmatite. Comb quartz (5 to 20

cm) intergrowth with K-feldspar (10 to 30 cm) and plagioclase (5 to 20 cm) occurs along the contact margin. A few biotite megacrysts (50 cm long) grew from the top of the pegmatite inwards. The contact zone changes to a quartz-rich zone in which individual K-feldspar crystals (0.1 to 0.8 m) are embedded. The pegmatite core consists of megacrystic K-feldspar graphically intergrown with quartz. An aplite vein borders the pegmatite bottom. Coarse-grained granite with a few K-feldspar megacrysts (30 to 50 cm) occurs below the vein.

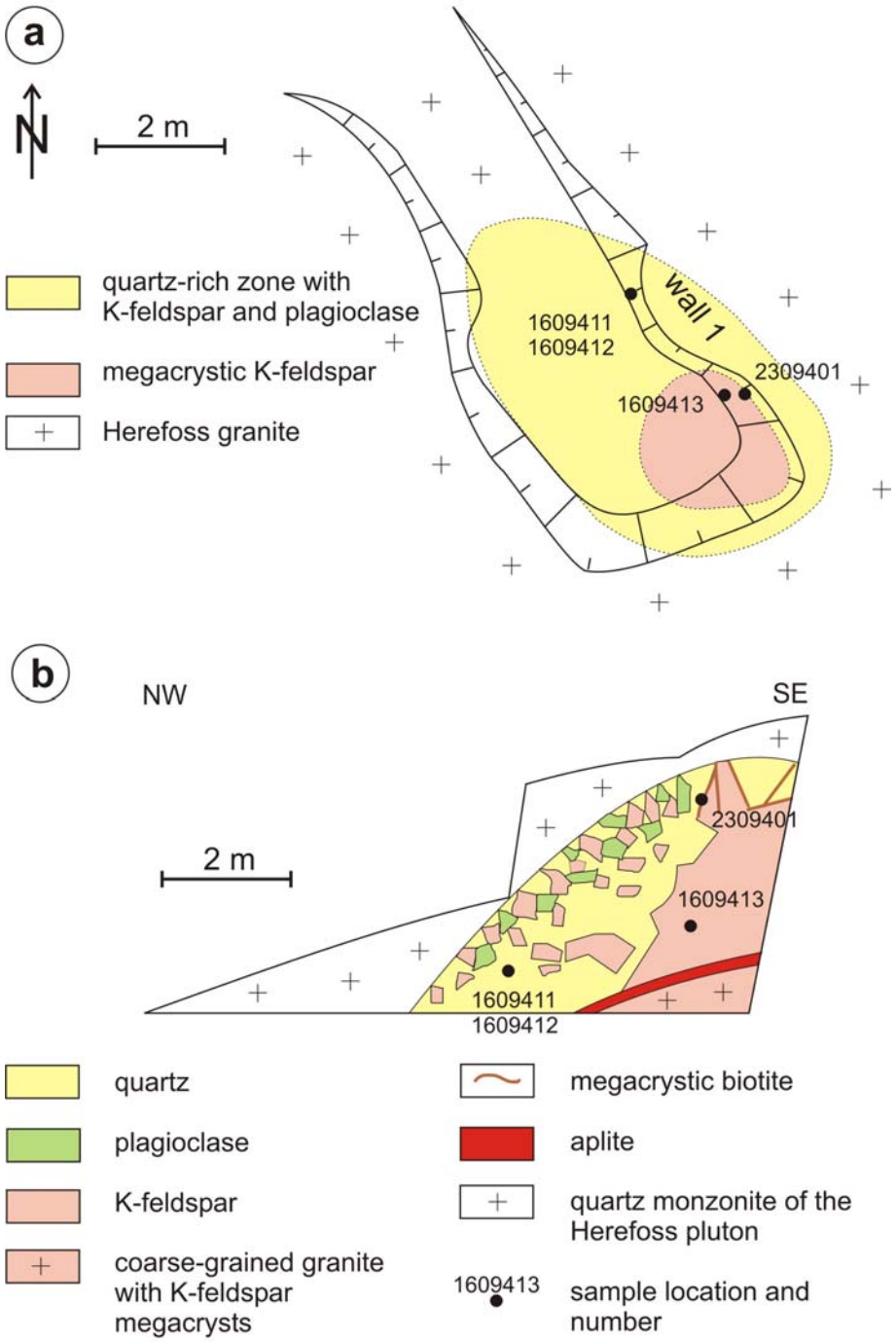

Fig. 20. *(a) Outline and (b) view of the wall 1 of the Fossheia, øst pegmatite with sample locations.*

4.13 Locality 13: Husefjell

A pinkish, coarse-grained, K-feldspar-quartz-rich porphyritic biotite leuco-granite is exposed in a road cut about 7 km NW of Grimstad. The pinkish K-feldspar phenocrysts are up to 3 cm long. The leuco-granite represents the early stage of the composite Herefoss pluton. The granite was sampled to determine the quartz and feldspar chemistry of a granite.

4.14 Locality 14: Metveit

The 1 m wide, steeply dipping pegmatite dyke occurs in small road cut W of Metveit. It is hosted by medium-grained porphyritic quartz monzonite of the Herefoss pluton which is the same granite facies which hosts the pegmatites Fossheia, vest and øst. The granite contains pinkish K-feldspar phenocrysts up to 1.5 cm long. The K-feldspar-rich granitic pegmatite (HP) is zoned exhibiting plagioclase-rich margin (10 to 25 cm) with embedded euhedral K-feldspar crystals and a massive quartz core zone. The core zone contains red K-feldspar megacrysts up to 50 cm in size. At the bottom the pegmatite changes gradually into coarse-grained K-feldspar-rich granite with large biotite crystals (5 cm). The latter is crosscut by aplite which borders the pegmatite dyke along its upper contact.

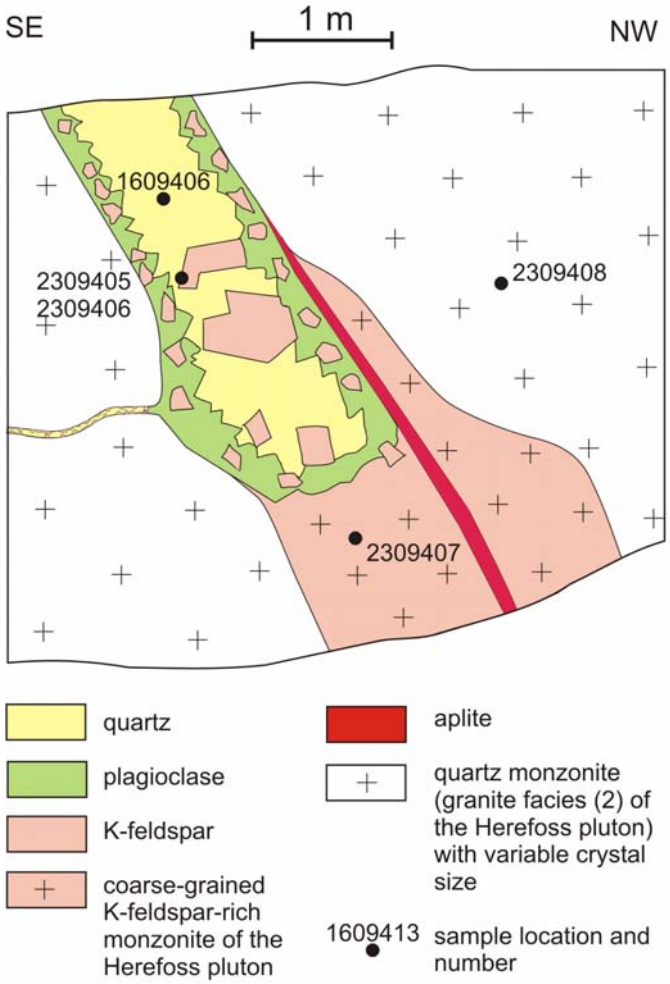

Fig. 21. *Schematic drawing of the road cut exposure at Metveit with sample localities.*

4.15 Locality 15: Heimdal

The pegmatite batch at Heimdal occurs in coarse-grained porphyritic granite with pink aligned K-feldspar megacrysts (up to 4 cm) in the western part of the Herefoss pluton, west of the Porsgrunn-Kristiansand Fault Zone. The pegmatite consists of 1.2 m long and 0.3 m wide quartz core. Up to 8 cm long K-feldspar crystals form comb-shaped growth structures indicating that they grew from the pegmatite contact towards the centre. Biotite (3 cm) and plagioclase (2 cm) rarely occur in the quartz core. The pegmatite thins outs towards the bottom and changes gradually to pure K-feldspar rock and further to porphyritic granite. The pegmatite represents a K-feldspar-rich granitic pegmatite related to an early stage of the Herefoss pluton formation (HP).

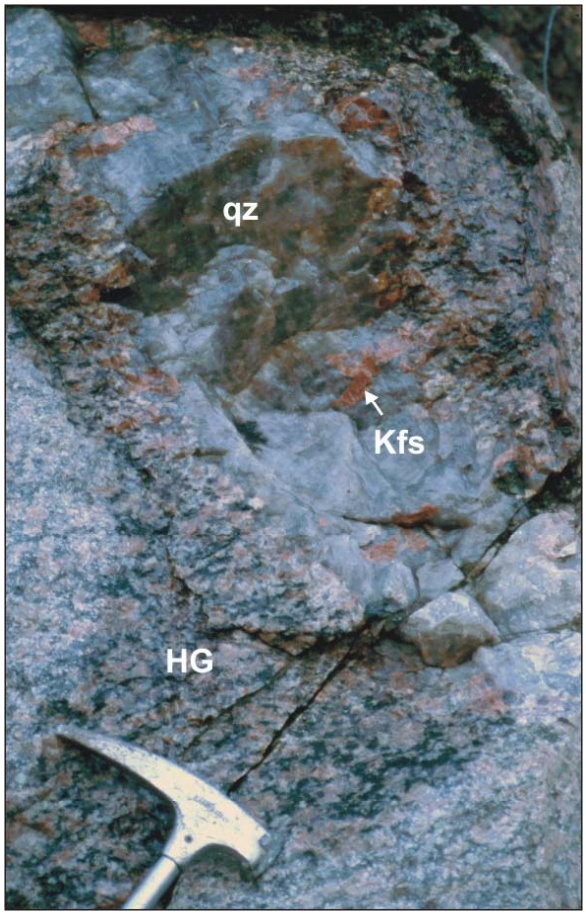

Fig. 22. *Quartz-rich pegmatite pocket at Heimdal hosted by the Herefoss granite (HG). Red euhedral K-feldspar crystals (Kfs) grew from the pegmatite contact into the quartz core (qz).*

5. Methods

5.1 Laser ablation inductively coupled mass spectrometry of quartz

A double focusing sector field inductively coupled mass spectrometer (Finnigan MAT, model-ELEMENT) was used for the determination of concentrations of Li, Be, B, Mn, Ge, Rb, Sr, Pb, Na, Mg, Al, P, K, Ti and Fe in quartz from the Froland pegmatites. Flem et al. (2002) give detailed description of the measurement procedure applied in the laboratory of NGU. Operating conditions of the laser ablation inductively coupled mass spectrometer (LA-ICP-MS) are listed in Table 1. The laser used for ablation was a Finnigan MAT, UV laser probe operating at 266 nm. The laser was run with a pulse width of 3 ns (Q-switched), a shot frequency of 20 shots s-1, pulse energy of 0.7-0.8 mJ and 30 µm spot size on rasters not larger than 180 x 250 µm.

Table 1. *Operating parameter of the LA-ICP-MS and key method parameters.*

plasma conditions	
plasma power	1075 W
auxiliary gas flow	0.89 l/min
sample gas flow	1.1 – 1.2 l/min
cone	high performance Ni
CD-1 guard electrode	yes
data collection	
scan type	E-scan
no. of scans	15

The existence of spectroscopic interferences required the use of variable mass resolutions. Li, Be, B, Mn, Ge, Rb, Sr and Pb were analysed at low mass resulotion ($m/\Delta m \approx 3500$), but Al, Na, P, Cl, Mg, Ti and Fe required medium mass resolution ($m/\Delta m = 300$) and K high mass resolution ($m/\Delta m > 8000$). The isotope ^{29}Si, was used as internal standard at low mass resolution, and ^{30}Si at medium and high mass resolution.

External calibration was achieved by using four silicate glass reference materials produced by the National Institute of Standards and Technology (NIST SRM 610, NIST SRM 612, NIST SRM 614, NIST SRM 616). In addition, the standard reference material 1830, soda-lime float glass (0.1 wt.% Al_2O_3) from NIST, the high purity silica BCS 313/1 reference sample from the Bureau of Analysed Samples, UK, the certified reference material "pure substance No. 1" silicon dioxide SiO_2 from the Federal Institute for Material Research and Testing, Berlin, Germany and the Qz-Tu synthetic pure quartz monocrystal provided by Andreas Kronz from the Geowissenschaftliches Zentrum Göttingen (GZG), Germany, were used.

Each measurement consists of 15 scans of each isotope, with a measurement time varying from 1 s per scan of K in high resolution to 0.02 s per scan of, e.g. Mn in low resolution. An Ar-blank was run before each standard and sample measurement. The background signal was subtracted from the instrumental response of the standard before normalisation against the internal standard. This was done to avoid memory effects between samples. A weighted linear regression model including several measurements of the different standard was used for calculation of the calibration curve for each element.

10 successive measurements on the Qz-Tu were used to estimate the limits of detections (LODs). LODs are based on 3 times standard deviation (3σ) of the 10 measurements divided by the sensitivity S. Typical detection limits are given in Table 2.

Table 2. *Limits of detection (LOD) are based on 10 measurements on the Qz-Tu synthetic quartz. Concentrations of Qz-Tu represent the average of three measurements applying the LA-ICP-MS the measurement procedure of Flem et al. (2002) at NGU.*

isotope	^{7}Li	^{9}Be	^{11}B	^{24}Mg	^{27}Al	^{31}P	^{39}K	^{47}Ti	^{55}Mn	^{56}Fe	^{74}Ge	^{85}Rb	^{88}Sr	^{208}Pb
LOD (ppm)	1.6	0.3	1	10	4	10	1	0.5	0.2	0.2	0.2	0.2	0.05	0.01
Qz-Tu (ppm)	1.832	<0.25	0.382	66.6	8.03	33.17	3.61	<0.1	2.544	<3.97	<0.54	0.224	<0.20	0.016

5.2 Electron probe micro-analysis of quartz

Trace element abundances of Al, K, Ti, and Fe in quartz were performed with a JEOL 8900 RL electron microprobe at the Geowissenschaftliches Zentrum Göttingen, Germany. These elements are the most common trace elements in natural quartz beside H, Na and Li. K was selected as representative of the interstitial monovalent ions, because the detection limit of Na (~90 ppm) was higher than the typical concentrations and Li and H cannot be measured by electron probe micro analysis (EPMA). The tetravalent Ti^{4+} substitutes for Si. The substituted trivalent Al^{3+} and Fe^{3+} are compensated by interstitial ions such as Li^{+}, Na^{+}, K^{+}, H^{+} and Fe^{2+} or by coupled substitution of a pentavalent ion, e.g. P^{5+} (e.g., Götze et al. 2001 and references therein). For high precision and sensitivity, a beam current of 80 nA, a beam diameter of 5 µm, and counting times of 15 s for Si, and of 300 s for Al, Ti, K, and Fe were used. Detection limits (3σ of single point background) were 60 ppm for Al, 18 ppm for K, 33 ppm for Ti, and 27 ppm for Fe.

5.3 X-ray fluorescence spectrometry of feldspar and mica

Major and trace element concentrations of feldspars and micas were determined by X-ray fluorescence spectrometry (XRF) using Phillips PW1480 spectrometer equipped with a Sc/W X-ray tube at NGU, Trondheim. Ca. 3 g sample material milled to ~40 µm are fused at 1030°C for 10 min. Loss on ignition (LOI) is determined gravimetrically and it is used as an approximate measure of volatiles such as H_2O and CO_2. 0.6 g of the sample material used for major element determination is then fused in a Pt-crucible with lithium tetra borate ($Li_2B_4O_7$) at 1120°C yielding a homogeneous, optically flat glass disc. Major element analysis is carried out on fused glass discs for Na, Mg, Al, Si, P, K, Ca, Ti, Mn and Fe. The total Fe concentration is calculated as Fe_2O_3. Accuracy and limits of detection of major elements are listed in Table 3.

Table 3. *Accuracy and limits of detection for XRF feldspar and mica analyses of major elements.*

oxide	SiO_2	Al_2O_3	Fe_2O_3	TiO_2	MgO	CaO	Na_2O	K_2O	MnO	P_2O_5
$K_{element}$*	0.053	0.038	0.045	0.020	0.077	0.045	0.050	0.036	0.010	0.025
limits of detection (wt.%)	0.1	0.1	0.01	0.01	0.01	0.01	0.1	0.01	0.01	0.01

*Accuracy = $K_{element} \cdot \sqrt{}$(concentration in sample + 0.1) [%]

For trace elements, pressed powder pellets using binding agent wax Hoechst C are analysed for Rb, Sr, Y, Zr, Nb, Ba, Pb, Th, U, Sc, V, Cr, Co, Ni, Cu, Zn, Ga, Mo, As, Sb, Sn, Ce, Nd, La, W, Cs, Ta, Pr, Hf, S, Cl and F. Accuracy and limits of detection of trace elements are listed in Table 4.

Table 4. *Accuracy and limits of detection (LOD) for XRF feldspar and mica analyses of trace elements.*

element	Ba	Sb	Sn	Ga	Zn	Cu	Ni	Yb	Co	Ce	Nd	La	W	Cs	Ta	Pr	Mo
$K_{element}$*	1.6	0.75	0.73	0.52	0.86	1.3	0.68	0.8	0.46	1.1	1.0	0.52	0.8	1.13	0.79	0.72	0.64
LOD (ppm)	10	10	10	10	5	10	5	15	5	10	10	10	10	10	10	10	5

element	Nb	Zr	Y	Sr	Rb	U	Th	Pb	Cr	V	As	Sc	Hf	S	Cl	S
$K_{element}$*	0.35	0.48	0.28	0.42	0.37	0.48	0.49	0.86	3.5	1.3	0.47	0.51	0.55	0.33	0.08	0.15
LOD (ppm)	5	5	5	5	5	10	5	10	10	10	5	10	10	1000	1000	1000

*Accuracy = $K_{element} \cdot \sqrt{}$(concentration in sample + 10) [ppm]

5.4 Inductively coupled mass spectrometry of feldspar

Rare earth elements of feldspar were determined by inductively coupled mass spectrometry (ICP-MS) following a $LiBO_2$ fusion and nitric acid digestion of a 0.2 g sample. The analyses were performed at the ACME Analytical Laboratories Ltd. in Vancouver, Canada. Limits of detection are given in Table 5.

Table 5. *Limits of detection (LOD) for ICP-MS feldspar analyses of rare earth elements.*

element	La	Ce	Pr	Nd	Sm	Eu	Gd	Tb	Dy	Ho	Er	Tm	Yb	Lu
LOD (ppm)	0.5	0.5	0.02	0.4	0.1	0.05	0.05	0.01	0.05	0.05	0.05	0.05	0.05	0.01

6. Micro-textures in cathodoluminescence images of quartz

Scanning electron microscope cathodoluminescence (SEM-CL) has been applied to quartz in order to reveal possible growth zoning, alteration structures and different quartz generations at micro scale (<1 mm). Grey-scale contrasts visualised by SEM-CL are caused by the heterogeneous distribution of lattice defects (e.g., oxygen and silicon vacancies, broken bonds) and trace elements in the crystal lattice (*e.g.*, Sprunt 1981, Ramseyer et al. 1988, Perny et al. 1992, Stevens Kalceff et al. 2000, Götze et al. 2001, 2004, 2005). Although the physical

background of the CL of quartz has not been fully understood the structures revealed by CL give information about the crystallisation and alteration history of the rock. Two or one thin sections of representative samples from each deposit were investigated by SEM-CL.

Generally, five types of secondary structures hosted in primary crystallised quartz (pqz) can be distinguished (Figs. 23 to 29):

1) Thin (<5 µm) healed cracks connecting nearly non-luminescent domains around secondary fluid inclusions. These structures appear black in the SEM-CL image and they are named secondary quartz 1 (sqz1; Figs. 25c, 27e, f, 28c, e, f).
2) Irregular patterns or domains of low-luminescent quartz enveloping commonly sqz1. Occasionally, the pattern seems to be preferentially oriented into certain directions which may correspond to the crystallographic orientation of quartz. These structures appear grey in the SEM-CL image and are named secondary quartz 2 (sqz2; Figs. 23b, d, 24d, e, 25c, 26a).
3) Diffuse alteration zones along grain boundaries and contacts to feldspar and mica. These structures appear dark grey in the SEM-CL image and they are named secondary quartz 3 (sqz3; Figs. 23f, 25a, 28a, b, 29e, f).
4) Bright circular radiation halos (sqz4) around radioactive inclusions, e.g. zircon (Fig. 26b). The α-radiation causes the damage of the quartz structure (metamictisation) and the change of CL properties.
5) Non-luminescent (black), thin crystal coatings and fillings at triple junctions of crystal boundaries of recrystallised quartz named secondary quartz 5 (sqz5; Figs. 26e, 27b).

Apart from the radiation halos all secondary structures appear darker in the SEM-CL image than the primary crystallised quartz. Growth zoning in primary quartz has not been observed.

Late- to post-magmatic fluid-driven overprint causes small-scale quartz dissolution and precipitation (healing) along grain boundaries and micro-cracks resulting in the formation of sqz1 to sqz3. Micro-fractures providing the pathways for fluids can be related to external deviatoric stress but also to internal stresses at grain scale resulting from the strong thermal contraction of quartz (Vollbrecht et al. 1991, 1994). The crack systems were formed by shearing and tensional strain, if the intra-granular crack system is symmetrically (Vollbrecht et al. 1991, 1994). The α/β-transition of quartz which causes an anisotropic contraction of 0.86 vol.% vertical to the c-axis and 1.3 vol.% parallel to the c-axis (e.g., Blankenburg et al. 1994), imposes additional stress within and between quartz crystals.

Dense network of sqz1-healed cracks connecting low-luminescent domains around fluid inclusions are a widespread phenomenon in quartz from igneous rocks (Sprunt & Nur 1979, Behr & Frentzel-Beyme 1989, Valley & Graham 1996, D'Lemos *et al*. 1997, Van den Kerkhof & Hein 2001, Van den Kerkhof *et al*. 2001, 2004, Müller *et al*. 2000, 2002b, Rusk & Reed 2002). The CL intensity of such structures may increase after several minutes of electron beam exposure using high beam power densities $>10^{+4}$ W/cm^2 (see chapter 7.2).

Quartz from the Løvland pegmatite is partially strongly recrystallised caused by rotation recrystallisation. Grain margins of quartz are covered by thin films (<3 µm) of newly crystallised, non-luminescent (black) quartz (Figs. 23a, b). The micro scale deformations is in agreement with observations made at macro scale (see chapter 4.1).

An exceptional micro-structure is developed in the quartz form the Fossheia, vest and Vaselona pegmatite. The pegmatite quartz was completely mylonitised which caused the deletion of pre-existing textures (sqz1-4) and the formation of micro-crystalline quartz (<1 to 20 µm; Figs. 26a-f, 27a-c). The grain boundaries are healed by thin coatings of non-luminescent quartz (sqz5). The degree of quartz mylonitisation is stronger in the Fossheia, vest sample than in the sample from Vaselona.

Pegmatite quartz from Metveit and the granite quartz from Husefjell exhibit commonly non-luminescent 1-5 µm small circular spots (Figs. 28d, 29a-d). These spots are not related to fluid inclusions or mineral inclusions (compare Figs. 29a and b). Some of the spots disappear after several minutes of electron bombardment (compare Figs. 29c and d). Stenina et al. (1984) described similar spots and identified these structures as amorphous (non-crystalline) micro-domains using TEM imaging. These disordered domains contain molecular water and are considered as defect clusters.

Table 6 summarises the observed of micro textures of secondary quartz in pegmatite quartz. For this study it is important to know the approximately volume portion which occupy secondary quartz within primary quartz. Therefore, the abundance of secondary quartz estimated from area analyses of SEM-CL images is shown in Table 6. The knowledge is essential because primary and secondary quartz may have different trace element concentrations which has influence of the average trace element content of quartz of the bulk deposit (see chapter 7.4).

Table 6. *Observed of micro textures of secondary quartz in pegmatite quartz and their estimated abundance in vol.%. The abundance of sqz4 is to low (<<1 vol.%) to be considered.*

locality Nr.	locality name	pegmatite type	sqz1	sqz2	sqz3	sqz4	sqz5	specific micro textures	vol.% of sqz1	vol.% of sqz2/3
1	Løvland	KP	x	x	x	x	x	strongly recrystallised and wide-spread formation of secondary quartz along newly formed grain boundaries, broad healed fluid inclusion trails (up to 500µm)	<1	5-10
2	Hellheia, midtre	NaP	x	x	x	x	-		<1	2-5
3	Hellheia, nordre	NaP	x	x	x	x	-	sporadic inclusions of rutile needles	<1	2-5
4	Bjortjørn	NaP	x	x	x	x	-	wide-spread sqz1, sqz2 and sqz3	1-2	5-10
5	Haukemyrliene	GP	x	x	x	x	-		<1	2-5
6	Skåremyr	ZoP	x	x	x	x	-	grey-scale contrast between pqz and sqz2 is very low	~1	2-5
7	Sønnristjern	ZoP	x	x	x	x	-		<1	2-5
8	Lille Kleivmyr	GP	x	x	x	x	-		~1	2-5
9	Våtåskammen	PGr	x	x	x	x	-		~1	2-5
10	Vaselona	sheared ZoP	-	-	-	-	x	extremely mylonitised, no pre-mylonitisation texture preserved	0	0
11	Fossheia, vest	sheared ZoP	-	-	-	-	x	extremely mylonitised, no pre-mylonitisation texture preserved	0	0
12	Fossheia, øst	HP	x	-	x	-	-	wide-spread sqz1, no sqz2, sporadic inclusions of rutile needles	1-2	3-5
13	Husefjell	monzonite	x	x	x	x	-	non-luminescent defect clusters (<5 µm)	~1	2-5
14	Metveit	HP	x	x	x	-	-	non-luminescent defect clusters (<5 µm), very unstable CL	~1	2-5
15	Heimdal	HP	x	x	x	-	-		~1	2-5

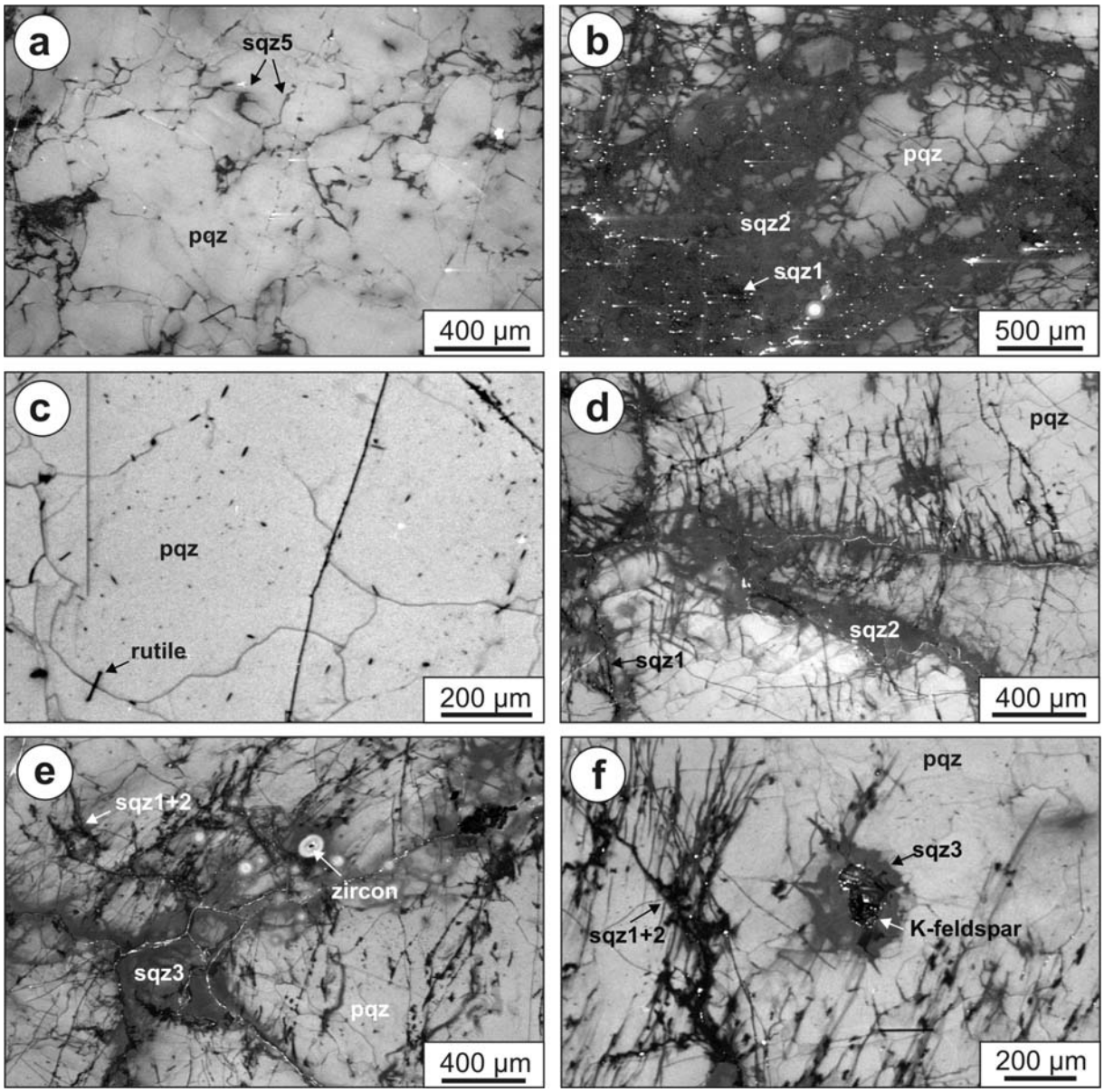

Fig. 23. *SEM-CL images of pegmatite quartz from Løvland and Hellheia, midtre.*
a – Quartz from Løvland showing thin films of sqz5 along grain boundaries of subgrains formed due to rotation recrystallisation (black). b – The same structure as in (a) were subsequently penetrated by fluids resulting in broad (up to 500 µm), healed fluid pathways containing fluid inclusions with a luminescence-active phases (bright dots). c - Quartz from Hellheia, midtre. Primary quartz containing rare sqz1 and a few inclusions of rutile needles. d – Quartz from Hellheia, midtre. Sqz2 pattern with preferentially orientation. e – SEM-CL image of pegmatite quartz from Hellheia, midtre. Textures formed by sqz, sqz2 and sqz3. Zircons are surrounded by bright luminescent, circular radiation halos. f- Quartz from Hellheia, midtre. Textures formed by sqz1 and sqz2. The K-feldspar inclusion is surrounded by alteration zone (sqz3).

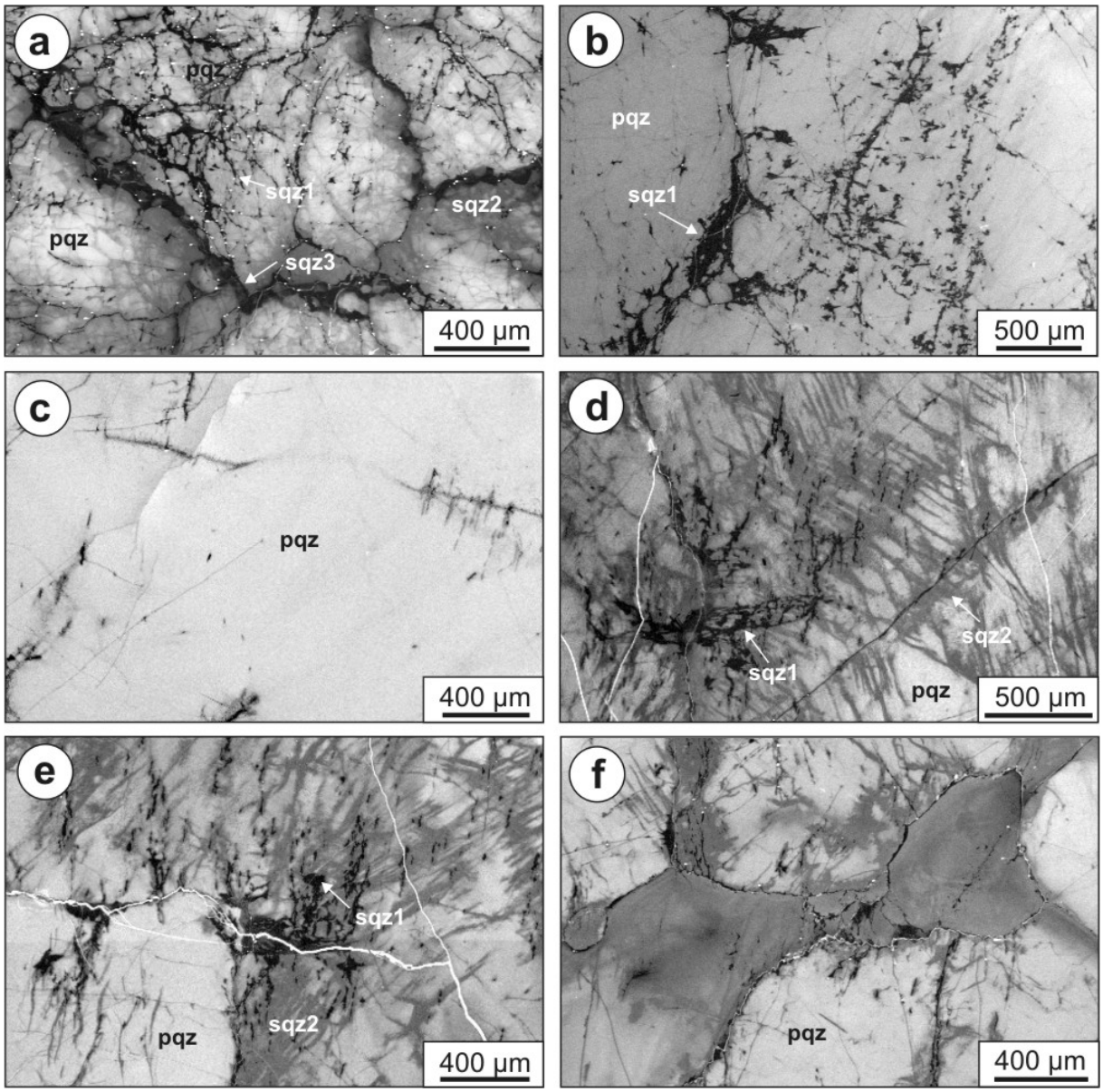

Fig. 24. *SEM-CL images of pegmatite quartz from Bjortjørn, Skåremyr and Sønnristjern. a – Quartz from Bjortjørn showing the distribution of sqz1, sqz2 and sqz3. The network of sqz1 is more dense and irregular than in other pegmatite samples. b - Quartz from Skåremyr. Pqz with relative dense network of sqz1. The grey-scale contrast between pqz and sqz2 is very low and hard to distinguish in the image. c - Pqz from Sønnristjern with scarce sqz1 and sqz2. d - Quartz from Sønnristjern showing textures formed by sqz1 and sqz2. e – Same as (d). f – Quartz from Sønnristjern with two small interstitial grains of lower luminescence. The grains were affected by alteration during rotation recrystallisation resulting in sqz3.*

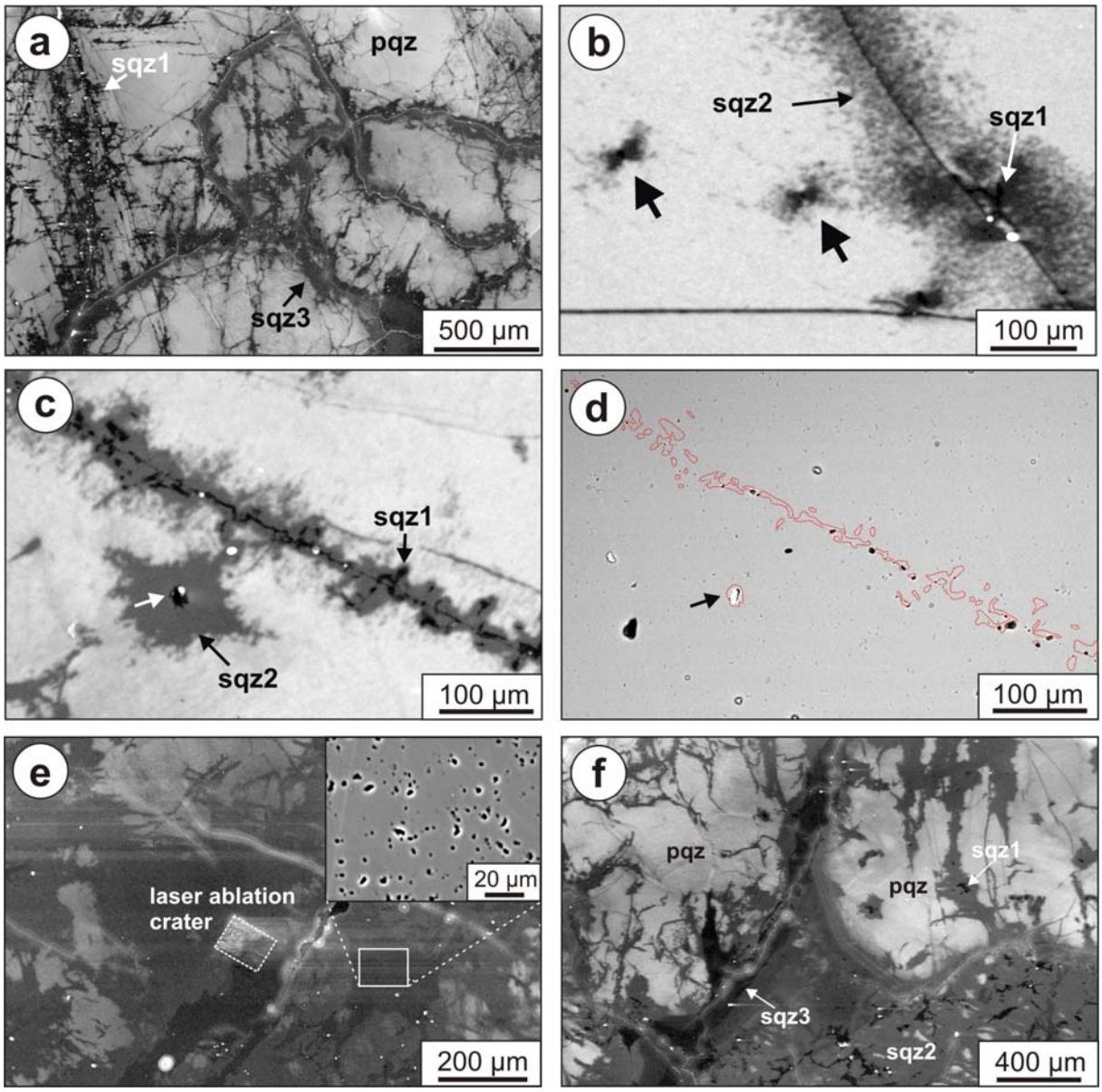

Fig. 25. *SEM-CL images of pegmatite quartz from Lille Kleivmyr.*
a – Quartz showing the distribution of sqz1 and sqz3. b – Quartz with butterfly structures of sqz2 around secondary fluid inclusions (black arrows). The fluid inclusions are bordered by a thin film of sqz1 in the centre of the "butterflies" (see also (e) and (f)). c - Quartz showing a fluid inclusion bordered by thin film of sqz1 (white arrow). Both are embedded in sqz2. f – Backscattered electron image of the same section as in (c). The thin red dashed lines correspond the extension of sqz1 in (e). The fluid inclusion hole (black arrow) is smaller than the black area in (e) (white arrow), which indicates clearly that sqz1 envelopes the fluid inclusion. e – Quartz after LA-ICP-MS analyses. It is one of the few analyses which could be clearly placed in secondary quartz (laser ablation crater). The backscattered electron image inset illustrates the high porosity (black spots) of secondary quartz.

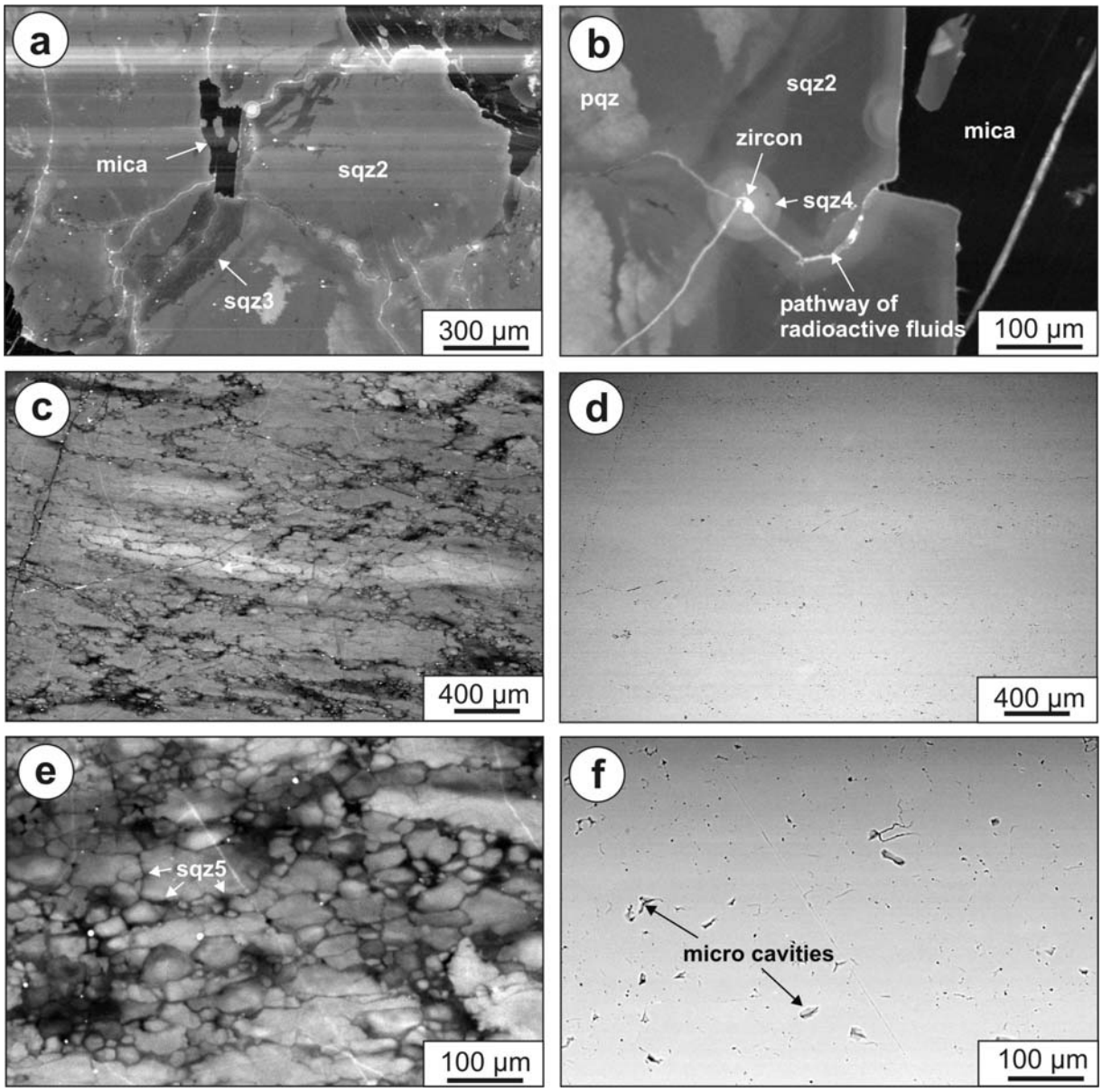

Fig. 26. *SEM-CL images of pegmatite quartz from Lille Kleivmyr and Vaselona. a – Strongly altered quartz from Lille Kleivmyr next to mica. The structure of sqz3 corresponds the former fluid pathway. b – Detail of pegmatite quartz from Lille Kleivmyr. α-radiation of the zircon caused the damage of surrounding quartz resulting in a bright luminescent halo (sqz4). The zircon is situated at the former pathway of radioactive fluids. c – Overview picture of quartz from Vaselona showing the mylonitised and healed micro-crysttaline texture. d - Backscattered electron image of the same section as in (c). e - Detail of (c) illustrating the small crystal size of the mylonitised quartz which is healed by non-luminescent (black) sqz5. f - Backscattered electron image of the same section as in (e). Most of the grain boundaries of the small crystals are healed by sqz5 (compare with (e)) and only a few micro cavities are left.*

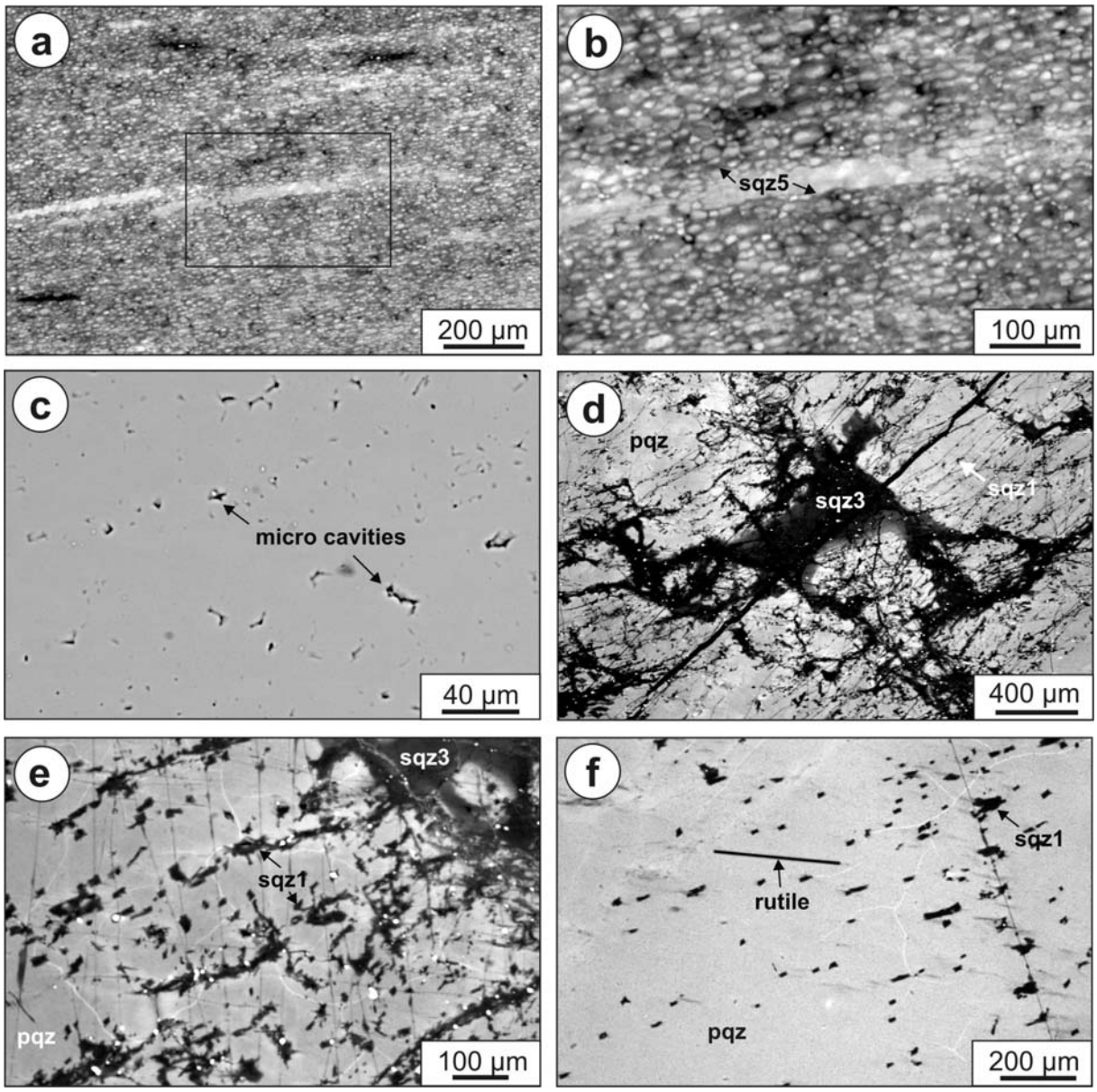

Fig. 27. *SEM-CL images of pegmatite quartz from Fossheia, vest and Fossheia, øst. a - Overview picture of quartz from Fossheia, vest showing the mylonitised and healed micro-crystalline texture. b - Detail of (a) illustrating the small crystal size of the mylonitised quartz which is healed by non-luminescent (black) sqz5. c - Backscattered electron image of the same section as in (b). Most of the grain boundaries of the small crystals are healed by sqz5 (compare with (b)) and only a few micro cavities are left. d - Quartz from Fossheia, øst showing the typical development of sqz1 and sqz3. e – Quartz from Fossheia, øst showing an area with a dense network of sqz1. f - Quartz from Fossheia, øst showing an area with scarce sqz1 and a rutile inclusion.*

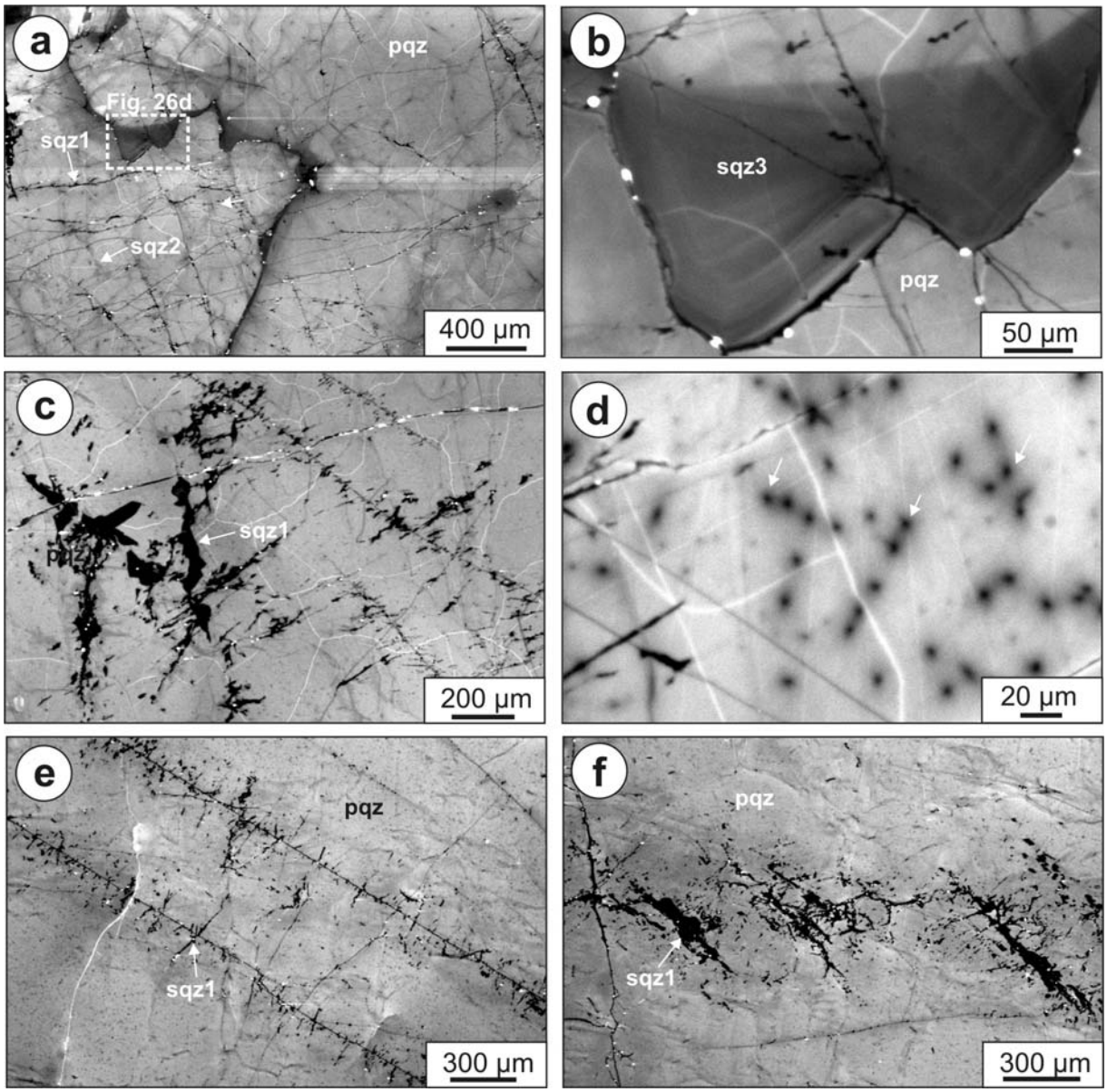

Fig. 28. *SEM-CL images of granite and pegmatite quartz from Husefjell and Metveit, respectively. a - Pqz of the granite from Husefjell showing a dense network of thin cracks healed by black sqz1 and grey sqz2. b - Weak oscillatory zoning in sqz3 which replaces pqz along a grain boundary (grain boundary migration). c - Pqz from Husefjell with relative dense network of sqz1. d – Detailed SEM-CL image of granite quartz from Husefjell. The quartz exhibits non-luminescent spots (black; some spots are marked with white arrows) which are interpreted as water-bearing defect clusters. e -Quartz from Metveit. Sqz1 forms straight thin healed cracks connecting non-luminescence domains around secondary fluid inclusions. f - Quartz from Metveit. Sqz1 forming an en echelon structure.*

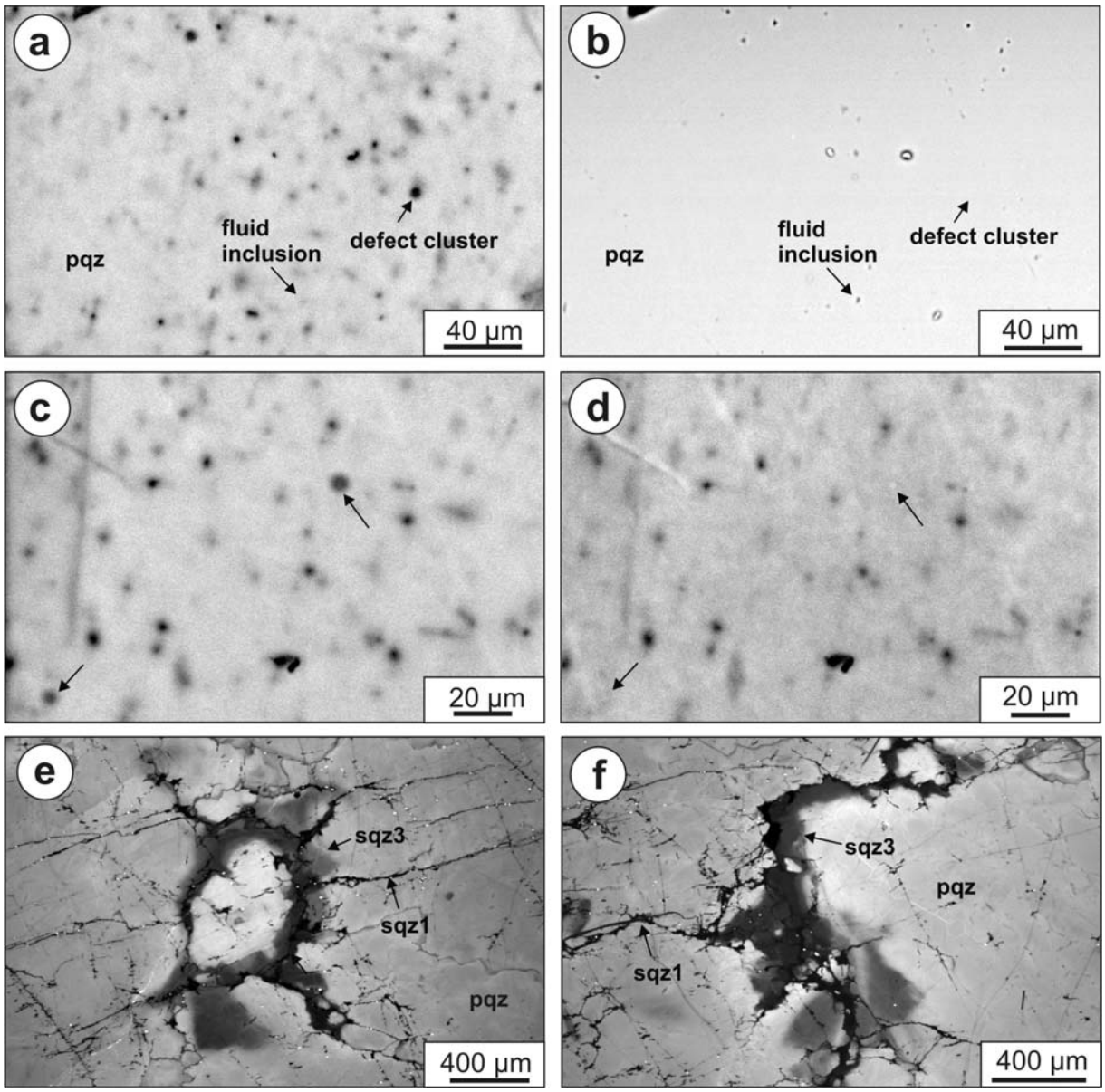

Fig. 29. *SEM-CL images of pegmatite quartz from Metveit and Heimdal.*
a - Detail of quartz from Metveit. The quartz exhibits a dotted micro texture in CL which are interpreted as water-bearing defect clusters. b - Backscattered electron image of the same section as in (a). The comparison with the SEM-CL image (a) indicates that the black dots observed in SEM-CL are not fluid or mineral inclusions. c – Detail of quartz from Metveit showing defect clusters at the beginning of electron beam exposure. d – Same section as in (c) after 3 min electron radiation. Some of the defect clusters increased their CL intensity and they are not visible anymore (arrows). e, f - Quartz from Heimdal showing the textural pattern of sqz1 and sqz3.

7. Trace elements of magmatic quartz

7.1 Variation of quartz chemistry between different pegmatite types and deposits

Concentrations of trace elements in quartz determined by LA-ICP-MS are listed in Appendix B. Variation diagrams of Al vs. Ti and Li vs. Ge are given in Appendix C and D. For better illustration Al vs. Ti and Li vs. Ge in quartz are plotted as concentration fields for the different pegmatite types in Fig. 30. Average trace element concentrations in quartz of the different pegmatite and granite types are listed in Table 7 and that of the different deposits are shown in Table 8. The average concentrations of the deposit do not include analyses of PD and biotite granite dykes because they occupy less than 3 vol.% of deposit. Concentrations of secondary quartz (spz) are also not considered in the average value of deposits.

Al content in quartz from PGr, GP, NaP, ZoP and KP is in the same range (Table 7). The concentrations range between 21.5 and 64.6 ppm. Ti is low in the PGr, GP NaP and KP varying from 3.8 to 6.1 ppm. ZoP contain quartz which has slightly higher average Ti of 7.2 ppm. Quartz of pegmatitic granites (PGr) exhibits the highest average Li of 10.2 ppm followed by granite pegmatites and Na-rich pegmatites with 8.7 ppm and 8.3 ppm, respectively. Quartz of K-rich pegmatites (ZoP and KP) has low average Li (6.9 and 5.9). Concentrations of trac elements in the mylonitised pegmatite quartz from Vaselona and Fossheia (ZoP) show significant differences compared to concentrations of the un-deformed ZoP quartz. The quartz from Fossheia, vest has high Ge (2.4 ppm) and Ti (29 ppm), and exceptional low Li (0.3 ppm) and Al (26.2 ppm). The quartz from Vaselona has highest Ge (2.8 ppm), high Ti (16.3 ppm), and relative low Li (4.3 ppm). The mylonitisation which is much stronger developed in the Fossheia, vest pegmatite may have caused the different trace element patterns.

The chemistry of the quartz in the biotite granite dykes crosscutting the pegmatites is characterised by lower average Al (18.3 ppm) and Ge (1.0 ppm) and slightly higher Ti (7.4 ppm) compared to that of the PGr, GP, NaP and KP. However, the concentration differences between the older pegmatite group and the biotite granite dykes are minor.

Muscovite-bearing pegmatite dykes (PD) are divided into two subtypes basing on the differences of Li, Al, Ti, K and Fe content (Table 7). However, both PD subtypes have high average Ge (2.0 and 2.1 ppm) compared to the other pegmatite types. The PD at Haukemyrliene exhibit a very distinct quartz trace element signature with very high Al (122 ppm), Ti (15.5 ppm), K (18.2 ppm) and Fe (1 ppm) and low Li (3.6 ppm). Moreover the macro-scale structures of the dykes is different.

Quartz in the quartz monzonites is characterised by high average Ti (28.8 ppm), K (4.8 ppm) and Fe (0.6 ppm) and low Ge (0.8 ppm). Quartz of the pegmatites inside the Herefoss pluton (HP) has high Ti (20.4 ppm), Fe (1.0 ppm) and low Li (4.3 ppm) compared to the old pegmatite group. Similar Li, Al, K and Fe concentrations of the quartz monzonites and HPs reflect their genetic relationship. However, the lower Ti in the HPs is probably related to the lower formation temperature of the pegmatites compared to the host monzonite. The higher Ge of HP may indicate that Ge separates preferentially into the vapour phase during pluton crystallisation.

Fig. 30 and Table 8 show that most of the older pegmatites (Løvland, Hellheia, midtre and nordre, Bjortjørn, Skåremyr Sønnristjern, Lille Kleivmyr) contain quartz of medium raw material quality with relative consistent trace element concentrations independently from the pegmatite type. However, old pegmatites, which occur in the contact aureole of the Herefoss pluton and in mega enclaves within the Herefoss pluton are characterised by relative high Ti. Most of the HPs contain low quality quartz. Quartz of the Fossheia øst pegmatite is the only HP quartz which has medium quality.

Table 7. *Average concentrations of trace elements in quartz of the different pegmatite and granite types (biotite granite dykes, Herefoss quartz quartz monzonites). Two different PD populations are distinguished based on the significant differences of the average Li, Al, Ti and Fe concentration. Average concentrations of quartz from the Vaselona and Fossheia pegmatite are given separately due to their deformation resulting in the redistribution of trace elements. Pegmatite types which are marked with yellow contain quartz of medium quality whereas the not marked pegmatite types contain quartz of low quality.*

pegmatite type	locality name	number of analyses	Li	Be	B	Na	Al	Ge	Mn	Rb	Sr	Pb	Mg	P	Ti	K	Fe
PGr	Våtåskammen	4	10.2	<0.3	<1.0	<50	34.4	0.88	<0.2	<0.2	0.06	0.01	<10	<10	3.8	<1	<0.2
GP	Sønnristjern, Lille Kleivmyr, Haukemyrliene	43	8.7	<0.3	<1.4	<50	40.3	1.37	<0.2	<0.2	0.06	<0.01	<10	<10	6.1	<1	<0.2
NaP	Hellheia, midtre and nordre, Bjortjørn	33	8.3	<0.3	<1.0	<50	40.5	1.80	<0.2	<0.2	0.12	0.01	34.9	<10	4.9	<1	<0.2
ZoP	Skåremyr, Sønnristjern	43	6.9	<0.3	<1.4	<50	36.2	1.31	<0.2	<0.2	0.06	<0.01	<17.1	<10	7.2	<1	<0.2
KP	Løvland	8	5.9	<0.3	<1.6	<50	43.7	1.70	<0.2	<0.2	0.04	0.01	11.3	<10	4.3	<1	<0.2
sheared ZoP	Vaselona	2	4.9	<0.3	<1.0	<50	40.7	2.77	<0.2	<0.2	0.05	<0.01	<10	<10	16.3	6.0	0.51
sheared ZoP	Fossheia, vest	2	0.3	<0.3	<1.0	<50	26.2	2.42	0.34	<0.2	0.30	0.17	58.3	<10	29.0	4.0	0.92
biotite granite dykes	Skåremyr, Sønnristjern	4	5.1	<0.3	<1.0	<50	18.3	1.01	<0.2	<0.2	0.06	0.01	15.9	<10	7.4	<1	<0.2
PD	Hellheia, midtre, Skåremyr	5	6.2	<0.3	<1.0	<50	37.8	1.97	<0.2	<0.2	0.06	0.01	<10	<10	8.5	<1	<0.2
PD	Haukemyrliene	4	3.6	0.41	<1.0	<50	122.2	2.07	0.45	0.78	0.07	0.02	<10	<10	15.5	18.2	1.01
Herefoss granites	Fossheia, vest, Husefjell, Metveit, Heimdal	10	4.7	<0.3	<1.0	<50	41.8	0.81	<0.2	<0.2	0.16	0.03	12.2	<10	28.8	4.8	0.62
HP	Fossheia, øst Metveit, Heimdal	12	4.3	<0.3	<1.0	<50	45.4	1.19	<0.2	<0.2	0.62	<0.19	<17.7	<10	20.4	<6.8	1.01

Table 8. *Average concentrations of trace elements in quartz of the different deposits.*
The granite outcrop 13 at Husefjell is not regarded as deposit. Only analyses of quartz types are included in the calculation which occupy more than 5 vol.% of the deposit. Pegmatites which are marked with yellow contain quartz of medium quality whereas the not marked pegmatites contain quartz of low quality.

locality nr.	locality	pegmatite type	number of analyses	Li	Be	B	Na	Al	Ge	Mn	Rb	Sr	Pb	Mg	P	Ti	K	Fe
1	**Løvland**	KP	8	5.9	<0.3	1.55	<50	43.7	1.70	<0.2	<0.2	0.04	0.01	11.3	<10	4.3	<1	<0.2
2	**Hellheia, midtre**	NaP	23	7.3	<0.3	1.54	<50	42.4	1.51	<0.2	<0.2	0.07	<0.01	31.3	<10	4.5	<1	0.41
3	**Hellheia, nordre**	NaP	4	9.0	<0.3	<1.0	<50	38.5	2.52	<0.2	<0.2	0.05	0.01	53.5	<10	3.8	<1	<0.2
4	**Bjortjørn**	NaP	6	9.2	<0.3	<1.0	<50	39.7	1.49	<0.2	<0.2	0.25	0.01	32.4	<10	6.5	5.7	<0.2
5	**Haukemyrliene**	GP	4	7.5	<0.3	1.21	<50	29.6	0.79	<0.2	<0.2	0.07	<0.01	<10	<10	9.1	<1	<0.2
6	**Skåremyr**	ZoP	25	6.2	<0.3	<1.0	<50	36.9	1.22	<0.2	<0.2	0.13	<0.01	18.5	<10	8.2	1.8	1.02
7	**Sønnristjern**	GP, ZoP	36	7.5	<0.3	1.57	<50	35.5	1.22	<0.2	<0.2	0.17	<0.01	<10	<10	5.9	<1	<0.2
8	**Lille Kleivmyr**	GP, GP	30	9.3	<0.3	<1.0	<50	42.8	1.35	<0.2	<0.2	0.05	0.01	16.9	<10	4.9	<1	<0.2
9	**Våtåskammen**	PGr	4	10.3	<0.3	<1.0	<50	34.4	0.88	<0.2	<0.2	0.06	<0.01	<10	<10	3.9	<1	<0.2
10	**Vaselona**	sheared ZoP	2	4.9	<0.3	<1.0	<50	40.7	2.77	<0.2	<0.2	0.05	<0.01	<10	<10	16.3	6.0	0.51
11	**Fossheia, vest**	sheared ZoP	2	0.3	<0.3	<1.0	<50	26.2	2.42	0.34	<0.2	0.30	0.17	58.3	<10	29.0	4.0	0.92
12	**Fossheia, øst**	HP	6	5.3	<0.3	1.28	<50	40.7	1.53	<0.2	<0.2	0.06	0.01	17.4	<10	16.7	<1	0.29
14	**Metveit**	HP	2	3.8	<0.3	<1.0	<50	100.3	1.06	0.33	<0.2	0.04	0.02	14.4	<10	20.0	19.3	0.42
15	**Heimdal**	HP	4	3.1	<0.3	<1.0	<50	24.8	0.75	0.51	0.50	1.77	0.40	19.8	<10	26.3	8.9	2.39

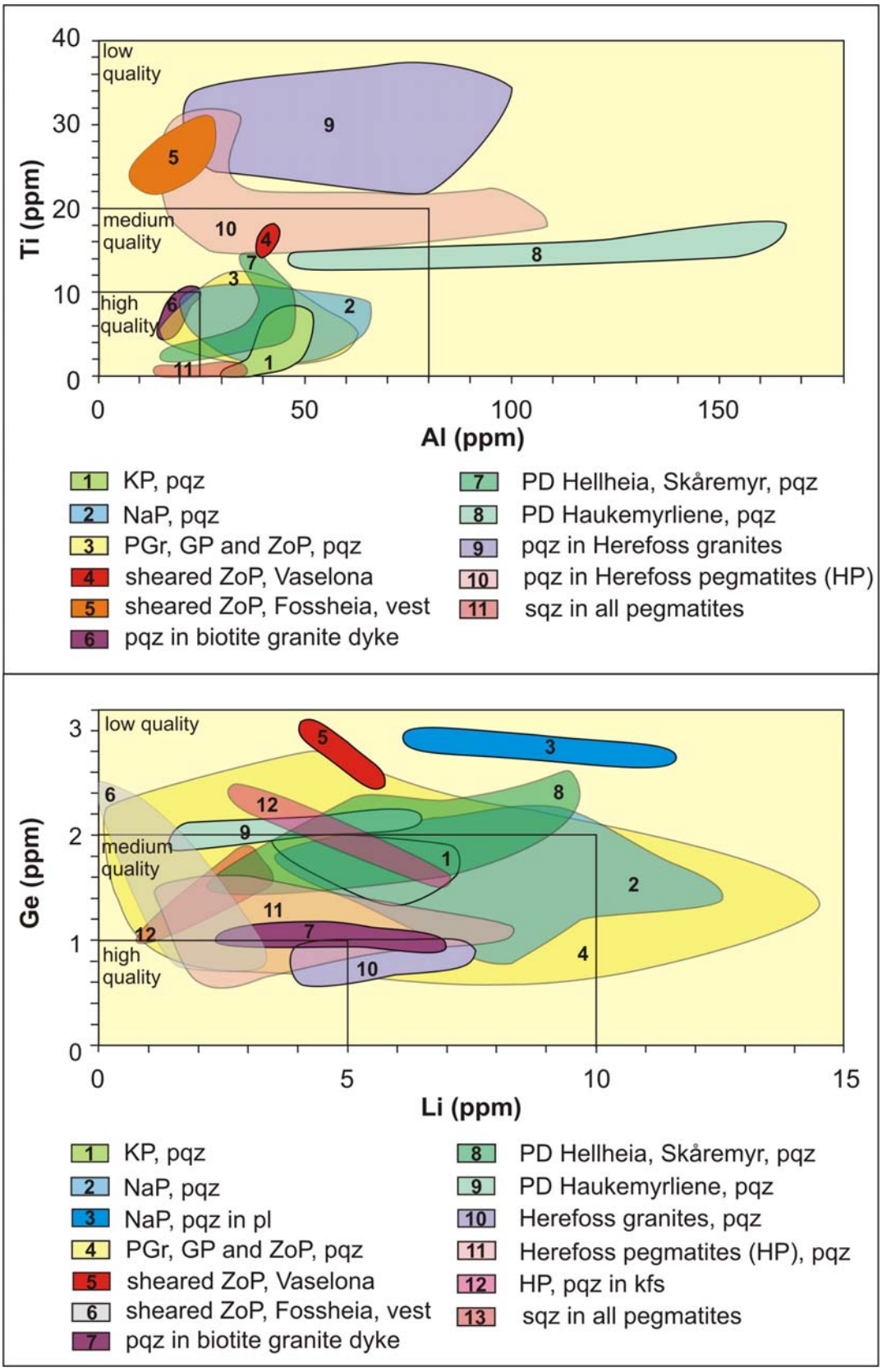

Fig. 30. *Diagrams of the variation of trace elements in quartz for the different pegmatite types.*

7.2 Variation of quartz chemistry in pegmatites

Sampling traverses were taken across the Løvland, Hellheia midtre, Skåremyr, Sønnristjern and Lille Kleivmyr pegmatite. Figs. 31 to 36 illustrate the distribution of the average (n = 2) Al, Ti, Li and Ge of pegmatite quartz in form of concentration columns. The concentration columns are placed at the sampling points on the outline maps of the pegmatite quarries.

Generally, the trace element concentrations of quartz are similar across pegmatites. The concentration variations between different sampling points are within the range of the standard deviation of the average values. The similarity of trace element concentrations in pegmatite quartz is best illustrated in Fig. 35. The concentration column diagram shows the Al, Ti, L,Ge concentration of quartz samples along a ca. 210 m long sampling profile crossing the Sønnristjern quarry (ZoP) and the granite pegmatite (GP). However, there are some exceptions. For example, analysis 2209405 of Løvland pegmatite quartz exhibits much lower Al, Ti and Li than the other samples (Fig. 31). This sample contains more than 10 vol.% of secondary quartz, which causes the lowering of the average trace element concentration of the quartz (see chapter 7.4). Samples 1809409 and 1809408 in the centre of the Hellheia, midtre pegmatite have slightly higher Al than samples at the pegmatite margin. However, the number of samples taken are to less to prove the general higher Al content in quartz of the pegmatite core.

Summarising, significant or systematic variations of the quartz trace element content across pegmatites could not be proofed. The results testify a rather homogeneous distribution of the tested trace elements Al, Ti, Li, Ge, Fe in quartz across different pegmatite zones.

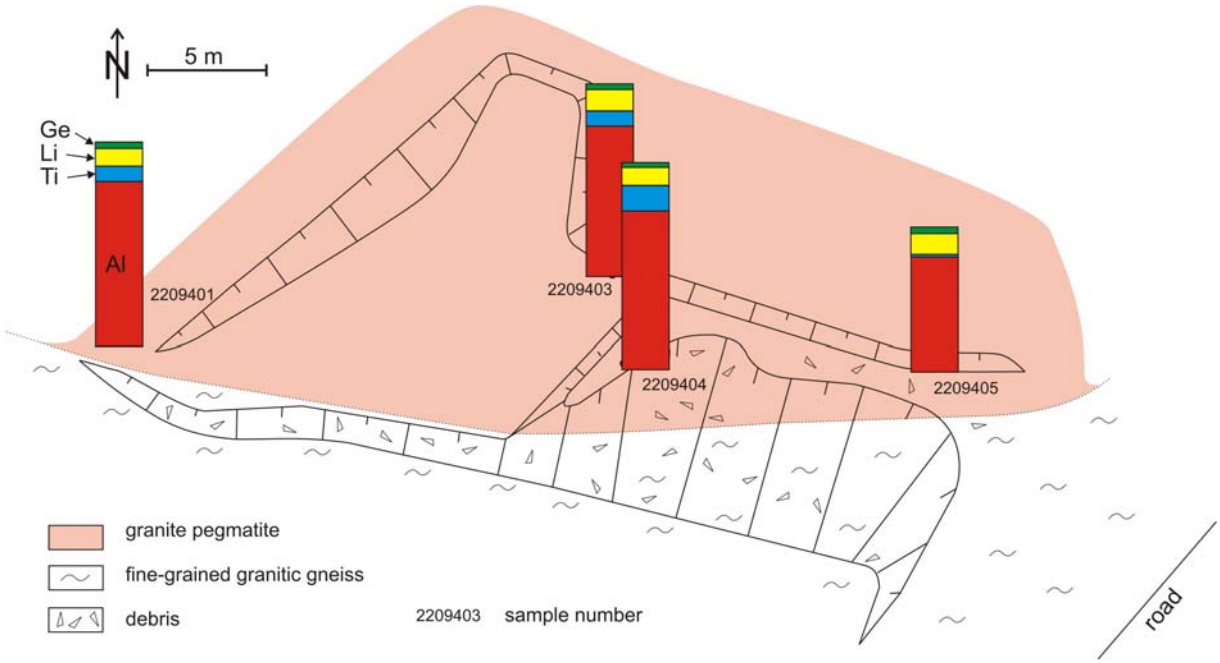

Fig. 31. *Outline of the Løvland quarry with concentration columns of trace elements in pegmatite quartz including Al (red), Ti (blue), Li (yellow) and Ge (green). The relative concentrations of one column are the average of 2 analyses. The columns are placed at the sampling point.*

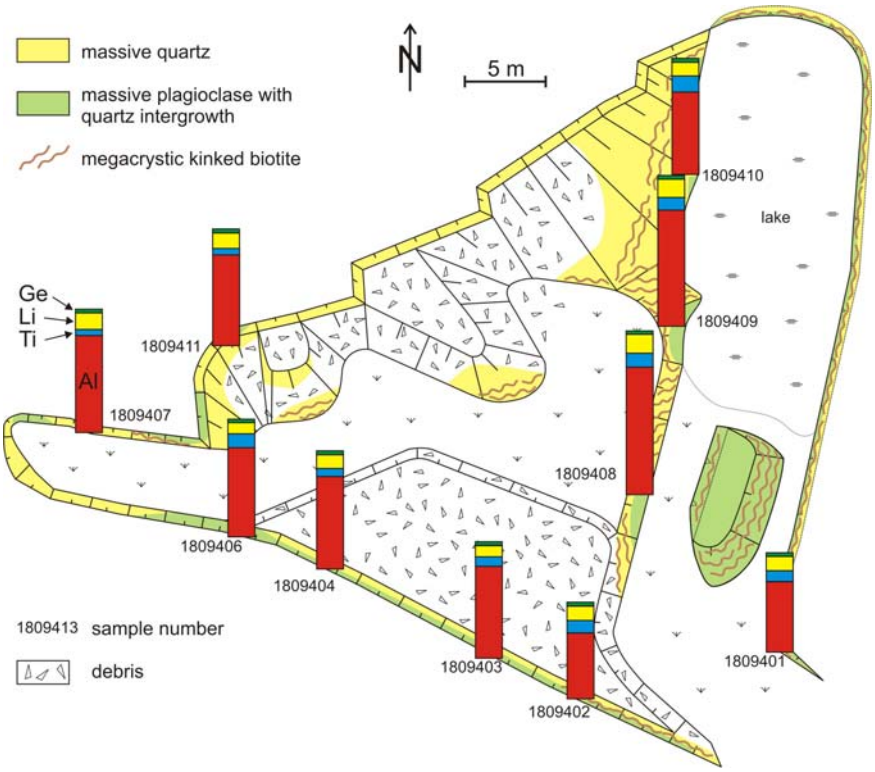

Fig. 32. *Outline of the Hellhia, midtre pegmatite with concentration columns of trace elements in pegmatite quartz including Al (red), Ti (blue), Li (yellow) and Ge (green). The relative concentrations of one column are the average of 2 analyses. The columns are placed at the sampling point.*

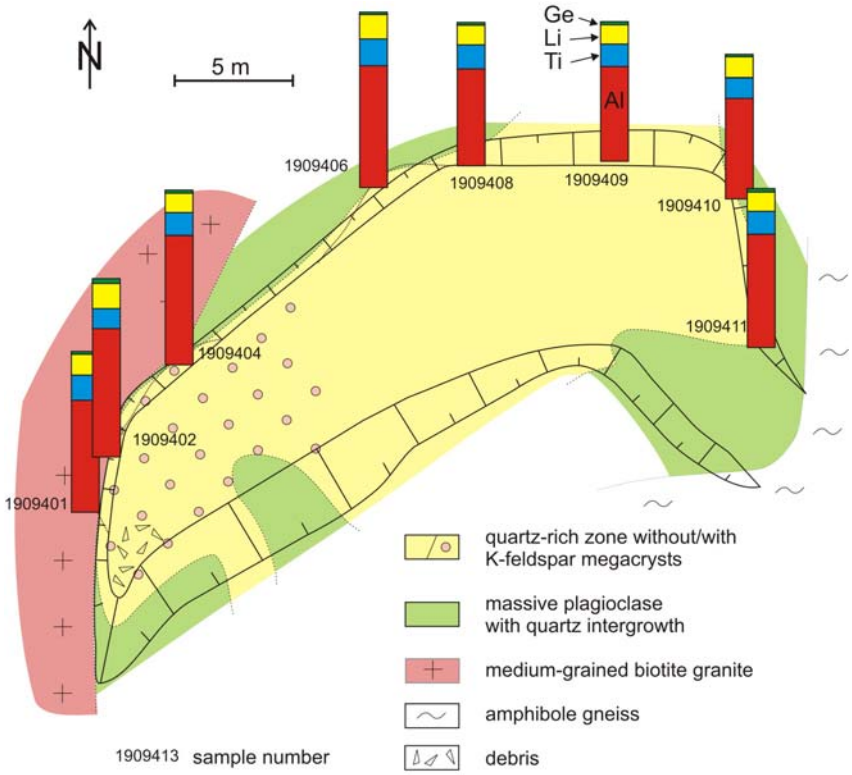

Fig. 33. *Outline of the Skåremyr pegmatite with concentration columns of trace elements in pegmatite quartz including Al (red), Ti (blue), Li (yellow) and Ge (green). The relative concentrations of one column are the average of 2 analyses. The columns are placed at the sampling point.*

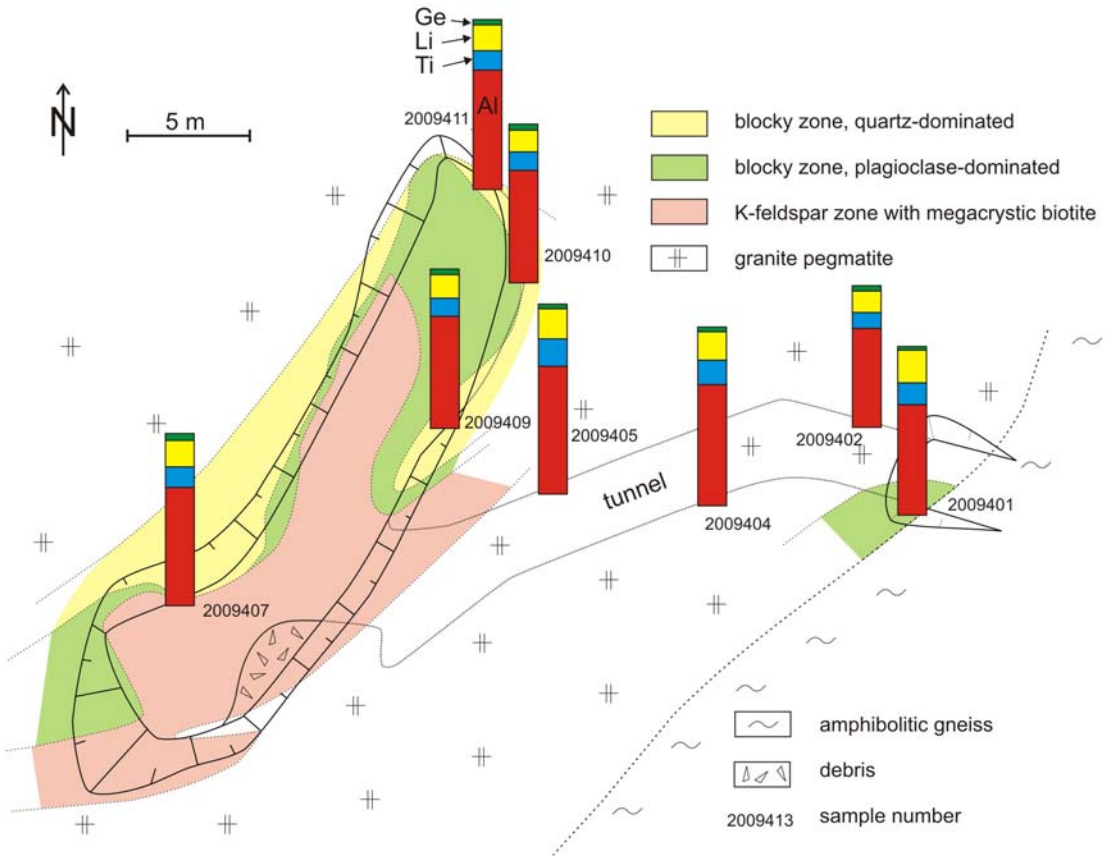

Fig. 34. *Outline of the Sønnristjern pegmatite with concentration columns of trace elements in pegmatite quartz including Al (red), Ti (blue), Li (yellow) and Ge (green). The relative concentrations of one column are the average of 2 analyses. The columns are placed at the sampling point.*

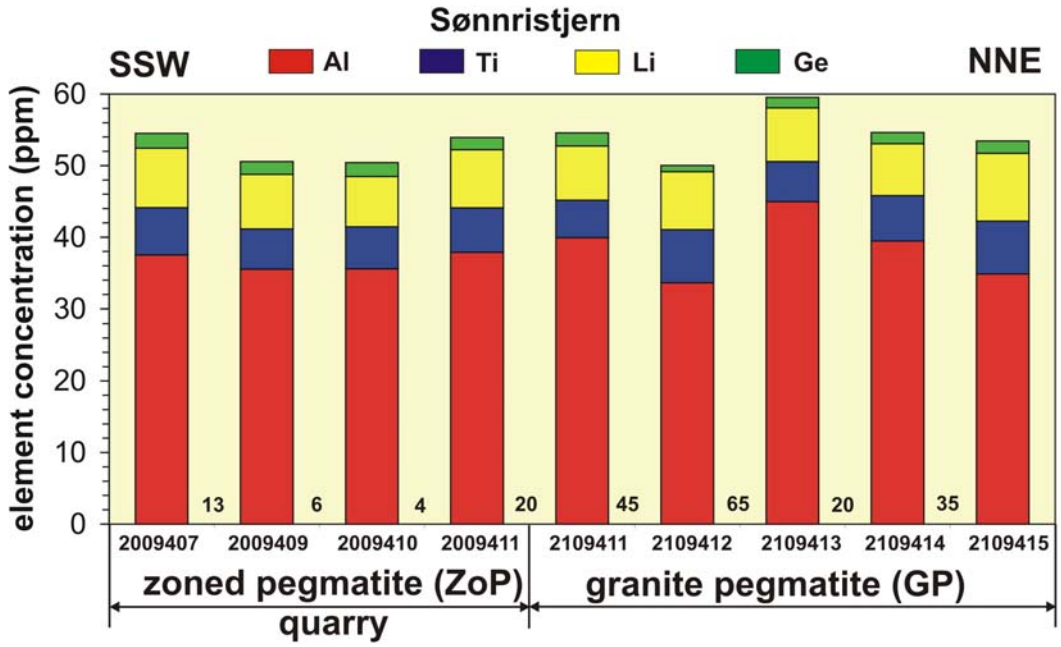

Fig. 35. *Stacked column diagram of Al, Ti, Li and Ge concentration of pegmatite quartz along a ca. 210 m long, SSW-NNE striking profile across the Sønnristjern pegmatite. Concentrations given for each locality are the average of two measurements. The numbers between the columns corresponds the distance between two sample points in meter.*

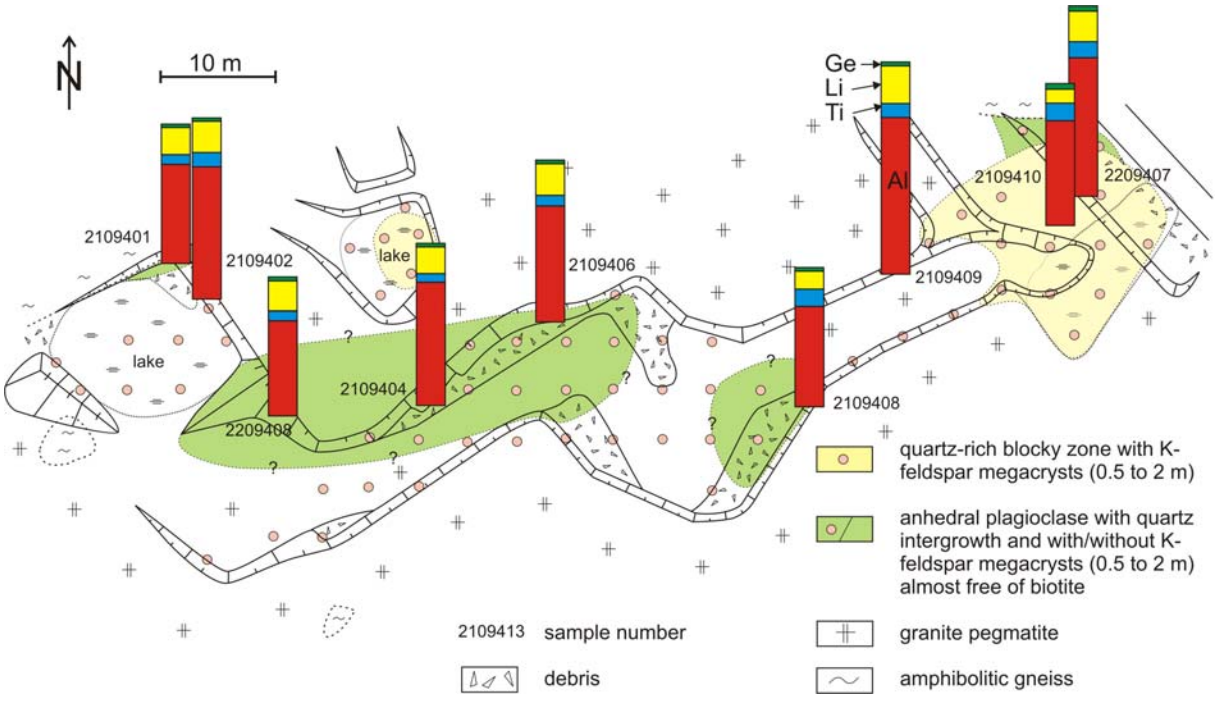

Fig. 36. *Outline of the Lille Kleivmyr pegmatite with concentration columns of trace elements in pegmatite quartz including Al (red), Ti (blue), Li (yellow) and Ge (green). The relative concentrations of one column are the average of 2 analyses. The columns are placed at the sampling point.*

7.3 Variation of quartz chemistry between quartz of different macro-structure, colour and transparency

Trace element concentration in quartz of different macro-structure (centimetre- to meter-scale), colour and transparency are shown in Table 9 and Apendix C and D. Macro-structure types include massive pegmatite quartz, quartz that is intergrown (commonly graphically) with plagioclase and K-feldspar, quartz segregations and mobilisations (centimetre-scale veins) in pegmatites and rock-forming interstitial quartz and quartz phenocrysts in the biotite granite dykes and Herefoss quartz monzonites and granites.

Generally, concentration variations among structurally different quartz types of the older pegmatite group are insignificant. However, quartz of NaP intergrown with plagioclase tends to have slightly lower Ti than massive quartz. Quartz intergrown with K-feldspar has slightly lower Li and Al (Lille Kleivmyr, Fossheia, øst) compared to massive pegmatite quartz. Mobilised quartz veins in GP from Haukemyrliene have somewhat lower Al and Li compared to surrounding pegmatitic quartz. Differences are rather distinct between the comb quartz and massive quartz within the muscovite PD at Haukemyrliene. The comb quartz has much higher Al, K and Fe and lower Li than the neighbouring massive (groundmass) quartz.

Trace element concentrations in smoky quartz and white quartz show no distinct differences (e.g., Hellheia, midtre and nordre; Table 9). This is agreement with the findings by Nassau and Prescott (1975; 1977) who suggested that the smoky colour is caused by post-crystallisation radiation damage of pre-existing substitutional Al defects. The smoky colour does not reflect necessarily differences of the Al content in quartz. It is a function of the radiation intensity and exposure time. Therefore, the most smoky quartz occurs next to K-feldspar crystals where the radiation damage is caused by β-radiation of the decaying isotope

K^{40}. The smoky colour is not stable above 180ºC which provide evidence that the smoky colouration occurred after quartz crystallisation (Blankenburg et al. 1994).

A visual distinction between milky and clear quartz was possible among samples from the Skåremyr pegmatite. However, significant differences in the trace element content of clear and milky quartz could not be determined. The result seems to be plausible, because the milky appearance of quartz is mainly caused by fluid inclusions which do not represent structural impurities and, thus, their were avoided during LA-ICP-MS analyses.

7.4 Variation of quartz chemistry between primary and secondary quartz

Due to the small size of textures formed by secondary quartz (usually <100 µm) only a few LA-ICP-MS analysis spots could be placed accurately in secondary quartz. However, an analytical distinction between sqz1 to 3 could not made caused by the large sampling volume of the laser (180 x 250 x 80 µm). Moreover, the high number of fluid inclusions within secondary quartz caused the adulteration of many of the analyses by elements originating from the fluid inclusions (e.g., Na, K, B). The contaminated analyses are not considered here. Secondary quartz (sqz1-4) revealed by SEM-CL studies is strongly depleted in Li, Al and Ti (Table 9; Fig. 30; Appendix C, D). The depletion of trace elements in secondary quartz found in granitic quartz has been described previously by Müller et al. (2002a; 2002b; 2003).

EPMA has been applied for more detailed analysis of the Al, Ti, K and Fe distribution across structures of secondary quartz, because EPMA provide *in situ* trace element data with a very good spatial resolution down to 5 µm. Fig. 37 shows 3 concentration profiles of Al across structures of secondary quartz in pegmatitic quartz from Bjortjørn, Sønnristjern and Lille Kleivmyr. Al is systemically depleted in secondary quartz. The depletion is stronger in sqz1 (Bjortjørn and Sønnristjern) than in sqz3 (Lille Kleivmyr). The CL intensity of secondary quartz in the Bjortjørn sample increased during electron exposure and, therefore, the contours are redrawn with white dashed lines. Concentration diagrams of Al vs. Al/Ti illustrating the depletion of Al and Ti in sqz1 and sqz3 are shown in Fig. 38.

The systematic reduction of Al, Ti and K within secondary quartz compared to the primary host quartz has been described previously (Müller et al. 2002b; 2003; Van den Kerkhof et al. 2004) and the process of quartz purification during retrograde, fluid-driven overprint seems to be a common phenomena in igneous and pegmatitic rocks.

Summarising, the presence of secondary quartz (sqz1-sqz3) in primary quartz lead to the slightly decrease of the average concentration of trace elements in bulk quartz analyses. However, the volume portion of secondary quartz in primary quartz is commonly less than 3 vol.%. Therefore, the influence of the chemistry of secondary quartz on the bulk quartz quality is minor in the case of the Froland pegmatite quartz. In samples, in which the volume of secondary quartz exceeds 10 vol.%, the average trace element concentration is significantly lower compared to the other quartz samples of the same deposit (e.g., sample 2209405, Løvland). However, it has to be considered that secondary quartz, is the main carrier of secondary fluid inclusions.

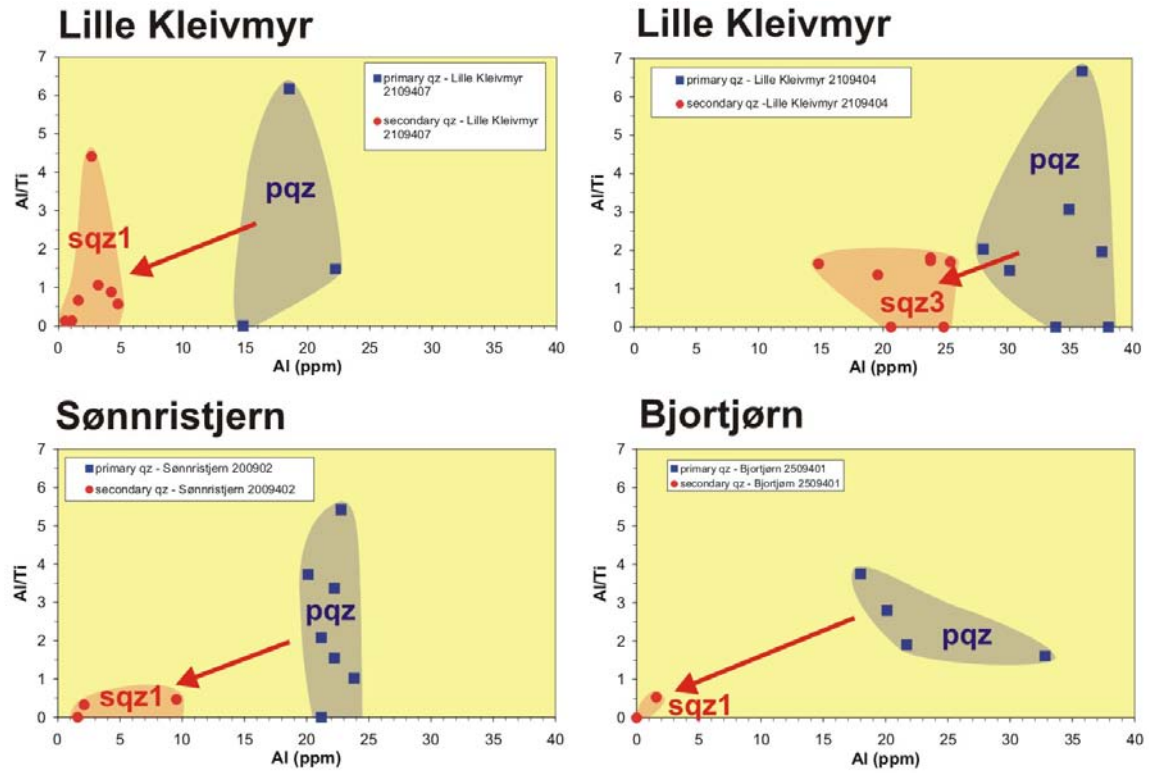

Fig. 37. *Concentration profiles of Al across structures of secondary quartz in pegmatite quartz from Bjortjørn, Sønnristjern and Lille Kleivmyr analysed by EPMA.*

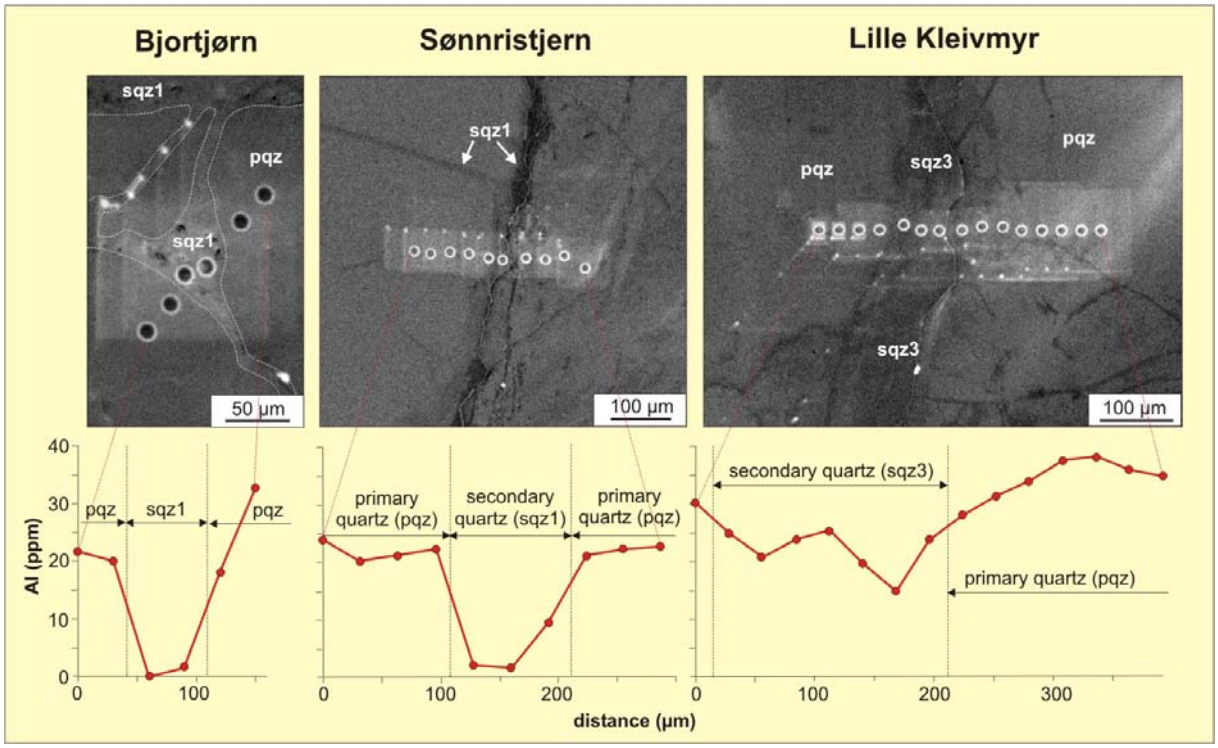

Fig. 38. *Variation diagrams of Al and Ti concentration in primary and secondary quartz. Concentrations were determined with EPMA.*

Table 9. *Average concentrations of trace elements in quartz with different macro structure (massive, intergrown with K-feldspar and plagioclase), micro structure distinguished by cathodoluminescence (primary and secondary quartz), colour (smoky, white) and transparency (clear, milky). Quartz samples which are not named "smoky" are white. Quartz types which are marked with orange have high quality, with yellow medium quality and white is low quality.*

locality nr.	locality name	pegmatite type	quartz type	number of analyses	Li	Be	B	Na	Al	Ge	Mn	Rb	Sr	Pb	Mg	P	Ti	K	Fe
1	Løvland	KP	smoky pqz	8	5.9	<0.3	1.55	<50	43.7	1.70	<0.2	<0.2	0.04	0.01	11.3	<10	4.3	<1	<0.2
		KP	sqz	1	3.2	<0.3	2.43	<50	28.0	1.71	<0.2	<0.2	0.22	0.01	29.4	<10	0.5	<1	<0.2
2	Hellheia, midtre	NaP	milky smoky pqz	4	7.0	<0.3	1.26	<50	33.1	1.91	<0.2	<0.2	0.06	<0.01	<10	<10	5.8	<1	0.26
		NaP	milky pqz	17	7.4	<0.3	2.21	<50	48.8	1.78	<0.2	<0.2	0.08	<0.01	46.8	<10	5.3	<1	0.72
		NaP	pqz in pl	2	7.7	<0.3	1.15	<50	45.1	0.86	<0.2	<0.2	0.08	<0.01	15.7	<10	2.5	<1	0.25
		PD	smoky pqz	3	7.7	<0.3	<1.0	<50	35.5	2.32	<0.2	<0.2	0.05	0.01	<10	<10	4.3	<1	0.23
3	Hellheia, nordre	NaP	milky pqz	2	9.1	<0.3	<1.0	<50	38.7	2.22	<0.2	<0.2	0.04	0.01	97.0	<10	5.0	<1	<0.2
		NaP	pqz in pl	2	8.8	<0.3	<1.0	<50	38.2	2.83	<0.2	<0.2	0.06	0.01	<10	<10	2.7	<1	<0.2
4	Bjortjørn	NaP	milky pqz	4	7.3	<0.3	<1.0	<50	46.6	1.61	<0.2	<0.2	0.44	0.01	54.8	<10	7.2	10.4	<0.2
		NaP	pqz in pl	2	11.2	<0.3	<1.0	<50	32.8	1.37	<0.2	<0.2	0.05	0.01	<10	<10	5.7	<1	<0.2
5	Haukemyrliene	GP	smoky pqz	2	8.8	<0.3	1.41	<50	34.9	0.70	<0.2	<0.2	0.06	<0.01	<10	<10	9.6	<1	<0.2
		GP	mobilised qz vein	2	6.2	<0.3	<1.0	<50	24.2	0.89	<0.2	<0.2	0.07	<0.01	<10	<10	8.6	<1	0.21
		PD	smoky comb pqz	2	1.7	0.46	<1.0	<50	158.6	2.01	0.53	1.36	0.06	<0.01	<10	<10	16.4	32.5	1.78
		PD	smoky pqz in kfs	2	5.5	0.35	<1.0	<50	85.9	2.14	0.36	<0.2	0.07	0.02	<10	<10	14.6	3.9	0.23
6	Skåremyr	ZoP	milky smoky pqz	13	6.5	<0.3	<1.0	<50	35.2	1.09	<0.2	<0.2	0.07	<0.01	18.9	<10	8.1	<1	0.34
		ZoP	clear smoky pqz	8	7.1	<0.3	<1.0	<50	40.7	0.87	<0.2	<0.2	0.27	<0.01	26.8	<10	8.2	3.1	0.43
		ZoP	pqz in pl	4	5.0	<0.3	<1.0	<50	34.8	1.70	<0.2	<0.2	0.05	<0.01	<10	<10	8.2	1.3	2.30
		ZoP	sqz	1	1.0	<0.3	1.61	<50	15.3	1.04	1.33	<0.2	0.60	0.34	54.4	<10	0.8	6.8	7.48
			pqz in biotite granite dyke	2	5.6	<0.3	<1.0	<50	20.0	1.02	0.35	<0.2	0.06	<0.01	<10	<10	9.2	<1	<0.2
		PD	milky smoky pqz	2	4.7	<0.3	<1.0	<50	40.1	1.62	0.30	<0.2	0.08	<0.01	<10	<10	12.7	<1	<0.2
7	Sønnristjern	GP	milky smoky pqz	18	8.6	<0.3	1.95	<50	38.1	1.41	<0.2	<0.2	0.05	<0.01	<10	<10	6.7	<1	<0.2
		ZoP	milky smoky pqz	14	7.7	<0.3	2.09	<50	35.5	1.80	<0.2	<0.2	0.54	<0.01	20.3	<10	6.1	<1	<0.2
		ZoP	smoky pqz in kfs	2	4.5	<0.3	<1.0	<50	34.3	0.89	<0.2	<0.2	0.05	<0.01	<10	<10	5.5	<1	<0.2
		ZoP	smoky pqz in pl	2	9.4	<0.3	1.26	<50	34.0	0.80	<0.2	<0.2	0.06	<0.01	<10	<10	5.1	<1	<0.2
			pqz in biotite granite dyke	2	4.6	<0.3	<1.0	<50	16.6	1.01	<0.2	<0.2	0.05	0.01	21.8	<10	5.6	<1	<0.2

Notes: pqz – primary quartz; sqz – secondary quartz; pl – placioclase; kfs – K-feldspar.

Table 9. *Continued.*

locality nr.	locality name	pegmatite type	quartz type	number of analyses	Li	Be	B	Na	Al	Ge	Mn	Rb	Sr	Pb	Mg	P	Ti	K	Fe
8	**Lille Kleivmyr**	GP	milky smoky pqz	14	10.4	<0.3	<1.0	<50	47.6	1.45	<0.2	<0.2	0.06	0.01	<10	<10	4.8	<1	<0.2
		GP	pqz in kfs	2	3.4	<0.3	<1.0	<50	34.9	1.18	<0.2	<0.2	0.05	0.02	41.5	<10	5.7	<1	<0.2
		GP	pqz in pl	6	10.8	<0.3	<1.0	<50	43.5	1.26	<0.2	<0.2	0.05	0.01	<10	<10	5.2	<1	<0.2
			pqz in garnet granite	8	9.9	<0.3	<1.0	<50	39.7	1.50	<0.2	<0.2	0.05	0.01	<10	<10	3.8	<1	0.27
9	**Våtåskammen**	PGr	smoky pqz	4	10.3	<0.3	<1.0	<50	34.4	0.88	<0.2	<0.2	0.06	<0.01	<10	<10	3.9	<1	<0.2
10	**Vaselona**	sheared ZoP	smoky pqz	2	4.9	<0.3	<1.0	<50	40.7	2.77	<0.2	<0.2	0.05	<0.01	<10	<10	16.3	6.0	0.51
11	**Fossheia, vest**	sheared ZoP	smoky pqz	2	0.3	<0.3	<1.0	<50	26.2	2.42	0.34	<0.2	0.30	0.17	58.3	<10	29.0	4.0	0.92
			pqz in adamelite	2	2.5	<0.3	<1.0	<50	12.2	0.84	<0.2	<0.2	0.06	<0.01	13.4	<10	23.2	<1	0.26
12	**Fossheia, øst**	HP	clear smoky pqz	2	3.2	<0.3	<1.0	<50	48.2	1.46	<0.2	<0.2	0.06	0.01	32.1	<10	16.2	1.5	0.37
		HP	smoky pqz	2	7.9	<0.3	1.17	<50	41.2	1.09	<0.2	<0.2	0.05	<0.01	<10	<10	15.6	<1	0.27
		HP	pqz in kfs	2	4.8	<0.3	1.68	<50	32.9	2.03	<0.2	<0.2	0.07	0.01	<10	<10	18.3	<1	0.23
13	**Husefjell**		pqz in Herefoss granite	2	7.3	<0.3	2.15	<50	84.4	0.89	0.39	0.26	0.15	0.04	<10	<10	35.2	9.7	1.15
14	**Metveit**	HP	smoky pqz	2	3.8	<0.3	<1.0	<50	100.3	1.06	0.33	<0.2	0.04	0.02	14.4	<10	20.0	19.3	0.42
			pqz in Herefoss granite	4	4.3	<0.3	<1.0	<50	47.3	0.81	<0.2	<0.2	0.39	0.02	15.2	<10	25.2	7.4	0.86
15	**Heimdal**	HP	milky smoky pqz	4	3.1	<0.3	<1.0	<50	24.8	0.75	0.51	0.50	1.77	0.40	19.8	<10	26.3	8.9	2.39
			pqz in Herefoss granite	2	4.6	<0.3	<1.0	<50	23.4	0.71	<0.2	<0.2	0.04	0.01	<10	<10	31.7	<1	<0.2

Notes: pqz – primary quartz; sqz – secondary quartz; pl – placioclase; kfs – K-feldspar.

8. Feldspar chemistry

Major and trace elements of 38 K-feldspar and 41 plagioclase samples were analysed by XRF. Additional major and trace element data of feldspars from the Froland pegmatites are published by Ihlen et al. (2002, 2003). Concentrations of K-feldspar are listed in Appendix E and of plagioclase in Appendix F. The elements Rb, Sr, and Ba in K-feldspar and plagioclase are sensitive to igneous differentiation and, thus, to the differentiation of the pegmatite-forming magma/fluid (Mehnert and Büsch 1981; Long and Luth 1986; Cox et al. 1996). Generally, Ba and Sr decrease and Rb increases in feldspar during magmatic differentiation. However, granite magmas crystallise under equlibrium conditions whereas pegmatite magmas/fluids crystallise under super-cooled conditions far fro the equilibrium or granite liquidus. Therefore, the crystal and, thus, the element fractionation can be very different, i.e. of Rb, Sr and Ba. Concentration diagrams of K_2O, Ba, Rb and Sr concentrations in K-feldspar and of the CaO, Ba, Rb and Sr concentrations in plagioclase are plotted in Fig. 39.

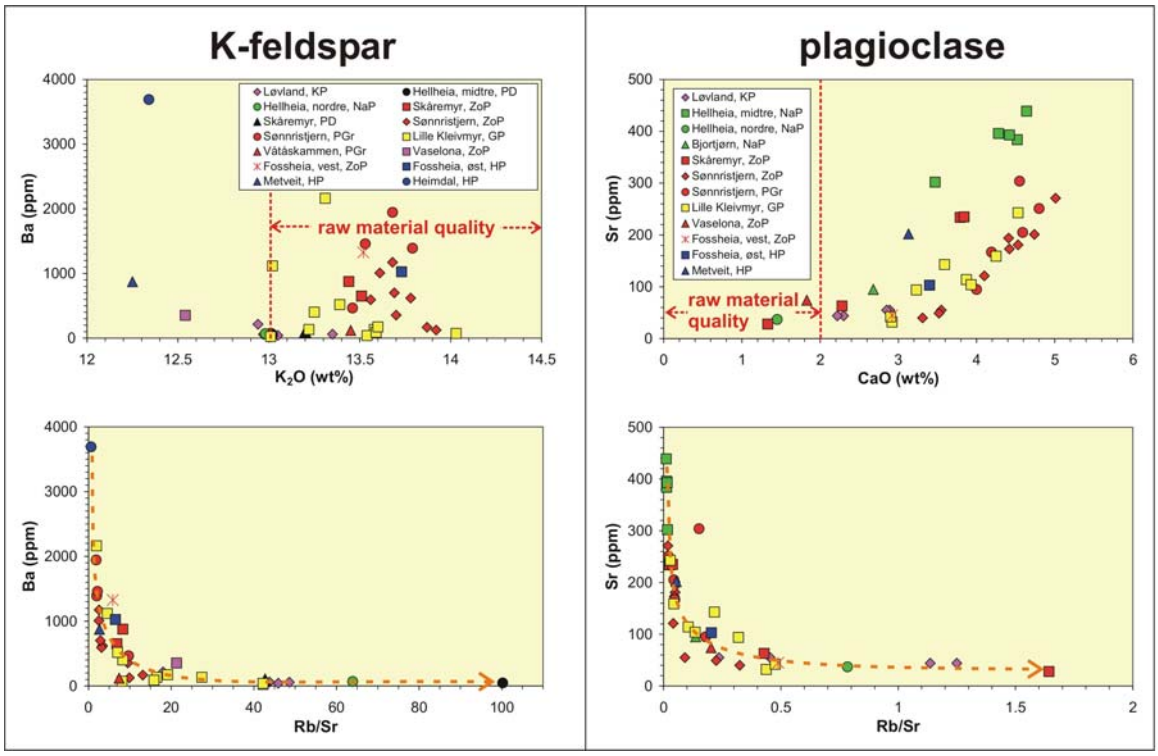

Fig. 39. *Concentration variation diagrams of major and trace elements in K-feldspar and plagioclase from Froland pegmatites. Concentrations of >13 wt.% K_2O in K-feldspar and of <2 wt.% CaO in plagioclase are the quality requirements for feldspar raw material. The arrows in the Ba vs. Rb/Sr and Sr vs. Rb/Sr diagram indicate the general magmatic differentiation trend.*

8.1 K-feldspar

K_2O content in K-feldspar ranges between 12.2 and 14.0 wt.% and the Ba content show a wide variation from 24 to 3691 ppm (Fig. 39). The K_2O variation of K-feldspar seems to be related to the pegmatite type whereas Ba exhibits large fluctuation within the pegmatites (e.g., Sønnristjern, Lille Kleivmyr). An important compositional requirement for glass- and ceramic-grade K-feldspar is that the K_2O content exceeds 13 wt.%. Generally, pale coloured K-feldspar has high K_2O, brick red and deformed and altered (sericitised, albitised) K-

feldspar has low K_2O (Ihlen et al. 2002). ZoP (Skåremyr, Sønnristjern), GP (Sønnristjern, Lille Kleivmyr) and PGr (Våtåskammen) have K-feldspar with the highest average K_2O concentration (>13.4 wt.%) and, therefore, they contain K-feldspar of good quality. However, the Vaselona ZoP contains K-feldspar with 12.5 wt.%. The low K_2O content in the Vaselona K-feldspar compared to that of the other ZoPs is probably caused by the deformation (shearing and mylonitisation at micro-scale; see chapter 6.). K-feldspar from Løvland (KP) has an average of 13.1 wt.% K_2O and low Ba of 94 ppm. The rare K-feldspar at Hellheia, nordre (NaP) contains 13.0 wt.%, whereas the NaPs Bjortjørn and Hellheia, midtre do not have K-feldspar apart from the small PD dykes crosscutting the pegmatites. The PDs itself consits of K-feldspar with 13.0 wt.% (Hellheia, midtre) and 13.2 wt.% (Skåremyr) and low Ba (47 and 96 ppm). Lowest K_2O content exhibit the two small HPs at Metveit and Heimdal with 12.25 and 12.34 wt.%, respectively. In contrast, the K-feldspars of the HPs at Fossheia, vest and Fossheia, øst contain 13.5 and 13.7 wt.% K_2O, respectively.

K-feldspars from Løvland (KP), PDs (Skåremyr and Hellheia, midtre), Hellheia, nordre (NaP), Vaselona (sheared ZoP) crystallised from the most evolved magmas/fluids of the Froland area. The moderate differentiation degree is represented by K-feldspar from Skåremyr (ZoP), Sønnristjern (ZoP, GP), Våtåskammen (PGr) deposits. The widest range of differentiation covers the K-feldpars from the Lille Kleivmyr pegmatite, which is the largest investigated pegmatite. HPs exhibit a relative primitive differentiation degree reflected by high Ba and low Rb/Sr ratio.

8.2 Plagioclase

Plagioclase of most of the pegmatites contain more than 2 wt.% CaO which makes them unsuitable as ceramic and glass raw material. Only three plagioclase samples from Vaselona, Hellheia, nordre and Skåremyr have less than 2 wt.% CaO. The picture of differention is slightly different if the K-feldpar chemistry is compared with the plagioclase chemistry. The most evolved chemistry is reflected by plagioclase of the Løvland (KP), Skåremyr (ZoP) and Hellheia, nordre pegmatite (NaP). Sønnristjern (ZoP, PGr), Lille Kleivmyr (GP, PGr), Vaselona (sheared ZoP), Bortjørn (NaP), and HPs contain plagioclase with a chemistry reflecting moderate differentiation degrees of the pegmatite forming magma/fluid. The most primitive plagioclase chemistry is represented by samples from the Hellheia, midtre pegmatite (NaP). However, if there is a discrepancy between the K-feldspar and plagioclase differenciation trends, e.g. like in Skåremyr and Vaselona, than one of these minerals was affected by post-crystallisation fluid-driven alteration which may result in mobilisation of Sr, Ba and/or Rb. The high differentiation degree of the NaP Hellheia, nordre pegmatite seems to be in conflict with the plagioclase-domincence in the pegmatite and the neighbouring Hellheia, midtre pegmatite which exhibits a rather primitive stage of magma evolution.

8.3 Variation of feldspar chemistry in pegmatites

The distribution of Rb/(Sr+Ba) ratio in K-feldspar and of the Rb/Sr ratio in plagioclase within pegmatites is shown in Figs. 40 to 45. Increasing ratios reflect increasing fractionation of the magma/fluid from which the feldspr grew, if the ratio is not disturbed by secondary feldspar alteration or influx of new magma batches.

The variation of the ratios across the Løvland pegmatite are minor (Fig. 40, compare also data in Fig. 39) which is in agreement with the structural homogeneity of the pegmatite. The Rb/Sr of plagioclase from the Hellheia, midtre pegmatite is more ore less constant (Fig. 41). A different pattern is observed in the zoned pegmatite at Skåremyr. The plagioclase shows a

strong increase in fractionation from SE towards the NW end of the pegmatite. A similar scenario was observed at Haukemyrliene where plagioclase presumably crystallised later than the K-feldspar-rich part of the pegmatite (Fig. 10).

A strong zoning Rb/(Sr+Ba) ratio in K-feldspar and of the Rb/Sr ratio in plagioclase is developed across the Sønnristjern pegmatite. The granite pegmatite hosting the zoned pegmatite has feldspar with constantly very low ratios (Figs. 42, 43). The ratios strongly increase within the zoned pegmatite reflecting a much higher fractionation degree. The core and margin composition of a plagioclase megacryst (Fig. 16d) were determined in order to reveal possible differences within crystals. The core of the megacryst has a significantly more primitive composition (sample 2009411; Rb/Sr = 0.04) than the crystal margin (sample 2009412; Rb/Sr = 0.22).

A similar differentiation pattern of the feldspar chemistry is developed in the Lille Kleivmyr pegmatite (Fig. 44). Feldspar megacrysts of blocky zones are chemically more differenciated (samples 2109403, 2109404, 2109406, 2109410) than feldspar of the granite pegmatite host (samples 2109408, 2109409). The trend is better reflected by the Rb/Sr ratio of plagioclase than by the Rb/(Sr+Ba) ratio of K-feldspar.

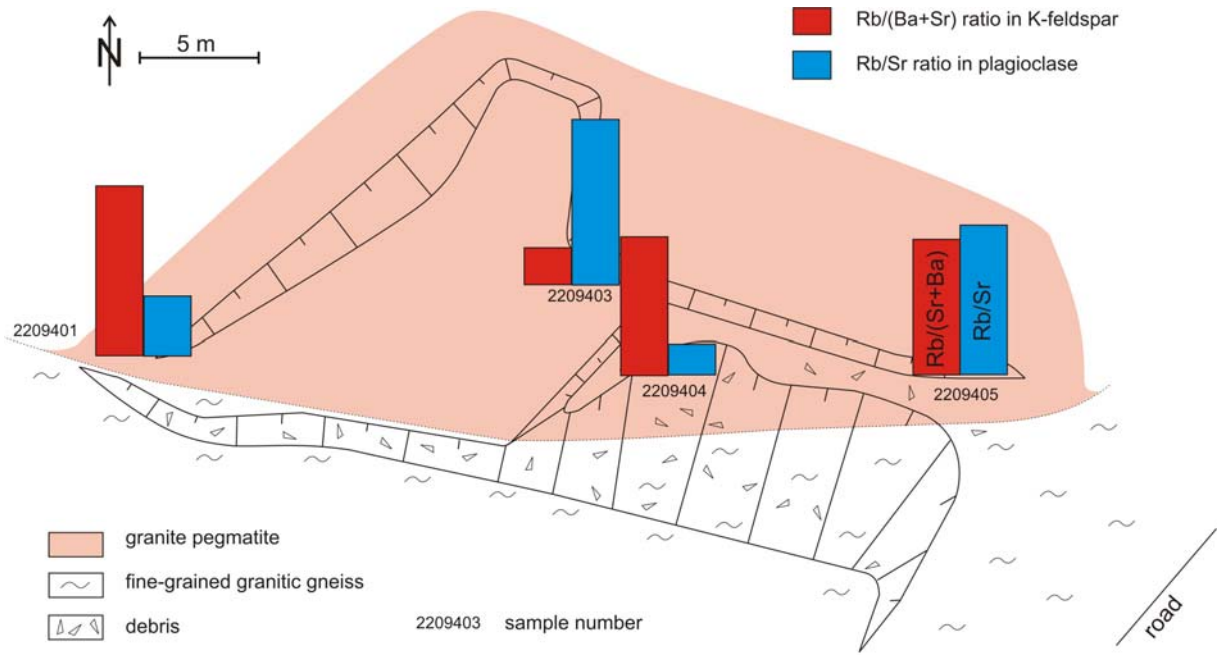

Fig. 40. *Outline of the Løvland quarry with columns of the Rb/(Ba+Sr) in K-feldspar (red) and Rb/Sr in plagioclase (blue). The columns are placed at the sampling point.*

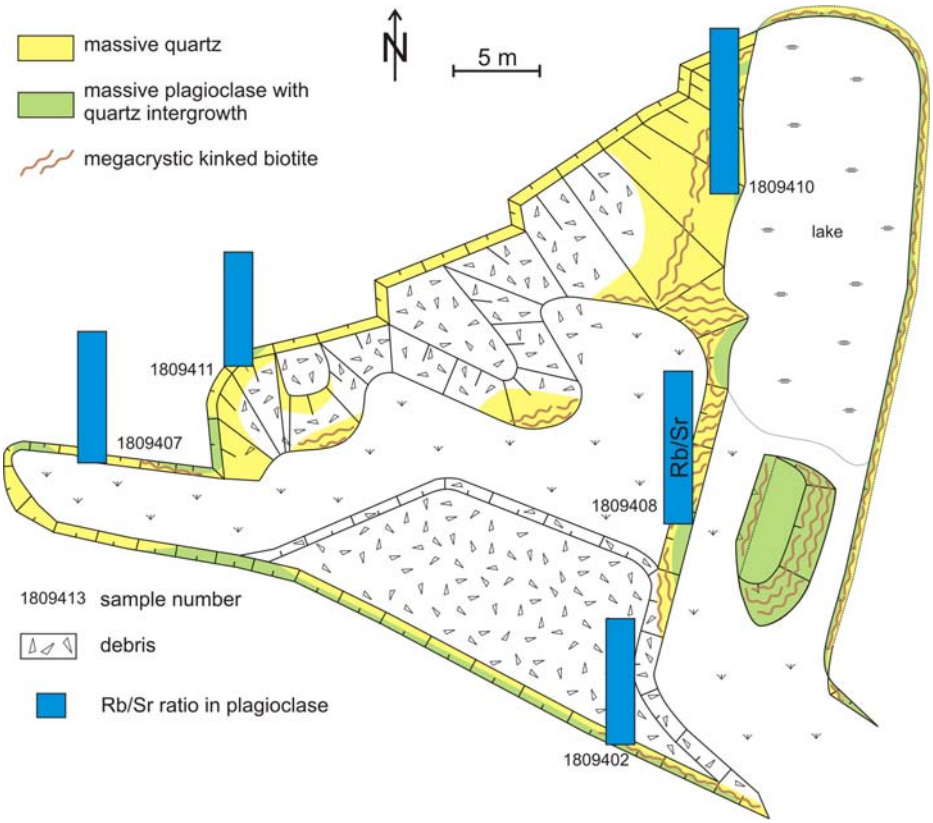

Fig. 41. *Outline of the Hellheia midtre quarry with columns of the Rb/(Ba+Sr) in K-feldspar (red) and Rb/Sr in plagioclase (blue). The columns are placed at the sampling point.*

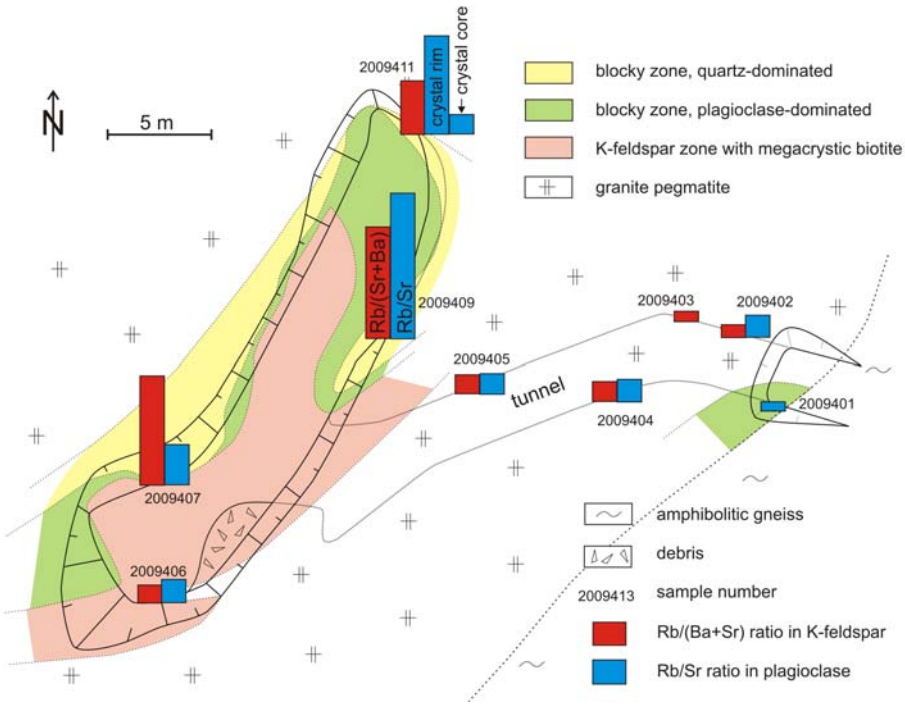

Fig. 42. *Outline of the Sønnristjern quarry with columns of the Rb/(Ba+Sr) in K-feldspar (red) and Rb/Sr in plagioclase (blue). The columns are placed at the sampling point. Compositional differences of the plagioclase megacryst core and margin are illustrated for sample 2009411.*

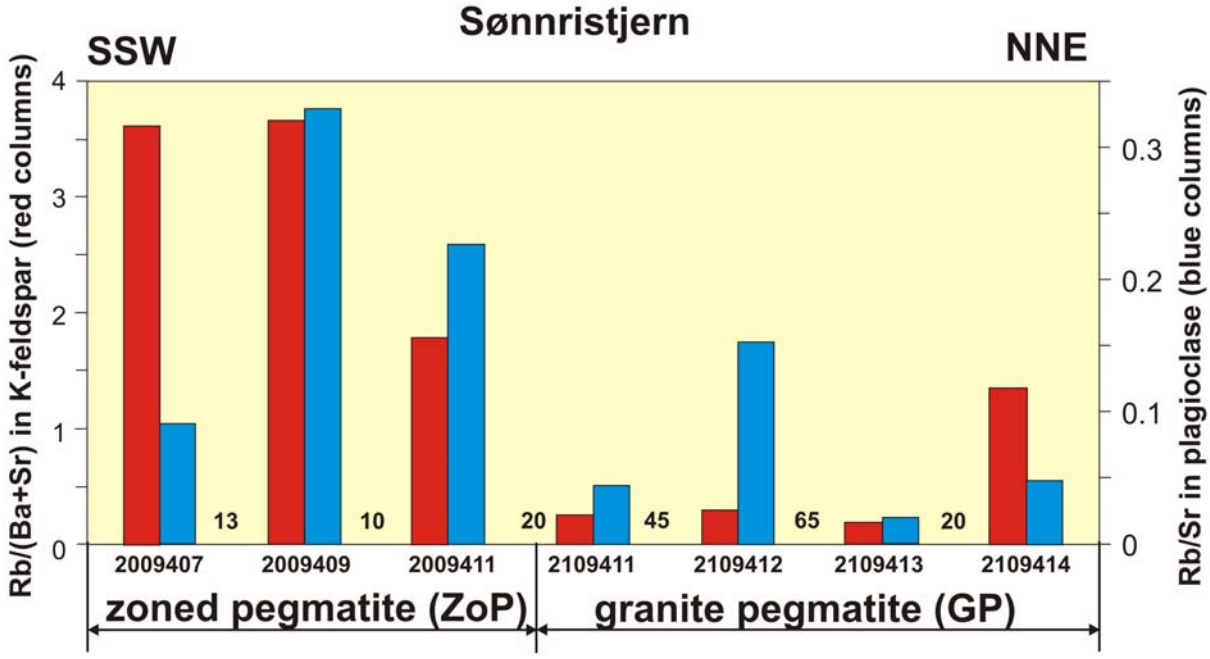

Fig. 43. *Column diagram of Rb/(Ba+Sr) ratio of K-feldspar along a ca. 170 m long, SSW-NNE striking profile across the Sønnristjern pegmatite. The numbers between the columns corresponds the distance between two sample points in meter.*

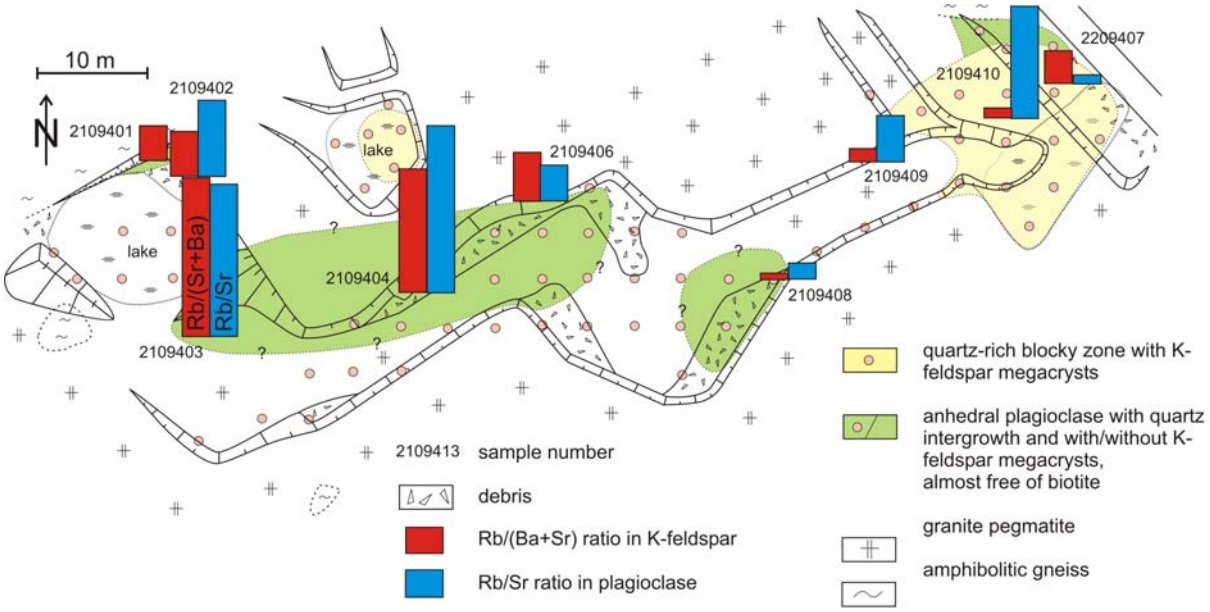

Fig. 44. *Outline of the Lille Kleivmyr quarry with columns of the Rb/(Ba+Sr) in K-feldspar (red) and Rb/Sr in plagioclase (blue). The columns are placed at the sampling point.*

9. Mica chemistry

Major and minor elements of 40 megacrystic mica samples and trace elements of 36 samples were analysed by XRF (Appendix G and H). Micas are useful as monitors of the physicochemical environment in which they grew, because they may incorporate a large number of elements depending on *PTX*-conditions during magmatic, metamorphic and

metasomatic/hydrothermal processes. Individual micas types are characteristic of different stages of pegmatite evolution (Černý and Burt, 1984). The mica chemistry is used in this study (1) to better discriminate the different pegmatite types (2) to get more information about the differentiation degree of the pegmatites (3) to verify if correlations among the chemistry of mica and quartz exist and (4) to trace metasomatic processes which may have overprinted the pegmatites.

Generally, the composition of biotites from Froland pegmatites is relative homogeneous and primitive in respect to granitic differentiation. The biotites of all pegmatites plot in the Mg-siderophyllite and Fe-phlogopite field in the discrimination diagram of Tischendorf et al. (2001; Fig. 45a). However, biotites from different pegmatite types exhibit slight variations in their composition. The most primitive composition (Fe-phlogopite) have the micas from pegmatites related to the Herefoss pluton (HP). Micas of NaP have transitional Fe-phlogopite – Mg-siderophyllite composition. Biotites of GP and ZoP reflect a slightly evolved differentiation.

Most of the biotites have low F contants (<1.4 wt.%; Appendix I). Biotites of HP and the Vaselona pegmatite (ZoP) are relative rich F. Trace element concentrations reveal that micas of each pegmatite have an individual micro-chemical signature: biotites from Skåremyr are rich in V, biotites from Lille Kleivmyr are enriched in Zn and micas of NaPs have high Ba (Appendix I). The high Ba in micas of NaP is presumably caused by the lack of K-feldspar which incorparates preferentially Ba. However, Ba in mica also depends on the pegmatite mineralogy beside K-feldspar and on the formation depth of the pegmatite. The outstanding composition of biotite (high Rb and F) and muscovite (high Ti, V and F) of the Vaselona pegmatite is presumably caused by the micro-shearing (see chapter 6.).

A number of pegmatites are crosscut by muscovite pegmatite dykes (PD). The muscovite of these dykes have zinnwaldite (Fe polylithionite) composition except the muscovite occurring in the Vaselona pegmatite, which has Li-Fe muscovite composition. The latter plot in the field of primary muscovite (Fig. 45b; Miller et al.,1981) whereas the composition of the muscovites in Hellheia midtre and nordre, Bjortjørn, Skåremyr corresponds to the composition of secondary muscovite.

Sampling profiles across the Hellheia midtre, Skåremyr, Sønnristjern and Lille Kleivmyr pegmatite were carried out in order to verify the chemical variability of the biotite chemistry within pegmatites (Figs. 46 to 49). The ratio of Mg – Li/Fe# (Fe# - Fe/(Fe+Mg) in atoms per formula unit) is used here to indicate the differentiation degree of biotites. The lower the ratio (small columns in Figs. 46 to 49) is the higher is the differentiation degree of the biotite. Biotites of the four pegmatites do not show systematic chemical zoning along the pegmatites like feldspar.

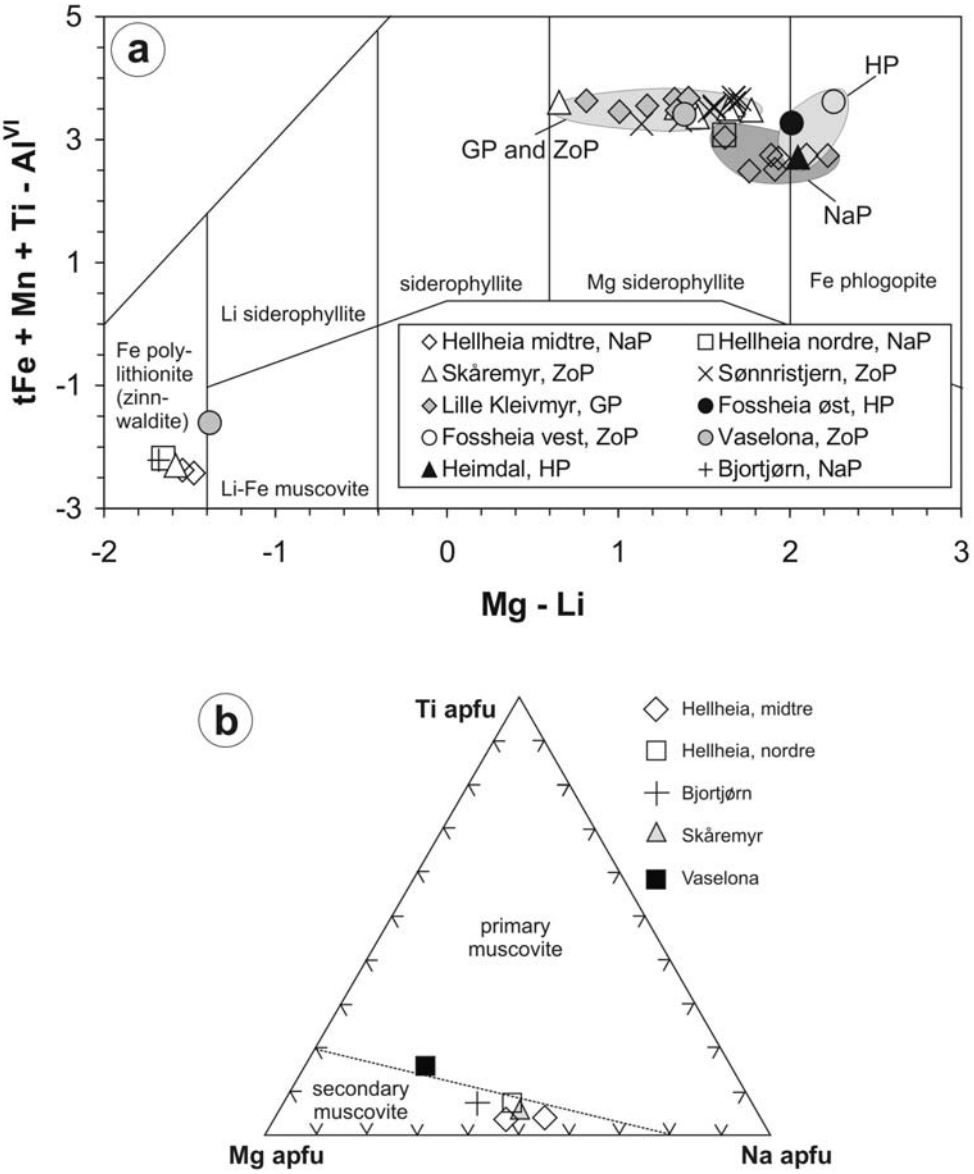

Fig. 45 *a - Mica chemistry of pegmatites plotted in the nomenclature diagram of Tischendorf et al. (2001). tFe – Fe total. b – Fe-Li muscovite and zinnwaldite composition of Froland pegmatites plotted in the Na-Mg-Ti diagram (Miller et al., 1981). apfu – atoms per formula unit.*

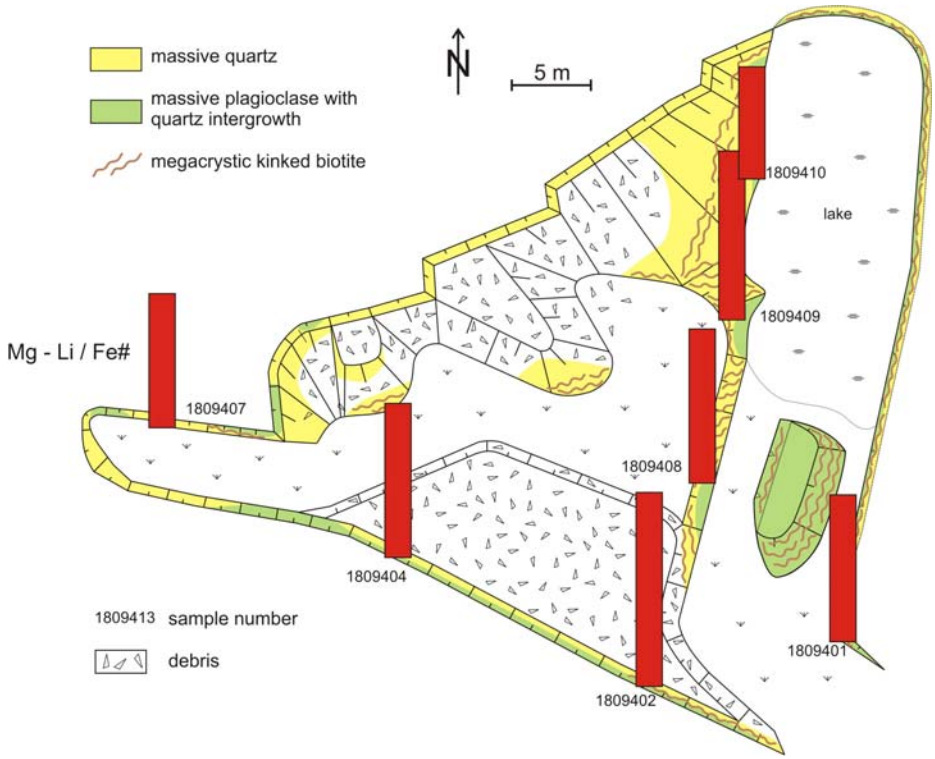

Fig. 46. *Outline of the Hellheia midtre quarry with red columns of the Mg - Li/Fe# ratio of biotite. The columns are placed at the sampling point.*

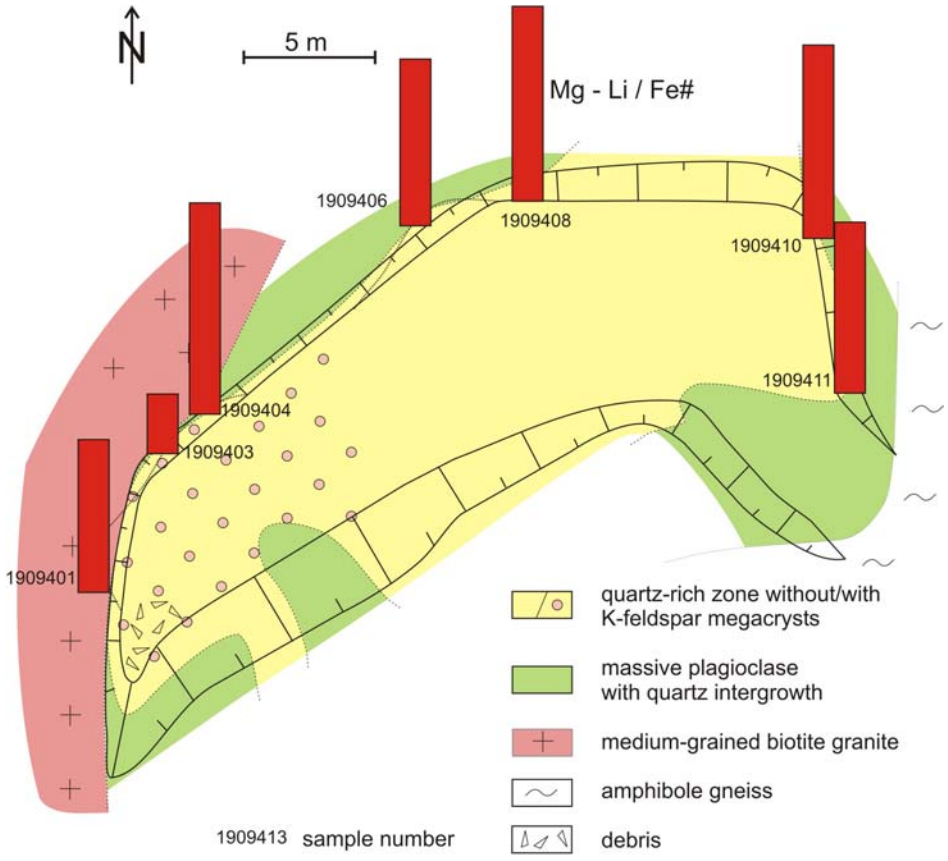

Fig. 47. *Outline of the Skåremyr quarry with red columns of the Mg - Li/Fe# ratio of biotite. The columns are placed at the sampling point.*

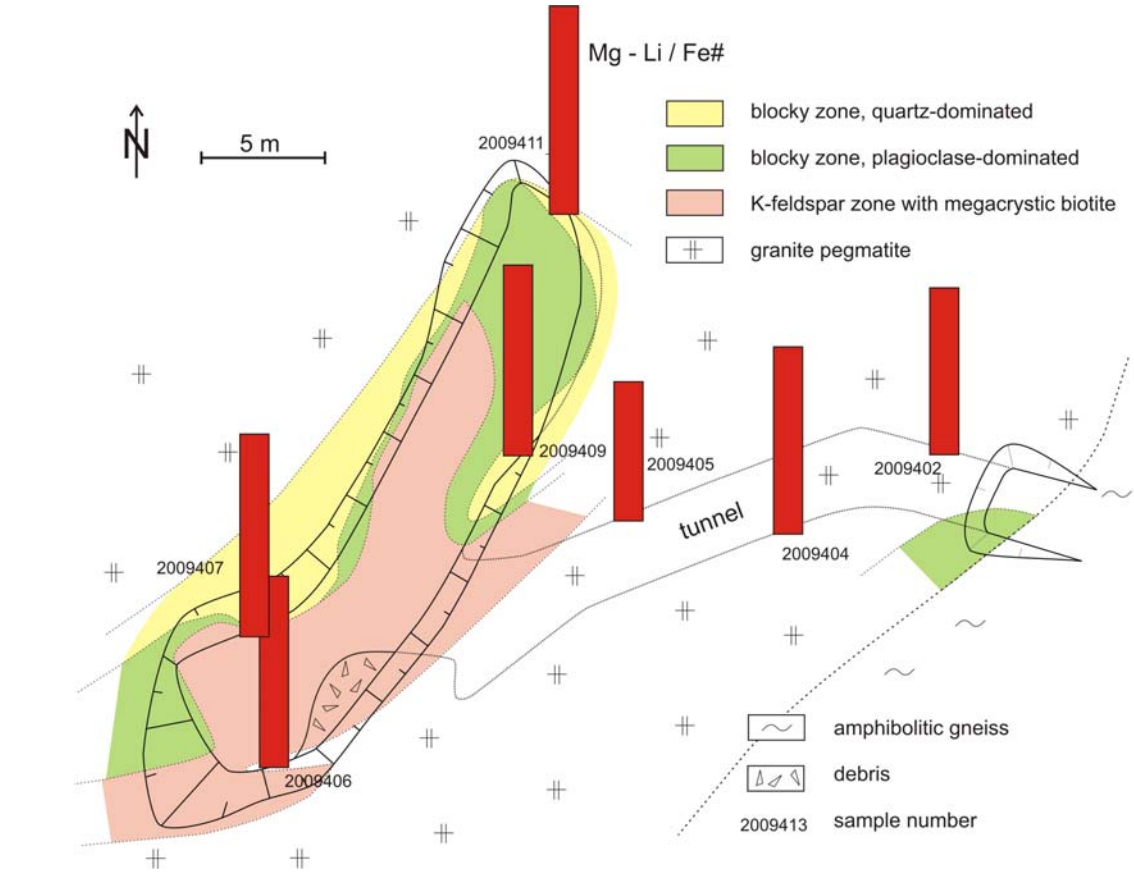

Fig. 48. *Outline of the Sønnristjern quarry with red columns of the Mg - Li/Fe# ratio of biotite. The columns are placed at the sampling point.*

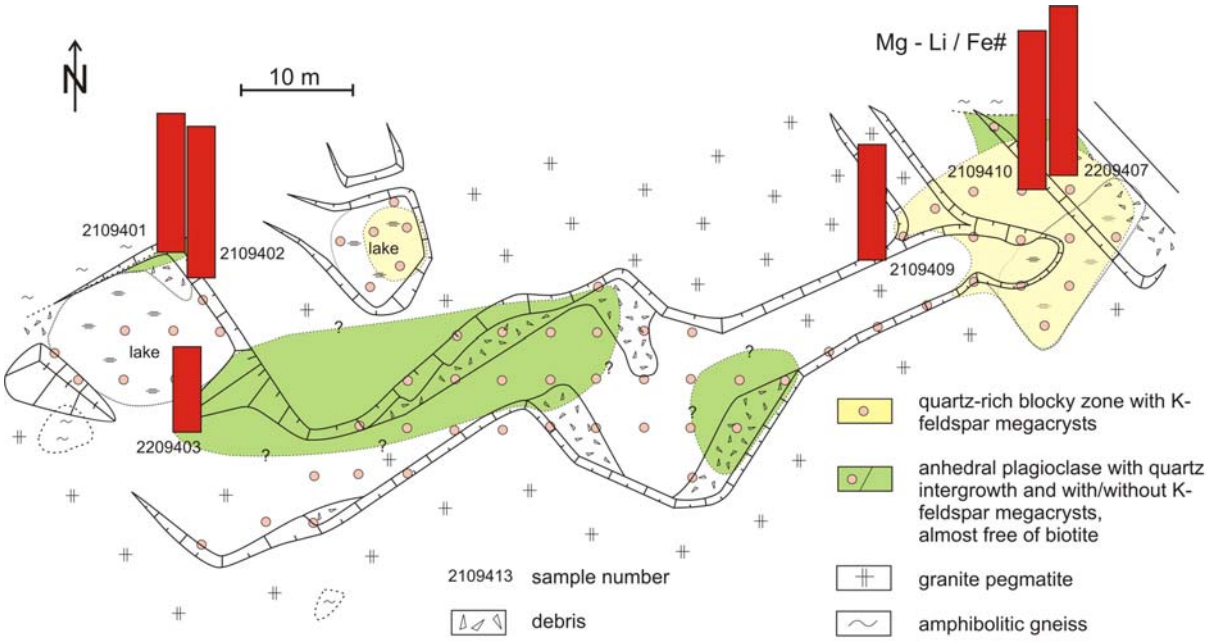

Fig. 49. *Outline of the Lille Kleivmyr quarry with red columns of the Mg - Li/Fe# ratio of biotite. The columns are placed at the sampling point.*

10. Summary

Quartz, feldspar and mica of 14 representative pegmatite of different type and relative age were sampled and analysed in order to determine the chemical quality of quartz and feldspar and to reveal relationships between of quartz, feldspar and mica chemistry and the pegmatite types.

Most of the older pegmatites (Løvland, Hellheia, midtre and nordre, Bjortjørn, Skåremyr Sønnristjern, Lille Kleivmyr, Vaselona) contain quartz of medium raw material quality with relative constant trace element concentrations independent of the pegmatite type. However, the older generation of pegmatites, which occur in mega enclaves within the Herefoss pluton are characterised by relative high Ti. Most of the HPs contain low quality quartz. Quartz of the Fossheia øst pegmatite is the only HP quartz which has medium quality. Significant systematic variations of the trace element content of quartz across pegmatites could not be proofed. The results testify a rather homogeneous distribution of trace elements in quartz across the pegmatites.

The presence of micro-scale secondary quartz in pegmatite quartz revealed by cathodoluminescence lowers slightly the average concentration of trace elements in bulk quartz analyses by LA-ICP-MS. However, the volume portion of secondary quartz in primary quartz is commonly less than 3 vol.%.

ZoP (Skåremyr, Sønnristjern, Fossheia, vest), GP (Lille Kleivmyr, Sønnristjern), PGr (Våtåskammen) and the Fossheia, øst HP contain K-feldspar with good quality of >13.4 wt.% K_2O. K-feldspars of Løvland (KP), Hellheia, nordre (NaP) and of PDs have 13.0 to 13.2 wt.% K_2O which is still in the range of economic quality. The Vaselona ZoP and the HPs at Metveit and Heimdal contain low-quality K-feldspar with 12.5 wt.%, 12.2 and 12.3 wt.% K_2O, respectively. The NaPs Bjortjørn and Hellheia, midtre do not contain K-feldspar apart from the small PD dykes crosscutting the pegmatites. Feldspar is the most sensitive indicator of the fractionation of the pegmatite-forming magma in comparison with quartz and mica. Plagioclase in most of the pegmatites contain more than 2 wt.% CaO which makes them unsuitable as raw material for ceramics and glass. Only three plagioclase samples from Vaselona, Hellheia, nordre and Skåremyr have less than 2 wt.% CaO. Mineralogically heterogeneous pegmatites, such as plagioclase-dominated pegmatites (NaP), granitic pegmatites (GP) and zoned pegmatites, exhibit distinct variation of the Rb/Sr ratio in plagioclase and Rb/(Sr+Ba) ratio in K-feldspar across the pegmatite. Feldspars in the pegmatite cores are more fractionated than those at the pegmatite margin. Moreover, feldspar megacrysts occurring in pegmatites show a more primitive composition in their cores compared to the crystal margins. However, the variation of the Rb/Sr and Rb/(Sr+Ba) ratios has no influence on the economic quality of feldspar. The opposite is the case, i.e. the K_2O content influences the uptake of Rb, Sr and Ba.

Generally, the composition of biotites from Froland pegmatites is relative homogeneously and primitive in respect to granitic differentiation. However, small variations of the mica chemistry help to classify the different pegmatite types. The most primitive composition is found in the micas from pegmatites related to the Herefoss pluton (HP) followed by the micas of NaP. Biotites of GP and ZoP reflect a slightly evolved pegmatite-forming magma. A systematic chemical variation of biotites across pegmatites could not be proofed.

11. References

Alirezaei, S. 2000. Geochemical investigation of the lower crustal rocks in Bamble Shear belt, southern Norway: implications for the source of gold in lode gold deposits. Unpublished Ph.D. thesis, University of Ottawa, 343 pp.

Andersen, T. 1997. Radiogenic isotope systematics of the Herefoss Granite, South Norway; an indicator of Sveconorwegian (Grenvillian) crustal evolution in the Baltic Shield. Chemical Geology 135: 139-158.

Behr, H.-J., Frentzel-Beyme, K. 1989. Permeability and paleoporosity in crystalline bedrocks of the Central European basement-studies of cathodoluminescence. In: Boden, A., Eriksson, K.G. (eds.) Exploration of the deep continental crust. Deep drilling in crystalline bedrock Volume 2. Springer, Berlin Heidelberg New York, pp. 477-497.

Bingen, B., Boven, A., Punzalan, L., Wijbrans, J.R., Demaiffe, D. 1998. Hornblende 40Ar/39Ar geochronology across terrane boundaries in the Sveconorwegian Province of S. Norway. Precambrian Research 90, 159-185.

Blankenburg, H.-J., Götze, J., Schulz, J. 1994. Quarzrohstoffe. Deutscher Verlag für Grundstoffindustrie, Leipzig-Stuttgart, 296 pp.

Černy, P. 1991. Rare element granitic pegmatites. Part I: Anatomy and internal evolution of pegmatite deposits. Geoscience Canada 18: 49-67.

Černý, P., Burt, D.M. 1984. Paragensis, crystallochemical properties, and chemical evolution of micas in granite pegmatites. In: Bailey, S.W. (ed) Micas. Reviews in Mineralogy vol. 13, 257-297.

Cox, R.A., Dempster T.Y., Bell B.R., Rogers, G. 1996. Crystallization of the Shap Granite: Evidence from zoned K-feldspar megacrysts. Journal of the Geological Society of London 153, 625-635.

Elders, W.A. 1963. On the form and mode of emplacement of the Herefoss granite. Norwegian Geological Survey Bulletin 214, 1 – 50.

Falkum, T., Petersen, J.S. 1980. The Sveconorwegian orogenic belt, a case of late-Proterozoic plate-collision. Geologische Rundschau 69, 622-647.

Flem, B., Larsen, R.B., Grimstvedt, A., Mansfeld, J. 2002. In situ analysis of trace elements in quartz by using laser ablation inductively coupled plasma mass spectrometry. Chemical Geology 182, 237-247.

Götze, J., Plötze, M. and Habermann, D. 2001. Origin, spectral characteristics and practical applications of the cathodoluminescence (CL) of quartz – a review. Mineralogy and Petrology 71, 225-250.

Götze, J., Plötze, M., Graupner, T., Hallbauer, D.K., Bray, C.J. 2004. Trace element incorporation into quartz: A combined study by ICP-MS, electron spin resonance, cathodoluminescence, capillary ion analysis, and gas chromatography. Geochimica et Cosmochimica Acta 68, 3741-3759.

Götze, J., Plötze, M., Trautmann, T. 2005. Structure and luminescence characteristics of quartz from pegmatites. American Mineralogist 90, 13-21.

Henderson, I., Ihlen, P.M. 2004. Emplacement of polygeneration pegmatites in relation to Sveco-Norwegian contractional tectonics: examples from southern Norway. Precambrian Research 133, 207-222.

Ihlen, P.M., Henderson, I., Larsen, R.B., Lynum, R. 2002. Potensielle ressurser av kvarts- og feldspat- råstoffer på Sørlandet, II: Resultater av undersøkelsene i Frolandsområdet i 2001. Norwegian Geological Survey Report 2002.009, 28 pp.

Ihlen, P.M., Henderson, I., Larsen, R.B., Lynum, R., Furuhaug, L. 2003. Potentielle ressurser av kvarts- og feldspat-råstoffer på Sørlandet, III: Sporelementsammensetningen av

pegmatittisk og hydrothermal kvarts i Froland, Østre Froland of Lillesand. Status quo ved utgangen av 2002. Norwegian Geological Survey Report 2003.035, 38 pp.
Long, P.E., Luth, W.C. 1986. Origin of K-feldspar megacrysts in granitic rocks: Implication of a partitioning model for barium. American Mineralogist 71, 367-375.
Mehnert, K.R., Büsch, W. 1981. The Ba content of K-feldspar megacrysts in granites: a criterion for their formation. Neues Jahrbuch für Mineralogie Abhandlungen 140, 221-252.
Miller, C.F., Stoddard, E.F., Larry J.B., Wayne, A.D. 1981. Composition of plutonic muscovites: genetic implications. Canadian Mineralogist 19, 25-34.
Morgan, G.B., London, D. 1999. Crystallization of the Little Three layered pegmatite-aplite dike, Ramona District, California. Contributions to Mineralogy and Petrology 136, 310-330.
Müller, A., Kronz, A., Breiter, K. 2002a. Trace elements and growth patterns in quartz: a fingerprint of the evolution of the subvolcanic Podlesí Granite System (Krušne Hory, Czech Republic). Bulletin of the Czech Geological Survey 77/2, 135-145.
Müller, A., Lennox, P., Trzebski, R. 2002b. Cathodoluminescence and micro-structural evidence for crystallisation and deformation processes of granites in the Eastern Lachlan Fold Belt (SE Australia). Contributions to Mineralogy and Petrology 143, 510-524.
Müller A., Rene M., Behr H.-J., Kronz A. 2003. Trace elements and cathodoluminescence of igneous quartz in topaz granites from the Hub Stock (Slavkovský Les Mts., Czech Republic). Mineralogy and Petrology 79, 167-191.
Nassau, K., Prescott, B.E. 1975. A reinterpretation of smoky quartz. Physica Status Solidi 29, 659-663.
Nassau, K., Prescott, B.E. 1977. Smoky, blue, greenish yellow, and other irradiation-related colors in quartz. Mineralogical Magazine 41, 301-312.
Nilsson, B. 1970. Samarskites. Chemcial composition, formula and crystalline phases produced by heating. Norsk Geologisk Tidsskrift 50, 357-373.
Perny, B., Eberhardt, P., Ramseyer, K., Mullis, J., Pankrath, R. 1992. Microdistribution of aluminium, lithium and sodium in a quartz: possible causes and correlation with shored lived cathodoluminescence. American Mineralogist 77, 534-544.
Ramseyer, K., Baumann, J., Matter, A., Mullis, J. 1988. Cathodoluminescence colours of α-quartz. Mineralogical Magazine 52, 669-677.
Rusk, B., Reed, M. 2002. Scanning electron microscope-cathodoluminescence analysis of quartz reveals complex growth histories in veins from the Butte porphyry copper deposit, Montana. Geology 30, 727-730.
Sprunt, E.S. 1981. Causes of quartz cathodoluminescence colors. Scanning Electron Microscopy 1981, 525-535.
Stenina, N.G., Bazarov, L.S., Shcherbakova, M.Y., Mashkovtsev R.I., 1984. Structural state and diffusion of impurities in natural quartz of different genesis. Physics and Chemistry of Minerals 10, 180-186.
Stevens Kalceff, M.A., Phillips, M.R., Moon, A.R., Kalceff, W. 2000. Cathodoluminescence microcharacterization of silicon dioxide polymorphs. In: Pagel, M., Barbin, V., Blanc, P., Ohnenstetter D. (eds.) Cathodoluminescence in Geosciences (. Springer, Berlin, pp. 193-279.
Søvegjarto, U. 2001. Geologisk 1:5000/1:2000 kartlegging i pegmatitt-felter ved Middagsknatten-Massævatn og Haukedalen, Froland Kommune 5.-9. jun 2001. Intern rapport, North Cape Minerals AS, Lillesand, 1 p., 9 maps.
Tischendorf, G., Förster, H.-J., Gottesmann, B. 2001. Minor- and trace-element composition of trioctahedral micas: a review. Mineralogical Magazine 65, 249-276.

Valley, J.W., Graham, C.M. 1996. Ion microprobe analysis of oxygen isotope ratios in quartz from Skye granite: healed micro-cracks, fluid flow, and hydrothermal exchange. Contributions to Mineralogy and Petrology 124, 225-234.
Van den Kerkhof, A.M., Hein, U. 2001. Fluid inclusion petrography. Lithos 55, 27-47.
Van den Kerkhof, A.M., Kronz, A., Simon, K. 2001. Trace element redistribution in metamorphic quartz and fluid inclusion modification: observations by cathodoluminescence. XVI ECROFI, Porto 2001, Departomento Geologica Memória 7, 447-450.
Van den Kerkhof, A.M., Kronz, A., Simon, K., Scherer, T. 2004. Fluid-controlled quartz recovery in granulite as revealed by cathodoluminescence and trace element analysis (Bamble sector, Norway). Contributions to Mineralogy and Petrology 146, 637-652.
Vollbrecht, A., Olesen, N.O., Schmidt, N.H., Weber, K. 1994. Crystallographic microcrack orientation in quartz from a granite – a combined ECP/U stage study. In: Bunge, H.J., Siegesmund, S., Skrotzki, W., Weber, K. (eds.) Textures of Geological Materials. DGM Informationsgesellschaft Verlag, Oberursel, pp. 345-352.
Vollbrecht, A., Rust, S., Weber, K. 1991. Development of microcracks in granites during cooling and uplift: examples from the Variscan basement in NE Bavaria, Germany. J. Struct. Geol. 13, 787-799.

Appendix A. *Sample list.*

locality nr.	locality name	sample nr.	UTM (WGS84)		map sheet 1:50000	locality description	pegmatite type	sample description
			Øst	Nord				
1	Løvland	2209401	469594	6496668	Nelaug	quarry ca. 500 m SW Lauvland farm at a district road, 3 km ENE Hynnekleiv	KP	fine- to medium-grained milky smoky quartz
		2209401k					KP	K-feldspar
		2209401p					KP	plagioclase
		2209402					KP	polished slab with 3-cm-magnetite
		2209403					KP	smoky quartz
		2209403k					KP	K-feldspar
		2209403p					KP	plagioclase
		2209404					KP	smoky quartz
		2209404k					KP	K-feldspar
		2209404p					KP	plagioclase
		2209405					KP	smoky quartz
		2209405k					KP	K-feldspar
		2209405p					KP	plagioclase
		2209406					KP	polished slab with typical DKP-texture and magnetite
2	Hellheia, midtre	1809401a	466955	6487785	Mykland	quarry 1.5 km S Lauvrak farm at the end of a forest road, S flank of the Hellheia hill (568 m a.s.l.), 5 km E Herefoss	NaP	smoky (black) quartz with biotite
		1809401b					NaP	quartz intergrown with plagioclase
		1809401d					NaP	plain biotite
		1809402					NaP	massive milky smoky quartz
		1809402d					NaP	plain biotite
		1809402p					NaP	plagioclase
		1809403a					NaP	massive white milky quartz
		1809403b					NaP	polished slab of plagioclase megacryst bordered by folded biotite and crusscut by muscovite-bearing quartz veins
		1809404					NaP	white milky quartz
		1809404d					NaP	biotite intergrown with feldspar
		1809405					PD	coarse-grained muscovite granite
		1809406					NaP	white milky quartz close to plagioclase
		1809407					NaP	massive white milky quartz

Appendix A. *Sample list. Continued.*

Locality nr.	Locality name	sample nr.	UTM (WGS84)		map sheet 1:50000	locality description	pegmatite type	sample description
			Øst	Nord				
2	**Hellheia, midtre**	1809407d	466955	6487785	Mykland	quarry 1.5 km S Lauvrak farm at the end of a forest road, S flank of the Hellheia hill (568 m a.s.l.), 5 km E Herefoss	NaP	biotite intergrown with feldspar
		1809407p					NaP	plagioclase
		1809408					NaP	massive white milky quartz
		1809408d					NaP	plain biotite
		1809408p					NaP	plagioclase
		1809409					NaP	smoky milky quartz with biotite megacryst
		1809409d					NaP	plain biotite
		1809410					NaP	massive white milky quartz
		1809410d					NaP	biotite intergrown with feldspar
		1809410p					NaP	plagioclase
		1809411a					NaP	massive smoky milky quartz
		1809411d					NaP	muscovite
		1809411p					NaP	plagioclase
		1809414					PD	muscovite pegmatite dyke
		1809414k					NaP	K-feldspar
		1809415					NaP	muscovite intergrowth with quartz and feldspar
		1809416					NaP	biotite
3	**Hellheia, nordre**	2409401	467120	6488120	Mykland	quarry 1.2 km S Lauvrak farm at a forest road, NE flank of the Hellheia hill (568 m a.s.l.), 5 km E Herefoss	NaP	massive white milky quartz
		2409401d					NaP	slightly kinked biotite
		2409401e					NaP	muscovite
		2409401k					NaP	K-feldspar
		2409401p					NaP	plagioclase
		2409402					NaP	quartz intergrown with plagioclase megacryst core and muscovite

Appendix A. *Sample list. Continued.*

locality nr.	locality name	sample nr.	UTM (WGS84)		map sheet 1:50000	locality description	pegmatite type	sample description
			Øst	Nord				
4	**Bjortjørn**	2509401	468008	6495125	Mykland	cave S of the small Bjortjørn lake, 20 m above the national road 42 between Hynnekleiv and Hinnebu	NaP	fine- to medium-grained smoky milky quartz
		2509401e					NaP	muscovite
		2509401p					NaP	plagioclase
		2509402					NaP	allanite
		2509403					NaP	samarkite
		2509404					NaP	garnet
		2509405					NaP	quartz intergrown with muscovitised plagioclase
5	**Haukemyrliene**	1609415	464880	6486840	Mykland	road cut along the road between Herefoss and Mjåvatn, 700 m N Olavsheia top (339 m a.s.l.), 2.5 km ESE Herefoss	GP	coarse-grained quartz-feldspar intergowth
		1609416					GP	vein of mobilsied quartz within synkinematic pegmatite
		1609417					PD	smoky stockscheider quartz
		1609418					PD	smoky stockscheider quartz intergrown with K-feldspar
		1609419					PD	horizontal, cross-cutting, 0.5 m thick dyke with alternating pegmatitic and aplitic layers with garnet and molybdenite(?)
6	**Skåremyr**	1909401	463311	6487221	Mykland	quarry at the end of forest road, 600 m S Tereleiken top (317 m a.s.l.), 1.2 km E Herefoss	ZoP	massive smoky milky quartz
		1909401d					ZoP	slightly kinked biotite
		1909401k					ZoP	K-feldspar
		1909401p					ZoP	plagioclase
		1909402					ZoP	massive smoky milky quartz
		1909403					PD	quartz in young albite pegmatite dyke
		1909403d					PD	small biotite
		1909403k					PD	K-feldspar
		1909403p					PD	plagioclase
		1909404					ZoP	massive clear smoky quartz
		1909404d					ZoP	slightly kinked biotite
		1909404k					ZoP	K-feldspar
		1909404p					ZoP	plagioclase
		1909405						cross-cutting young, fine-grained biotite granite

Appendix A. *Sample list. Continued.*

locality nr.	locality name	sample nr.	UTM (WGS84)		map sheet 1:50000	locality description	pegmatite type	sample description
			Øst	Nord				
6	**Skåremyr**	1909406	463311	6487221			ZoP	massive clear smoky quartz
		1909406d					ZoP	plain biotite
		1909406p					ZoP	plagioclase
		1909407					ZoP	contact young biotite granite dyke with mega-plagioclase
		1909408					ZoP	massive smoky milky quartz
		1909408d					ZoP	plain biotite
		1909409					ZoP	massive milky smoky quartz
		1909410					ZoP	massive milky smoky quartz
		1909410d					ZoP	plain biotite
		1909410p					ZoP	plagioclase
		1909411					ZoP	massive clear smoky quartz
		1909411d					ZoP	plain biotite
		1909412					ZoP	fine- to medium-grained quartz in granitic dyke next to plagioclase megacryst at pegmatite contact
		1909413					ZoP	polished slab of plagioclase near pegmatite contact
		1909414a					ZoP	quartz intergrown with core of plagioclase megacryst
		1909415					ZoP	quartz vein in plagioclase
		1909416d					ZoP	muscovite pocket in plagioclase megacrystal
7a	**Sønnristjern**	2009401	466795	6494807	Mykland	quarry at the end of a forest road 1.2 km SE Hynnekleiv on a mountain ridge (349 m a.s.l.)	GP	smoky quartz intergrown with plagioclase
		2009401p					GP	plagioclase
		2009402					GP	smoky quartz
		2009402d					GP	plain biotite
		2009402k					GP	K-feldspar
		2009402p					GP	plagioclase
		2009403k					GP	K-feldspar
		2009404					GP	smoky quartz intergrown with feldspar
		2009404d					GP	plain biotite
		2009404k					GP	K-feldspar
		2009404p					GP	plagioclase
		2009405					GP	quartz intergrown with feldspar

Appendix A. *Sample list. Continued.*

locality nr.	locality name	sample nr.	UTM (WGS84)		map sheet 1:50000	locality description	pegmatite type	sample description
			Øst	Nord				
7a	**Sønnristjern**	2009405d	466795	6494807			GP	plain biotite
		2009405k					GP	K-feldspar
		2009405p					GP	plagioclase
		2009406a					ZoP	smoky quartz in K-feldspar
		2009406b					ZoP	smoky quartz in plagioclase
		2009406d					ZoP	plain biotite
		2009406k					ZoP	K-feldspar
		2009406p					ZoP	plagioclase
		2009407					ZoP	massive quartz
		2009407d					ZoP	plain biotite
		2009407k					ZoP	K-feldspar
		2009407p					ZoP	plagioclase
		2009408						fine-grained biotite granite dyke
		2009409					ZoP	massive smoky milky quartz
		2009409d					ZoP	plain biotite
		2009409k					ZoP	K-feldspar
		2009409p					ZoP	plagioclase
		2009410					ZoP	massive smoky milky quartz
		2009411					ZoP	massive smoky milky quartz
		2009411d					ZoP	plain biotite
		2009411k					ZoP	K-feldspar
		2009411p					ZoP	margin of plagioclase megacryst
		2009412					ZoP	smoky quartz
		2009412p					ZoP	core of plagioclase megacrystal
		2009413					ZoP	polished slab of plagioclase-quartz intergrowth in a megacrystal
		2009414					GP	polished slab of megacrystic granitic pegmatite
7b	**Sønnristjern**	2109411	466766	6494868			GP	smoky quartz intergrown with K-feldspar
		2109411d					GP	plain biotite
		2109411k					GP	K-feldspar
		2109411p					GP	plagioclase

Appendix A. *Sample list. Continued.*

locality nr.	locality name	sample nr.	UTM (WGS84)		map sheet 1:50000	locality description	pegmatite type	sample description
			Øst	Nord				
7c	**Sønnristjern**	2109412	466812	6494911			GP	quartz intergrown with K-feldspar
		2109412k					GP	K-feldspar
		2109412p					GP	plagioclase
7d	**Sønnristjern**	2109413	466875	6494961			GP	clear smoky quartz
		2109413d					GP	plain biotite
		2109413k					GP	K-feldspar
		2109413p					GP	plagioclase
7e	**Sønnristjern**	2109414	466876	6495031			GP	massive smoky milky quartz
		2109414d					GP	plain biotite
		2109414k					GP	K-feldspar
		2109414p					GP	plagioclase
7f	**Sønnristjern**	2109415	466910	6495045			GP	massive smoky milky quartz
		2109415k					GP	plagioclase
8	**Lille Kleivmyr**	2109401	469318	6495309	Nelaug	quarry 500 m W Øygarden farm, 500 m SW Våtåsen top (367 m a.s.l.), 3.5 km E Hynnekleiv	GP	quartz intergrowth with plagioclase and biotite 2 m from contact
		2109401ak					GP	K-feldspar
		2109401bk					GP	K-feldspar
		2109401d					GP	plain biotite
		2109401p					GP	plagioclase
		2109402					GP	quartz intergrown with plagioclase next to a garnet-bearing granite dyke
		2109402ak					GP	K-feldspar
		2109402bk					GP	K-feldspar
		2109402d					GP	plain biotite
		2109402p					GP	plagioclase
		2109403						garnet-bearing granite batch
		2109403d						biotite intergrown with garnet in garnet-bearing granite batch
		2109403k						K-feldspar in garnet-bearing granite batch
		2109403p						plagioclase in garnet-bearing granite batch
		2109404					GP	smoky quartz in K-feldspar next to a garnet-bearing granite dyke
		2109404k					GP	K-feldspar next to a garnet-bearing granite dyke

Appendix A. *Sample list. Continued.*

locality nr.	locality name	sample nr.	UTM (WGS84)		map sheet 1:50000	locality description	pegmatite type	sample description
			Øst	Nord				
8	**Lille Kleivmyr**	2109404p	469318	6495309	Nelaug		GP	plagioclase next to a garnet-bearing granite dyke
		2109405					GP	2-cm-garnet
		2109406					GP	quartz in medium- to coarse-grained granitic pegmatite
		2109406k					GP	K-feldspar
		2109406p					GP	plagioclase
		2109407						irregular quartz vein in garnet-bearing granite
		2109408a					GP	quartz intergrown with K-feldspar
		2109408b					GP	quartz intergrown with plagioclase
		2109408k					GP	K-feldspar
		2109408p					GP	plagioclase
		2109409					GP	quartz
		2109409d					GP	plain biotite
		2109409k					GP	K-feldspar
		2109409p					GP	plagioclase
		2109410					GP	massive smoky milky quartz of pegmatite core
		2109410d					GP	plain biotite
		2109410k					GP	K-feldspar
		2109410p					GP	plagioclase
		2209407					GP	smoky quartz from pegmatite core
		2209407d					GP	plain biotite
		2209407k					GP	K-feldspar
		2209407p					GP	plagioclase
		2209408						quartz in garnet-bearing granite
9	**Våtåskammen**	1709401a	469400	6495570	Nelaug	300 m W Våtåsen top (367 m a.s.l.), 700 m NE Øygarden farm, 3.7 km E Hynnekleiv	PGr	coarse-grained granite containing stretched and boudinaged K-feldspar megacrysts up to 1 m in length
		1709401b					PGr	medium-grained granite containing stretched and boudinaged K-feldspar megacrysts up to 1 m in length
		1709401k					PGr	coarse-grained K-feldspar
10	**Vaselona**	2309404	461358	6479100	Lillesand	quarry 1 km SSE Søre Herefoss, NW Begervannet	sheared ZoP	massive smoky quartz
		2309404d					sheared ZoP	slightly kinked biotite
		2309404k					sheared ZoP	K-feldspar
		2309404e					sheared ZoP	muscovite

Appendix A. *Sample list. Continued.*

locality nr.	locality name	sample nr.	UTM (WGS84)		map sheet 1:50000	locality description	pegmatite type	sample description
			Øst	Nord				
10	**Vaselona**	2309404p	461358	6479100			sheared ZoP	plagioclase
11	**Fossheia, vest**	2309402	460930	6478914	Lillesand	quarry at mountain top (231 m a.s.l.) 1.2 km S Søre Herefoss	sheared ZoP	massive smoky quartz
		2309402d					sheared ZoP	kinked biotite
		2309402k					sheared ZoP	K-feldspar
		2309402p					sheared ZoP	plagioclase
		2309403						medium-grained porphyritic adamelite, Herefoss pluton
12	**Fossheia, øst**	1609411	461024	6478881	Lillesand	small quarry 20 m above the road between Søre Herefoss and Metveit, 1.1 km S Søre Herefoss	HP	massive clear smoky quartz from pegmatite core
		1609412					HP	smoky quartz next to K-feldspar
		1609413					HP	quartz graphically intergrown with K-feldspar
		2309401d					HP	kinked biotite
		2309401k					HP	K-feldspar
		2309401p					HP	plagioclase
13	**Husefjell**	1609402	468867	6472150	Lillesand	road cut at the national road 404 between Risbruna and Skiftenes, E flank of Husefjell (227 m a.s.l.), 2.5 km WSW Skiftenes		pink, coarse-grained leuco-granite with K-feldspar phenocrysts (3 cm), Herefoss pluton
14	**Metveit**	1609405	464356	6474754	Lillesand	road cut at the national road 404 between Søre Herefoss and Risbruna, 600 m E Metveit farm		fine- to medium-grained porphyritic quartz monzonite with pink K-feldspar (1.5 cm), Herefoss pluton
		2309405					HP	massive smoky quartz
		2309405k					HP	K-feldspar
		2309405p					HP	plagioclase
		2309406					HP	idiomorpher kfs
		2309407						fine- to medium-grained monzonite from pegmatite bottom, Herefoss pluton
		2309408						porphyritic quartz monzonite, Herefoss pluton
15	**Heimdal**	1609409	458567	6480410	Lillesand	road cut at a forest road on the S side of Heimdalsvannet, 800 m E Lilleheimdal, 2.7 km WNW Søre Herefoss	HP	milky smoky, fine- to medium-grained quartz at contact with host granite
		1609409k					HP	K-feldspar
		2309409d					HP	plain biotite
		2309410						coarse-grained porphyritic monzonite, Herefoss pluton

Appendix B. *Trace element concentrations in quartz determined by LA-ICP-MS.*
Quartz analyses which are marked with orange have high quality, with yellow medium quality and white is low quality.

locality nr.	locality name	sample/ analyse nr.	pegmatite type	quartz type	Li	Be	B	Na	Al	Ge	Mn	Rb	Sr	Pb	Mg	P	Ti	K	Fe
1	Løvland	2209401-A	KP	smoky pqz	7.0	<0.30	<1.00	<50	47.7	1.61	<0.20	<0.20	0.04	<0.01	<10.0	<10.0	2.5	<1.0	<0.20
		2209401-B	"	"	3.6	<0.30	1.24	<50	50.0	1.96	<0.20	<0.20	0.05	0.01	12.1	<10.0	6.7	<1.0	<0.20
		2209403-A	KP	smoky pqz	7.0	<0.30	1.50	<50	48.2	1.63	<0.20	<0.20	0.02	0.01	<10.0	<10.0	4.8	<1.0	<0.20
		2209403-B	"	"	6.3	<0.30	1.14	<50	41.5	1.77	<0.20	<0.20	0.03	0.01	<10.0	<10.0	3.5	<1.0	<0.20
		2209404-A	KP	smoky pqz	5.2	<0.30	2.15	<50	51.3	1.50	<0.20	<0.20	0.04	<0.01	<10.0	<10.0	7.7	<1.0	<0.20
		2209404-B	"	"	6.0	<0.30	1.73	<50	42.5	1.41	0.25	<0.20	0.03	0.01	10.4	<10.0	7.4	<1.0	0.25
		2209405-C	KP	smoky pqz	5.4	0.30	<1.00	<50	32.6	1.86	<0.20	<0.20	0.05	0.01	<10.0	<10.0	0.7	<1.0	<0.20
		2209405-D	"	"	7.0	<0.30	<1.00	<50	35.8	1.83	<0.20	<0.20	0.04	0.01	<10.0	<10.0	0.8	1.2	<0.20
		2209405-A	KP	sqz	3.3	<0.30	2.43	135	34.7	1.60	<0.20	<0.20	0.35	0.01	44.6	11.2	0.9	18.7	0.93
		2209405-B	"	"	3.0	<0.30	<1.00	<50	21.3	1.83	<0.20	<0.20	0.09	0.01	14.3	<10.0	0.1	<1.0	<0.20
2	Hellheia, midtre	1809401A-A	NaP	milky smoky pqz	7.1	<0.30	1.59	<50	35.3	1.78	<0.20	<0.20	0.07	<0.01	<10.0	<10.0	5.5	<1.0	<0.20
		1809401A-B	"	"	7.0	<0.30	1.12	<50	33.1	1.84	0.28	<0.20	0.08	<0.01	<10.0	<10.0	5.1	1.1	0.21
		1809401B-A	NaP	pqz in pl	7.1	<0.30	1.15	<50	42.8	0.91	<0.20	<0.20	0.07	0.01	17.7	<10.0	2.9	<1.0	0.25
		1809401B-B	"	"	8.2	<0.30	<1.00	<50	47.5	0.81	<0.20	<0.20	0.08	<0.01	13.6	<10.0	2.2	<1.0	<0.20
		1809402-A	NaP	milky smoky pqz	7.1	<0.30	1.24	<50	28.0	1.89	0.45	<0.20	0.03	<0.01	15.3	<10.0	4.8	<1.0	0.37
		1809402-B	"	"	6.7	<0.30	1.08	<50	36.1	2.12	0.33	<0.20	0.07	0.01	15.8	<10.0	7.7	1.0	0.22
		1809403-A	NaP	milky pqz	5.5	0.42	1.45	<50	48.5	1.72	0.28	<0.20	0.09	<0.01	35.6	11.8	5.5	<1.0	<0.20
		1809403-B	"	"	5.5	0.44	1.25	<50	41.0	1.89	0.39	<0.20	0.06	<0.01	64.7	<10.0	3.9	<1.0	0.26
		1809404-A	NaP	milky pqz	7.0	<0.30	<1.00	<50	47.2	1.88	0.21	<0.20	0.06	<0.01	74.6	<10.0	4.0	1.3	0.28
		1809404-B	"	"	6.5	0.44	<1.00	<50	42.8	1.85	0.34	<0.20	0.06	<0.01	30.4	<10.0	3.7	1.2	0.48
		1809406-A	NaP	milky pqz	5.5	<0.30	1.14	<50	44.4	1.99	<0.20	<0.20	0.06	<0.01	67.3	10.0	7.2	<1.0	<0.20
		1809406-B	"	"	5.4	<0.30	<1.00	<50	42.4	1.40	0.28	<0.20	0.09	<0.01	71.6	<10.0	6.2	<1.0	0.26
		1809407-A	NaP	milky pqz	8.2	<0.30	1.78	<50	46.5	1.69	<0.20	<0.20	0.05	<0.01	22.7	10.6	3.1	<1.0	<0.20
		1809407-B	"	"	7.8	<0.30	1.79	<50	48.1	1.80	<0.20	<0.20	0.08	<0.01	12.7	<10.0	3.0	1.1	0.22
		1809408-A	NaP	milky pqz	8.1	<0.30	2.10	<50	62.3	1.68	<0.20	<0.20	0.09	0.01	111.0	19.3	5.3	<1.0	0.53
		1809408-B	"	"	8.4	<0.30	1.61	<50	59.5	1.73	<0.20	<0.20	0.07	0.02	126.3	11.1	6.0	2.0	1.30
		1809408-C	"	"	11.0	0.34	8.23	333	64.6	1.80	0.92	0.31	0.40	0.02	59.4	11.6	8.8	19.3	4.41

Appendix B. *Trace element concentrations in quartz determined by LA-ICP-MS. Continued.*

locality nr.	locality name	sample/ analyse nr.	pegmatite type	quartz type	Li	Be	B	Na	Al	Ge	Mn	Rb	Sr	Pb	Mg	P	Ti	K	Fe
2	**Hellheia, midtre**	1809409-A	NaP	milky pqz	7.7	<0.30	<1.00	<50	55.7	1.66	<0.20	<0.20	0.05	<0.01	11.6	<10.0	7.3	<1.0	0.42
		1809409-B	"	"	9.8	<0.30	<1.00	<50	57.2	1.90	0.23	<0.20	0.04	<0.01	11.0	<10.0	5.1	<1.0	0.40
		1809410-A	NaP	milky pqz	6.7	<0.30	1.57	<50	39.2	1.76	<0.20	<0.20	0.05	<0.01	25.4	<10.0	8.4	<1.0	0.23
		1809410-B	"	"	6.8	<0.30	1.77	<50	41.4	1.79	0.20	<0.20	0.02	0.01	30.8	<10.0	7.0	<1.0	<0.20
		1809411-A	NaP	milky pqz	6.9	<0.30	1.64	<50	42.6	1.87	<0.20	<0.20	0.07	<0.01	21.9	11.9	3.3	<1.0	0.28
		1809411-B	"	"	8.3	<0.30	<1.00	<50	46.2	1.81	0.34	<0.20	0.09	<0.01	19.2	<10.0	2.7	<1.0	0.27
		1809405-A	PD	smoky pqz	5.1	<0.30	<1.00	82	17.3	2.29	<0.20	<0.20	0.05	0.01	37.9	10.4	3.0	4.4	<0.20
		1809405-B	"	"	9.5	<0.30	<1.00	<50	43.6	2.54	0.20	<0.20	0.06	0.01	<10.0	<10.0	4.9	<1.0	0.23
		1809405-C	"	"	8.5	0.31	<1.00	<50	45.7	2.12	<0.20	<0.20	0.05	0.01	<10.0	<10.0	5.1	1.2	0.22
3	**Hellheia, nordre**	2409401-A	NaP	milky pqz	9.3	<0.30	<1.00	<50	43.7	2.25	<0.20	<0.20	0.05	0.01	108.7	<10.0	5.3	<1.0	<0.20
		2409401-B	"	"	9.0	<0.30	<1.00	<50	33.8	2.19	<0.20	<0.20	0.04	0.01	85.4	<10.0	4.6	<1.0	<0.20
		2409402-A	NaP	pqz in pl	11.4	<0.30	<1.00	<50	44.0	2.74	<0.20	<0.20	0.06	<0.01	<10.0	<10.0	3.3	<1.0	<0.20
		2409402-B	"	"	6.3	<0.30	<1.00	<50	32.4	2.91	0.28	<0.20	0.05	0.01	<10.0	<10.0	2.2	<1.0	<0.20
4	**Bjortjørn**	2509401-A	NaP	milky pqz	10.3	<0.30	<1.00	<50	40.4	1.42	<0.20	<0.20	0.05	0.01	42.6	<10.0	6.7	<1.0	<0.20
		2509401-B	"	"	9.6	0.31	<1.00	<50	57.5	1.58	<0.20	<0.20	0.05	0.01	47.5	<10.0	7.7	<1.0	<0.20
		2509401-C	"	"	3.7	0.41	2.57	192	44.4	1.78	<0.20	<0.20	1.42	0.02	59.4	<10.0	6.7	28.9	0.57
		2509401-D	"	"	5.5	<0.30	5.06	205	43.9	1.65	<0.20	<0.20	0.23	0.01	69.6	<10.0	7.7	10.8	0.22
		2509405-A	NaP	pqz in pl	9.9	<0.30	<1.00	<50	24.6	1.31	<0.20	<0.20	0.06	<0.01	<10.0	<10.0	5.3	<1.0	<0.20
		2509405-B	"	"	12.4	<0.30	<1.00	<50	41.1	1.43	<0.20	<0.20	0.05	0.01	<10.0	<10.0	6.1	<1.0	<0.20
5	**Haukemyrliene**	1609415-A	GP	smoky pqz	8.4	<0.30	1.54	<50	34.8	0.65	<0.20	<0.20	0.08	<0.01	<10.0	<10.0	10.0	<1.0	<0.20
		1609415-B	"	"	9.1	<0.30	1.29	<50	34.9	0.75	<0.20	<0.20	0.05	0.01	<10.0	<10.0	9.2	<1.0	<0.20
		1609416-A	GP	mobilised qz vein	6.8	<0.30	<1.00	<50	27.0	0.79	<0.20	<0.20	0.10	<0.01	<10.0	<10.0	8.8	<1.0	0.22
		1609416-B	"	"	5.5	<0.30	<1.00	<50	21.5	0.99	<0.20	<0.20	0.05	<0.01	<10.0	<10.0	8.5	<1.0	0.21
		1609417-A	PD	smoky comb pqz	1.7	0.46	1.13	<50	163.6	2.05	0.41	1.64	0.05	0.01	<10.0	<10.0	17.7	34.7	2.61
		1609417-B	"	"	1.6	<0.30	<1.00	<50	153.6	1.96	0.65	1.07	0.07	<0.01	<10.0	<10.0	15.2	30.3	0.95
		1609418-A	PD	smoky pqz in kfs	6.3	0.35	<1.00	<50	124.3	2.17	0.44	0.22	0.07	0.04	<10.0	<10.0	15.2	6.0	0.23
		1609418-B	"	"	4.6	<0.30	<1.00	<50	47.4	2.12	0.28	<0.20	0.08	0.01	<10.0	<10.0	14.0	1.8	<0.20
6	**Skåremyr**	1909401-A	ZoP	milky smoky pqz	7.8	<0.30	<1.00	<50	40.6	0.96	<0.20	<0.20	0.05	0.01	11.6	<10.0	6.5	5.4	0.34
		1909401-C	"	"	6.1	0.38	1.30	<50	35.8	1.08	<0.20	<0.20	0.06	0.01	20.7	<10.0	10.7	2.7	0.33

Appendix B. *Trace element concentrations in quartz determined by LA-ICP-MS. Continued.*

locality nr.	locality name	sample/ analyse nr.	pegmatite type	quartz type	Li	Be	B	Na	Al	Ge	Mn	Rb	Sr	Pb	Mg	P	Ti	K	Fe
6	Skåremyr	1909402-A	ZoP	milky smoky pqz	8.9	<0.30	<1.00	<50	41.2	1.59	<0.20	<0.20	0.07	<0.01	19.4	<10.0	6.6	<1.0	<0.20
		1909402-B	"	"	8.4	0.31	<1.00	<50	46.3	1.60	0.20	<0.20	0.08	<0.01	30.9	<10.0	7.2	1.4	0.32
		1909404-A	ZoP	clear smoky pqz	7.0	<0.30	1.51	<50	36.7	0.90	<0.20	<0.20	0.04	0.01	26.1	<10.0	8.1	<1.0	<0.20
		1909404-B	"	"	6.3	0.30	1.39	<50	51.6	1.08	0.26	<0.20	0.05	<0.01	<10.0	<10.0	7.5	5.0	0.60
		1909406-A	ZoP	clear smoky pqz	8.6	<0.30	1.01	<50	42.7	0.66	0.42	<0.20	0.06	<0.01	17.2	<10.0	10.6	1.7	<0.20
		1909406-B	"	"	8.1	<0.30	<1.00	<50	40.4	0.69	<0.20	<0.20	0.05	<0.01	<10.0	<10.0	8.1	<1.0	<0.20
		1909408-A	ZoP	milky smoky pqz	6.4	<0.30	<1.00	<50	31.9	0.79	<0.20	<0.20	0.06	<0.01	<10.0	<10.0	7.7	<1.0	<0.20
		1909408-B	"	"	7.3	<0.30	<1.00	<50	34.5	0.71	0.23	<0.20	0.06	<0.01	13.0	<10.0	8.4	<1.0	<0.20
		1909409-A	ZoP	milky smoky pqz	7.4	<0.30	<1.00	<50	35.3	0.84	<0.20	<0.20	0.06	<0.01	12.9	<10.0	8.3	<1.0	<0.20
		1909409-B	"	"	6.3	<0.30	<1.00	<50	29.3	0.87	<0.20	<0.20	0.05	<0.01	16.4	<10.0	6.8	<1.0	<0.20
		1909410-A	ZoP	milky smoky pqz	7.4	0.34	1.21	<50	33.4	0.85	<0.20	<0.20	0.05	<0.01	<10.0	<10.0	7.2	1.3	<0.20
		1909410-B	"	"	7.1	<0.30	<1.00	<50	35.2	0.90	<0.20	<0.20	0.07	0.01	<10.0	<10.0	6.8	<1.0	<0.20
		1909411-C	ZoP	milky smoky pqz	8.5	<0.30	<1.00	<50	51.3	0.92	<0.20	<0.20	0.06	0.01	29.3	<10.0	8.2	1.3	0.39
		1909411-D	"	"	8.1	<0.30	<1.00	<50	35.4	0.84	<0.20	<0.20	0.04	0.01	23.6	<10.0	7.6	1.0	<0.20
		1909401-D	ZoP	milky smoky pqz	3.1	<0.30	1.14	<50	23.3	1.11	<0.20	<0.20	0.20	0.04	21.0	<10.0	7.9	2.7	0.42
		1909411-A	ZoP	clear smoky pqz	6.5	<0.30	1.04	224	34.2	0.85	<0.20	<0.20	0.06	0.01	24.4	12.3	9.4	<1.0	0.29
		1909411-B	"	"	3.9	0.34	3.00	67	33.5	1.05	0.30	0.53	1.80	0.09	40.1	12.5	6.4	6.5	0.41
		1909412-A	ZoP	milky smoky pqz	0.5	<0.30	1.10	<50	38.9	1.47	<0.20	<0.20	0.06	<0.01	23.8	13.9	9.2	<1.0	0.43
		1909412-B	"	"	7.4	<0.30	<1.00	<50	31.5	1.35	<0.20	<0.20	0.06	<0.01	<10.0	<10.0	11.6	<1.0	0.21
		1909414-A	ZoP	pqz in pl	4.4	<0.30	<1.00	<50	40.5	2.70	<0.20	<0.20	0.04	<0.01	<10.0	<10.0	6.8	<1.0	<0.20
		1909414-B	"	"	4.1	<0.30	<1.00	<50	30.0	1.44	0.36	<0.20	0.06	<0.01	<10.0	<10.0	7.3	<1.0	<0.20
		1909415-A	ZoP	qz vein in pl	6.8	<0.30	<1.00	<50	28.9	1.31	0.52	<0.20	0.04	<0.01	<10.0	<10.0	8.1	1.3	2.30
		1909415-B	"	"	4.7	<0.30	<1.00	<50	39.8	1.34	0.10	<0.20	0.06	<0.01	<10.0	<10.0	10.8	<1.0	<0.20
		1909401-B	ZoP	sqz	1.0	<0.30	1.61	<50	15.3	1.04	1.33	<0.20	0.60	0.34	54.4	<10.0	0.8	6.8	7.48
		1909405-A		pqz in biotite granite dyke	6.5	<0.30	<1.00	<50	22.8	0.94	<0.20	<0.20	0.06	0.47	<10.0	<10.0	10.0	<1.0	<0.20
		1909405-B		"	4.6	<0.30	<1.00	<50	17.3	1.09	0.35	<0.20	0.07	<0.01	<10.0	<10.0	8.5	<1.0	<0.20
		1909403-A	PD	milky smoky pqz	2.4	<0.30	<1.00	<50	44.6	1.54	<0.20	<0.20	0.09	<0.01	11.9	<10.0	10.9	<1.0	<0.20
		1909403-B	"	"	7.0	<0.30	<1.00	<50	35.5	1.70	0.30	<0.20	0.06	<0.01	<10.0	<10.0	14.6	<1.0	<0.20

Appendix B. *Trace element concentrations in quartz determined by LA-ICP-MS. Continued.*

locality nr.	locality name	sample/ analyse nr.	pegmatite type	quartz type	Li	Be	B	Na	Al	Ge	Mn	Rb	Sr	Pb	Mg	P	Ti	K	Fe
7a	Sønnristjern	2009401-A	GP	milky smoky pqz	10.4	<0.30	<1.00	<50	38.5	1.14	<0.20	<0.20	0.08	<0.01	<10.0	<10.0	6.0	<1.0	<0.20
		2009401-B	"	"	10.6	<0.30	<1.00	<50	31.9	0.95	<0.20	<0.20	0.06	<0.01	<10.0	<10.0	7.8	<1.0	<0.20
		2009402-C	GP	milky smoky pqz	6.6	<0.30	1.31	<50	29.9	1.53	0.21	<0.20	0.06	0.01	<10.0	<10.0	4.0	<1.0	<0.20
		2009402-D	"	"	7.1	<0.30	<1.00	<50	35.4	1.52	<0.20	<0.20	0.05	0.01	<10.0	<10.0	4.8	<1.0	<0.20
		2009404-A	GP	milky smoky pqz	10.2	<0.30	<1.00	<50	46.2	1.38	0.22	<0.20	0.04	<0.01	<10.0	12.2	7.2	<1.0	0.38
		2009404-B	"	"	10.1	<0.30	<1.00	<50	36.9	1.37	<0.20	<0.20	0.06	<0.01	<10.0	<10.0	9.5	<1.0	<0.20
		2009405-A	GP	milky smoky pqz	8.9	<0.30	1.15	<50	36.9	1.26	<0.20	<0.20	0.08	<0.01	<10.0	<10.0	8.5	<1.0	0.47
		2009405-B	"	"	10.4	<0.30	1.42	<50	44.5	1.40	0.32	<0.20	0.06	<0.01	<10.0	<10.0	8.9	<1.0	<0.20
		2009406A-A	ZoP	smoky pqz in kfs	4.9	<0.30	1.10	<50	38.6	0.93	<0.20	<0.20	0.05	<0.01	<10.0	<10.0	5.4	<1.0	<0.20
		2009406A-B	"	"	4.2	<0.30	<1.00	<50	30.1	0.85	0.26	<0.20	0.06	<0.01	10.3	<10.0	5.6	<1.0	<0.20
		2009406B-A	ZoP	smoky pqz in pl	8.1	<0.30	1.11	<50	31.6	0.79	<0.20	<0.20	0.06	<0.01	<10.0	<10.0	5.3	<1.0	<0.20
		2009406B-B	"	"	10.7	<0.30	1.40	<50	36.5	0.81	0.23	<0.20	0.05	0.01	<10.0	<10.0	4.9	<1.0	0.26
		2009407-A	ZoP	milky smoky pqz	7.5	<0.30	2.47	<50	32.1	2.05	<0.20	<0.20	0.07	<0.01	24.1	<10.0	6.1	<1.0	0.20
		2009407-B	"	"	9.1	<0.30	3.09	<50	42.9	2.10	<0.20	<0.20	0.05	<0.01	19.7	<10.0	7.1	<1.0	<0.20
		2009409-C	ZoP	milky smoky pqz	8.4	<0.30	1.40	<50	38.8	1.80	<0.20	<0.20	0.05	<0.01	16.0	<10.0	5.8	<1.0	<0.20
		2009409-C1	"	"	7.9	<0.30	1.81	<50	32.5	1.89	<0.20	<0.20	0.04	<0.01	12.8	<10.0	4.7	<1.0	<0.20
		2009410-A	ZoP	milky smoky pqz	6.8	<0.30	1.17	<50	30.2	1.90	<0.20	<0.20	0.04	0.01	15.3	<10.0	5.6	<1.0	<0.20
		2009410-B	"	"	7.3	<0.30	2.11	<50	41.0	1.99	<0.20	<0.20	0.06	0.01	21.0	<10.0	6.2	<1.0	0.21
		2009411-A	ZoP	milky smoky pqz	8.6	<0.30	1.11	<50	36.4	1.63	<0.20	<0.20	0.06	<0.01	36.1	<10.0	6.5	<1.0	<0.20
		2009411-B	"	"	7.6	<0.30	<1.00	<50	39.4	1.76	<0.20	<0.20	0.04	<0.01	26.0	<10.0	5.9	<1.0	<0.20
		2009402-A	ZoP	milky smoky pqz	7.0	<0.30	1.39	<50	29.4	1.64	0.33	<0.20	0.04	0.01	<10.0	<10.0	5.0	<1.0	<0.20
		2009402-B	"	"	6.7	0.35	1.60	<50	32.1	1.85	<0.20	<0.20	0.17	0.01	11.8	<10.0	6.1	<1.0	<0.20
		2009404-C	ZoP	milky smoky pqz	8.8	<0.30	<1.00	<50	42.1	1.60	<0.20	<0.20	0.05	0.01	<10.0	<10.0	7.3	2.3	0.51
		2009404-D	"	"	7.5	<0.30	<1.00	<50	29.0	1.54	<0.20	<0.20	0.06	0.01	10.1	<10.0	6.9	<1.0	<0.20
		2009409-A	ZoP	milky smoky pqz	7.0	<0.30	4.93	238	31.0	1.69	0.76	1.73	6.80	0.11	32.4	<10.0	5.2	23.7	<0.20
		2009409-B	"	"	7.1	<0.30	1.88	<50	39.8	1.74	<0.20	<0.20	0.05	<0.01	18.0	<10.0	6.9	<1.0	0.20
		2009408-A		pqz in biotite granite dyke	6.8	<0.30	<1.00	<50	16.0	0.98	<0.20	<0.20	0.04	0.01	<10.0	<10.0	5.5	<1.0	<0.20
		2009408-B		"	2.5	<0.30	<1.00	<50	17.2	1.03	<0.20	<0.20	0.05	0.01	21.8	<10.0	5.8	<1.0	<0.20

Appendix B. *Trace element concentrations in quartz determined by LA-ICP-MS. Continued.*

locality nr.	locality name	sample/ analyse nr.	pegmatite type	quartz type	Li	Be	B	Na	Al	Ge	Mn	Rb	Sr	Pb	Mg	P	Ti	K	Fe
7b	**Sønnristjern**	2109411-A	GP	milky smoky pqz	7.3	<0.30	2.03	<50	36.7	2.13	<0.20	<0.20	0.02	<0.01	<10.0	<10.0	5.1	<1.0	<0.20
		2109411-B	"	"	7.8	<0.30	1.28	<50	43.1	1.51	<0.20	<0.20	0.02	<0.01	<10.0	<10.0	5.4	<1.0	<0.20
7c	**Sønnristjern**	2109412-A	GP	milky smoky pqz	8.1	<0.30	2.09	<50	32.4	0.73	<0.20	<0.20	0.02	<0.01	<10.0	<10.0	7.6	<1.0	<0.20
		2109412-B	"	"	8.1	<0.30	1.48	<50	34.9	1.03	0.22	<0.20	0.06	<0.01	<10.0	<10.0	7.3	1.1	0.26
7d	**Sønnristjern**	2109413-A	GP	milky smoky pqz	7.2	<0.30	2.33	<50	40.3	1.41	<0.20	<0.20	0.04	<0.01	<10.0	<10.0	5.3	<1.0	0.26
		2109413-B	"	"	7.8	<0.30	2.45	<50	49.6	1.51	0.30	<0.20	0.06	0.01	<10.0	<10.0	5.9	<1.0	<0.20
7e	**Sønnristjern**	2109414-A	GP	milky smoky pqz	8.0	<0.30	3.82	<50	46.4	1.54	<0.20	<0.20	0.03	<0.01	12.2	<10.0	6.5	<1.0	0.25
		2109414-B	"	"	6.4	<0.30	2.46	<50	32.5	1.60	0.33	<0.20	0.05	<0.01	<10.0	<10.0	6.2	<1.0	0.35
7f	**Sønnristjern**	2109415-A	GP	milky smoky pqz	8.9	<0.30	1.62	<50	27.9	1.68	0.51	<0.20	0.02	0.02	20.9	<10.0	7.8	<1.0	<0.20
		2109415-B	"	"	10.1	<0.30	1.93	<50	41.8	1.75	<0.20	<0.20	0.03	0.01	<10.0	<10.0	7.0	<1.0	0.53
8	**Lille Kleivmyr**	2109406-A	GP	milky smoky pqz	12.5	<0.30	<1.00	<50	45.6	1.27	0.24	<0.20	0.05	0.01	<10.0	10.6	3.2	<1.0	<0.20
		2109406-B	"	"	11.2	<0.30	<1.00	<50	40.4	1.20	<0.20	<0.20	0.04	0.01	<10.0	<10.0	4.5	1.6	<0.20
		2109409-A	GP	milky smoky pqz	13.4	<0.30	1.89	<50	59.9	1.18	<0.20	<0.20	0.04	0.02	<10.0	<10.0	5.7	<1.0	<0.20
		2109409-B	"	"	14.3	<0.30	1.30	<50	56.2	1.35	<0.20	<0.20	0.03	0.01	<10.0	<10.0	4.8	<1.0	<0.20
		2109402-A	GP	pqz in pl	10.4	<0.30	<1.00	<50	45.1	1.26	<0.20	<0.20	0.06	0.01	<10.0	<10.0	5.7	<1.0	<0.20
		2109402-B	"	"	12.9	<0.30	1.28	<50	52.8	1.05	<0.20	<0.20	0.04	0.01	<10.0	<10.0	4.7	<1.0	0.23
		2109404-A	GP	milky smoky pqz	11.1	<0.30	1.02	<50	36.1	1.25	0.21	<0.20	0.03	0.01	<10.0	<10.0	3.2	1.7	0.34
		2109404-D	"	"	13.3	<0.30	<1.00	<50	56.8	1.29	<0.20	<0.20	0.04	0.01	<10.0	<10.0	2.7	<1.0	0.24
		2109410-A	GP	milky smoky pqz	8.3	<0.30	1.30	<50	41.7	1.75	<0.20	<0.20	0.04	0.01	14.1	12.6	7.7	<1.0	<0.20
		2109410-D	"	"	0.4	<0.30	1.03	<50	37.5	2.23	<0.20	<0.20	0.13	0.03	20.6	13.5	4.1	7.7	<0.20
		2209407-A	GP	milky smoky pqz	11.1	<0.30	1.44	<50	54.4	1.44	<0.20	<0.20	0.02	0.01	<10.0	<10.0	6.0	<1.0	<0.20
		2209407-B	"	"	12.4	<0.30	1.07	<50	48.3	1.41	<0.20	<0.20	0.03	0.01	14.6	<10.0	5.8	<1.0	<0.20
		2109404-B	GP	milky smoky pqz	6.4	<0.30	1.06	<50	44.9	1.38	0.22	<0.20	0.07	0.01	26.0	<10.0	2.1	1.9	0.29
		2109404-C	"	"	5.5	<0.30	1.19	<50	50.1	1.48	<0.20	<0.20	0.08	<0.01	40.7	<10.0	2.4	1.0	<0.20
		2109410-B	GP	milky smoky pqz	3.5	<0.30	2.07	152	37.6	2.18	<0.20	<0.20	0.32	0.01	40.6	<10.0	7.6	13.3	0.36
		2109410-C	"	"	8.7	<0.30	<1.00	<50	38.4	2.21	0.21	<0.20	0.04	0.01	<10.0	<10.0	7.0	<1.0	0.21
		2109408A-A	GP	smoky pqz in kfs	4.9	<0.30	<1.00	<50	31.1	1.18	<0.20	<0.20	0.05	<0.01	32.7	13.1	5.3	1.7	<0.20
		2109408A-B	"	"	2.0	<0.30	<1.00	<50	38.7	1.19	<0.20	<0.20	0.04	0.02	50.2	11.2	6.1	1.9	<0.20

Appendix B. *Trace element concentrations in quartz determined by LA-ICP-MS. Continued.*

locality nr.	locality name	sample/ analyse nr.	pegmatite type	quartz type	Li	Be	B	Na	Al	Ge	Mn	Rb	Sr	Pb	Mg	P	Ti	K	Fe
8	**Lille Kleivmyr**	2109408B-A	GP	smoky pqz in pl	10.4	<0.30	1.87	<50	36.3	1.21	<0.20	<0.20	0.03	0.01	<10.0	<10.0	6.1	<1.0	<0.20
0		2109408B-B	"	"	10.0	<0.30	1.38	<50	42.3	1.25	<0.20	<0.20	0.03	<0.01	<10.0	<10.0	7.6	<1.0	<0.20
		2109401-A	GP	smoky pqz in pl	9.3	<0.30	<1.00	<50	34.5	1.37	<0.20	<0.20	0.04	0.01	<10.0	<10.0	3.8	<1.0	<0.20
		2109401-B	"	"	10.6	<0.30	<1.00	<50	38.8	1.61	<0.20	<0.20	0.05	0.01	<10.0	<10.0	3.3	<1.0	<0.20
		2209408-A		pqz in garnet granite	11.0	<0.30	1.08	<50	34.9	1.31	<0.20	<0.20	0.04	0.01	<10.0	<10.0	3.6	<1.0	<0.20
		2209408-B		"	11.2	<0.30	<1.00	<50	35.5	1.42	<0.20	<0.20	0.06	0.01	<10.0	<10.0	3.8	<1.0	<0.20
		2109403-A		pqz in garnet granite	9.8	<0.30	<1.00	<50	39.5	1.18	<0.20	<0.20	0.04	0.01	<10.0	<10.0	3.3	<1.0	<0.20
		2109403-B		"	10.4	<0.30	<1.00	<50	33.7	1.13	<0.20	<0.20	0.05	0.01	<10.0	<10.0	2.5	<1.0	<0.20
		2109407-C		pqz in garnet granite	13.0	<0.30	<1.00	<50	48.3	1.72	0.23	<0.20	0.04	0.01	<10.0	<10.0	4.9	<1.0	<0.20
		2109407-D		"	11.9	<0.30	<1.00	<50	44.9	1.72	<0.20	<0.20	0.04	0.01	<10.0	<10.0	5.6	<1.0	0.27
		2109407-A		"	3.1	<0.30	<1.00	<50	36.9	1.77	<0.20	<0.20	0.05	0.01	84.2	<10.0	3.2	<1.0	0.29
		2109407-B		"	8.8	<0.30	<1.00	<50	43.5	1.74	<0.20	<0.20	0.08	0.01	<10.0	<10.0	3.5	<1.0	0.24
9	**Våtåskammen**	1709401A-A	PGr	smoky pqz	10.7	<0.30	<1.00	<50	35.5	0.92	<0.20	<0.20	0.06	0.01	<10.0	<10.0	4.9	<1.0	<0.20
		1709401A-B	"	"	11.0	<0.30	<1.00	<50	37.3	0.94	<0.20	<0.20	0.06	0.01	<10.0	<10.0	4.4	1.1	0.36
		1709401B-A	PGr	smoky pqz	9.0	<0.30	<1.00	<50	34.6	0.75	<0.20	<0.20	0.05	<0.01	<10.0	<10.0	2.6	<1.0	<0.20
		1709401B-B	"	"	10.3	<0.30	<1.00	<50	30.0	0.90	<0.20	<0.20	0.08	<0.01	<10.0	<10.0	3.5	<1.0	<0.20
10	**Vaselona**	2309404-A	sheared ZoP	smoky pqz	5.6	<0.30	<1.00	<50	41.5	2.52	<0.20	<0.20	0.04	<0.01	<10.0	<10.0	17.4	7.6	0.42
		2309404-B	"	"	4.2	<0.30	<1.00	<50	39.8	3.03	<0.20	<0.20	0.06	<0.01	<10.0	<10.0	15.2	4.4	0.60
11	**Fossheia, vest**	2309402-A	sheared ZoP	smoky pqz	0.4	<0.30	<1.00	<50	25.9	2.40	0.33	<0.20	0.29	0.13	66.1	<10.0	29.9	3.8	0.76
		2309402-B	"	"	0.2	<0.30	<1.00	<50	26.5	2.45	0.35	<0.20	0.30	0.21	50.4	11.4	28.1	4.1	1.09
		2309403-A		pqz in adamelite	3.2	<0.30	<1.00	<50	9.6	0.84	<0.20	<0.20	0.06	<0.01	<10.0	<10.0	23.8	<1.0	<0.20
		2309403-B		"	1.7	<0.30	<1.00	<50	14.9	0.84	0.20	<0.20	0.07	0.01	13.4	<10.0	22.7	<1.0	0.26
12	**Fossheia, øst**	1609411-A	HP	clear smoky pqz	3.4	<0.30	<1.00	<50	36.8	1.37	<0.20	<0.20	0.08	0.01	32.0	16.4	15.1	1.0	0.25
		1609411-B	"	"	3.1	<0.30	<1.00	<50	59.6	1.56	<0.20	<0.20	0.04	0.01	32.2	13.1	17.2	2.1	0.49
		1609412-A	HP	smoky pqz	7.5	<0.30	1.35	<50	37.6	1.07	<0.20	<0.20	0.04	<0.01	<10.0	<10.0	15.7	<1.0	0.27
		1609412-B	"	"	8.2	<0.30	1.00	<50	44.7	1.10	<0.20	<0.20	0.05	<0.01	<10.0	<10.0	15.4	<1.0	0.27
		1609413-A	HP	pqz in kfs	2.8	<0.30	2.09	<50	27.8	2.44	<0.20	<0.20	0.07	<0.01	<10.0	<10.0	15.4	<1.0	<0.20
		1609413-B	"	"	6.9	<0.30	1.27	<50	38.0	1.61	<0.20	<0.20	0.07	0.01	<10.0	<10.0	21.1	<1.0	0.23

Appendix B. *Trace element concentrations in quartz determined by LA-ICP-MS. Continued.*

locality nr.	locality name	sample/ analyse nr.	pegmatite type	quartz type	Li	Be	B	Na	Al	Ge	Mn	Rb	Sr	Pb	Mg	P	Ti	K	Fe
13	**Husefjell**	1609402-A		pqz in Herefoss granite	7.2	<0.30	2.60	<50	71.3	0.95	0.43	0.26	0.16	0.05	<10.0	<10.0	36.6	9.8	1.74
		1609402-B		"	7.3	<0.30	1.69	<50	97.4	0.82	0.34	<0.20	0.15	0.03	<10.0	<10.0	33.8	9.6	0.56
14	**Metveit**	2309405-A	HP	smoky pqz	4.1	<0.30	<1.00	<50	105.4	1.00	<0.20	<0.20	0.04	0.03	14.6	15.3	18.3	19.5	0.46
		2309405-B	"	"	3.4	<0.30	<1.00	<50	95.1	1.11	0.33	<0.20	0.04	0.02	14.2	10.9	21.7	19.2	0.38
		1609405-A		pqz in Herefoss granite	4.4	<0.30	1.30	<50	77.6	0.75	0.22	<0.20	0.24	0.04	<10.0	<10.0	22.2	10.6	1.16
		1609405-B		"	4.8	<0.30	<1.00	<50	61.7	0.83	<0.20	<0.20	0.11	0.02	<10.0	<10.0	24.9	6.2	0.89
		2309407-A		pqz in Herefoss granite	4.1	<0.30	1.06	<50	26.4	0.78	<0.20	<0.20	0.04	0.00	12.8	<10.0	25.6	<1.0	0.54
		2309407-B		"	4.1	<0.30	1.06	103	23.6	0.89	<0.20	<0.20	1.16	0.02	28.0	<10.0	28.1	5.4	<0.20
15	**Heimdal**	1609409-A	HP	milky smoky pqz	2.1	<0.30	<1.00	<50	18.1	0.64	<0.20	<0.20	0.10	0.01	20.5	<10.0	19.1	1.3	0.51
		1609409-D	"	"	4.4	<0.30	<1.00	<50	32.9	0.81	<0.20	<0.20	0.05	0.01	13.2	<10.0	30.8	2.1	0.60
		1609409-B	"	"	2.9	<0.30	<1.00	<50	29.9	0.89	0.28	0.71	0.79	0.68	17.4	<10.0	25.2	7.0	1.24
		1609409-C	"	"	3.0	<0.30	<1.00	234	18.3	0.65	0.73	0.29	6.14	0.90	28.0	<10.0	30.1	25.0	7.19
		2309410-A		pqz in Herefoss granite	4.2	<0.30	1.08	<50	24.2	0.64	<0.20	<0.20	0.05	0.02	<10.0	<10.0	33.2	<1.0	<0.20
		2309410-B		"	5.0	<0.30	<1.00	<50	22.7	0.79	<0.20	<0.20	0.04	0.01	<10.0	<10.0	30.2	<1.0	<0.20

Appendix C. *Concentration diagrams of Al vs. Ti in quartz determined by LA-ICP-MS.*

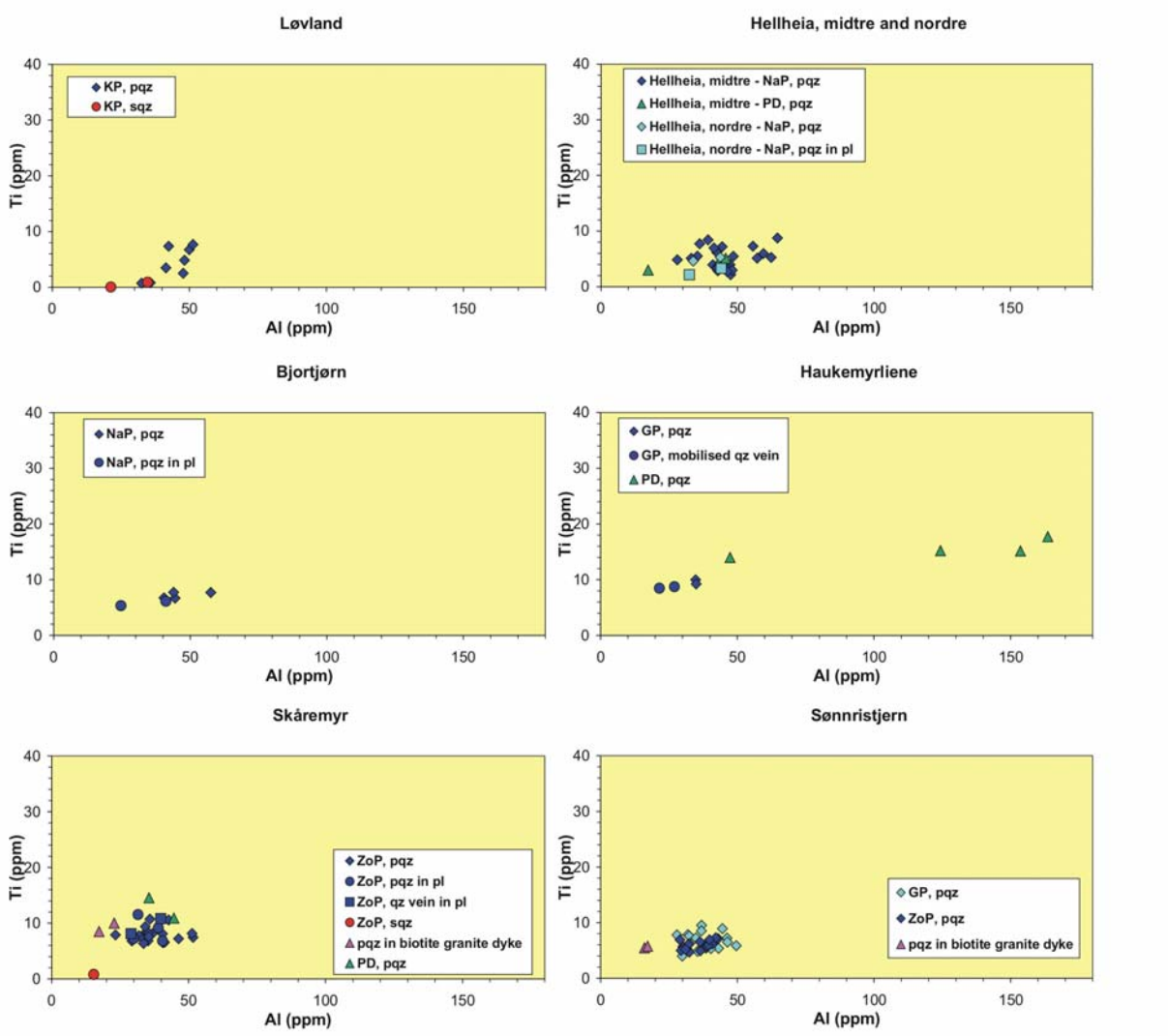

Appendix C. *Concentration diagrams of Al vs. Ti in quartz determined by LA-ICP-MS. Continued.*

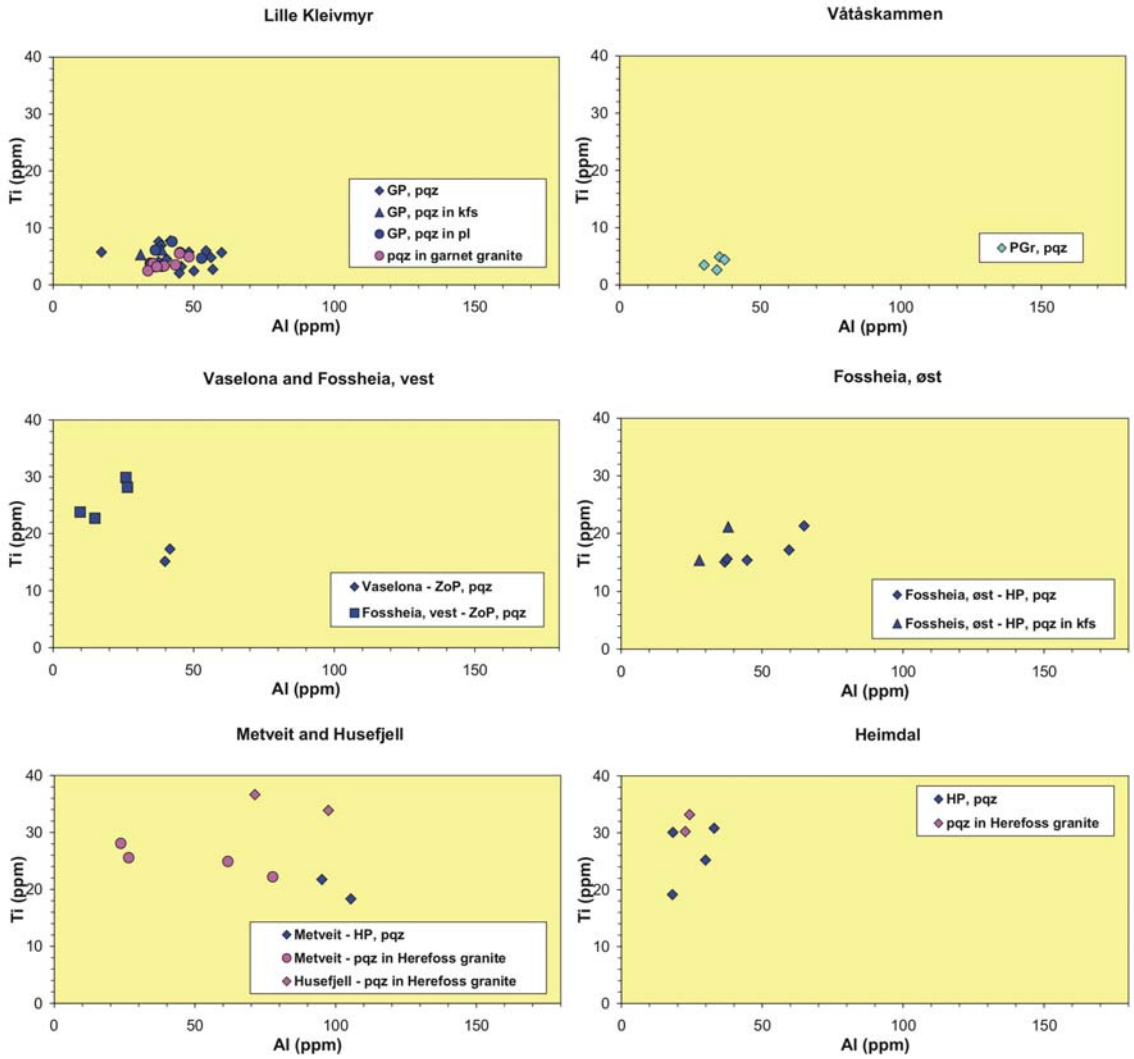

Appendix D. *Concentration diagrams of Li vs. Ge in quartz determined by LA-ICP-MS.*

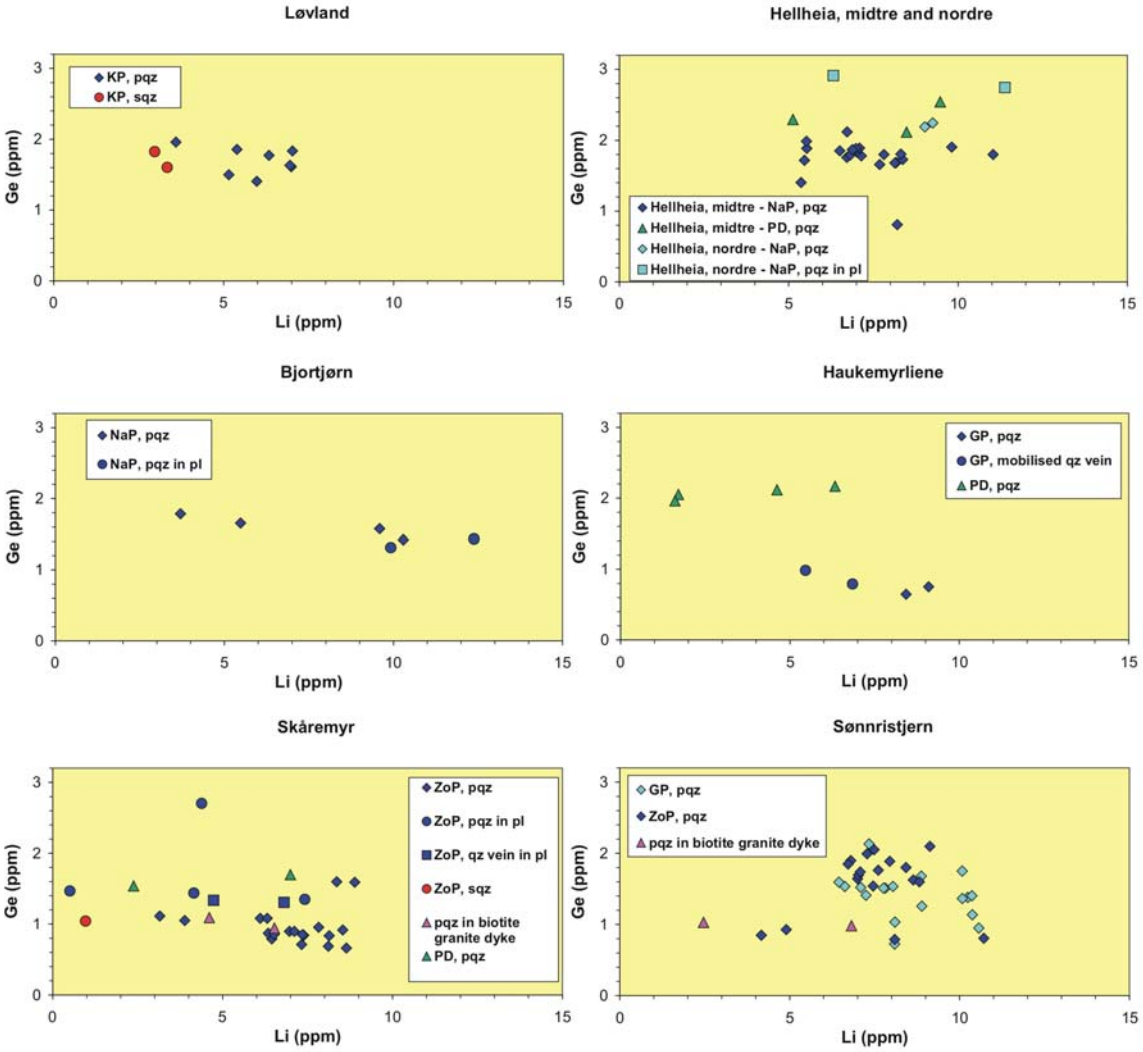

Appendix D. *Concentration diagrams of Li vs. Ge in quartz determined by LA-ICP-MS. Continued.*

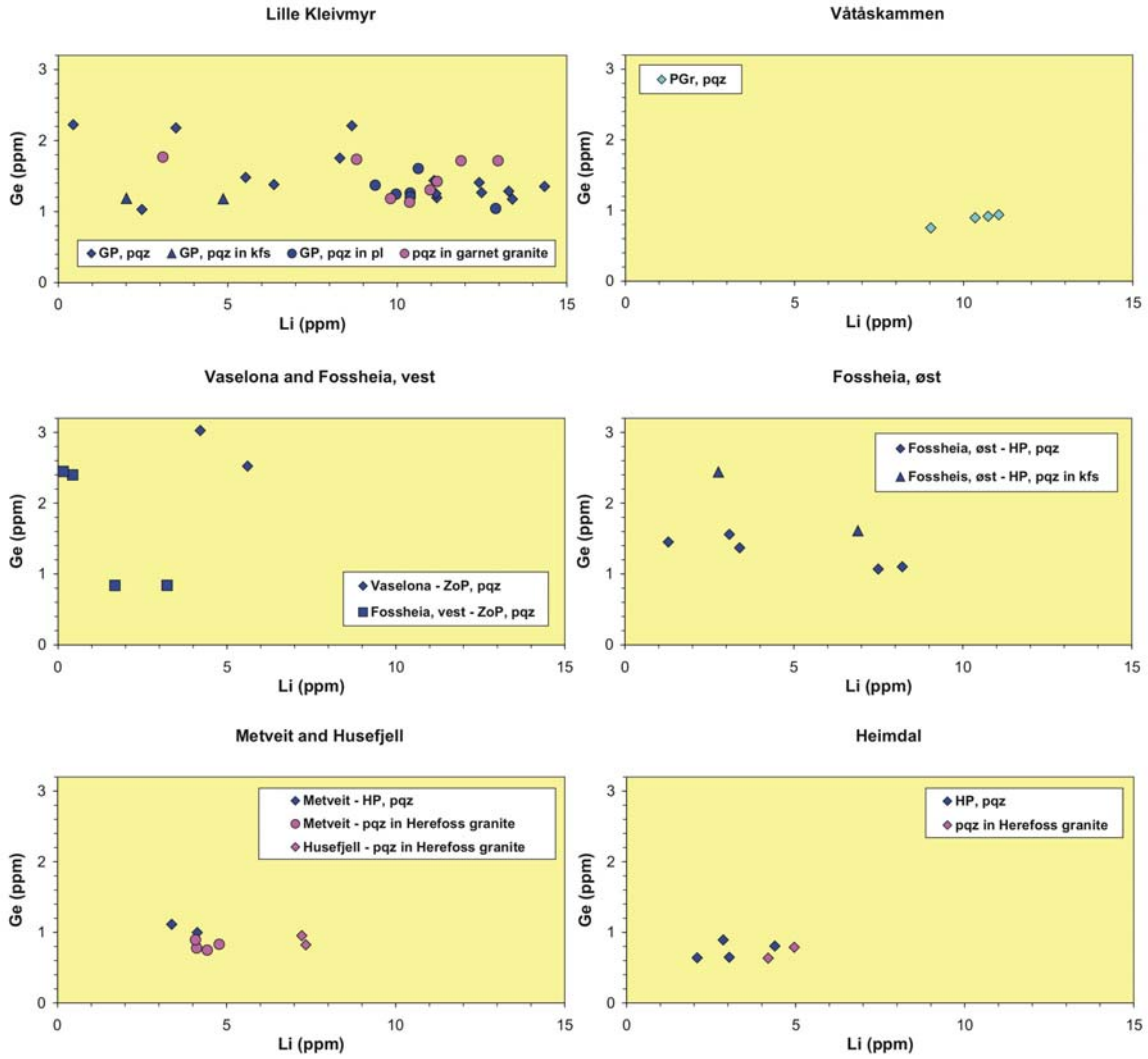

Appendix E. *Element concentrations of K-feldspar determined by XRF.*

locality nr.	locality name	sample nr.	pegmatite type	major and minor elements (wt.%)										trace elements (ppm)					
				SiO_2	Al_2O3	Fe_2O_3	TiO_2	CaO	Na_2O	K_2O	P_2O_5	LOI	total	Sr	Rb	Pb	Cr	Ba	Ga
1	**Løvland**	2209401k	KP	65.07	18.40	0.13	<0.01	0.07	2.26	13.05	0.02	0.14	99.16	20	918	182	63	42	27
		2209403k	KP	65.95	18.49	0.12	<0.01	0.08	2.29	12.94	0.01	0.51	100.40	45	811	188	52	215	25
		2209404k	KP	64.84	18.18	0.12	<0.01	0.07	2.26	12.97	0.02	0.15	98.63	19	923	187	56	58	26
		2209405k	KP	64.33	18.25	0.09	<0.01	0.06	2.16	13.35	<0.01	0.14	98.41	22	963	192	47	60	27
2	**Hellheia, midtre**	1809414k	PD	64.76	18.43	0.15	<0.01	0.08	2.15	13.01	0.02	0.19	98.83	17	1704	156	102	47	28
3	**Hellheia, nordre**	2409401k	NaP	65.78	18.59	0.08	<0.01	0.07	2.50	12.98	0.02	0.06	100.10	22	1406	136	46	69	30
6	**Skåremyr**	1909401k	ZoP	64.62	18.48	0.09	<0.01	0.07	1.96	13.44	0.02	0.10	98.81	76	629	100	66	876	26
		1909404k	ZoP	64.91	18.49	0.12	<0.01	0.17	1.80	13.51	0.01	0.19	99.26	88	604	107	80	651	18
		1909403k	PD	65.06	18.70	0.20	<0.01	0.13	2.11	13.20	<0.01	0.21	99.66	26	1111	122	110	96	40
7a	**Sønnristjern**	2009402k	ZoP	64.66	18.51	0.12	0.01	0.08	1.84	13.61	0.02	0.14	99.05	181	452	92	77	1007	11
		2009403k	ZoP	64.38	18.47	0.10	<0.01	0.12	1.86	13.68	0.01	0.17	98.81	180	458	85	50	1173	<10
		2009404k	ZoP	64.48	18.46	0.14	<0.01	0.16	1.75	13.78	<0.01	0.23	99.07	152	513	121	96	620	10
		2009405k	ZoP	64.96	18.41	0.10	<0.01	0.12	1.82	13.56	0.01	0.15	99.19	158	494	123	84	593	14
		2009406k	ZoP	65.13	18.42	0.12	<0.01	0.08	1.93	13.69	<0.01	0.14	99.57	171	492	108	95	701	<10
		2009407k	ZoP	64.84	18.53	0.09	<0.01	0.09	1.74	13.92	<0.01	0.11	99.38	72	711	167	65	125	13
		2009409k	ZoP	64.83	18.44	0.11	<0.01	0.06	1.71	13.87	0.01	0.18	99.27	65	853	225	58	168	18
7b	**Sønnristjern**	2009411k	ZoP	64.82	18.51	0.08	<0.01	0.13	1.82	13.70	<0.01	0.15	99.26	82	780	200	57	356	19
		2109411k	GP	64.92	18.57	0.10	<0.01	0.07	1.82	13.79	<0.01	0.11	99.39	207	405	90	51	1391	<10
7c	**Sønnristjern**	2109412k	GP	61.31	17.32	0.12	<0.01	0.13	1.87	13.53	0.02	0.35	94.71	224	481	88	66	1460	<10
7d	**Sønnristjern**	2109413k	GP	64.90	18.39	0.10	<0.01	0.06	1.86	13.68	0.02	0.13	99.17	224	407	75	57	1945	<10
7e	**Sønnristjern**	2109414k	GP	64.67	18.45	0.08	<0.01	0.07	1.88	13.46	0.01	0.17	98.84	76	735	200	50	466	11
8	**Lille Kleivmyr**	2109401ak	GP	64.67	18.4	0.08	<0.01	0.07	1.56	14.03	<0.01	0.19	99.05	78	631	150	75	73	17
		2109401bk	GP	64.92	18.54	0.10	<0.01	0.08	1.91	13.58	0.01	0.19	99.39	51	842	166	67	134	27
		2109402ak	GP	64.79	18.54	0.17	<0.01	0.07	2.11	13.22	0.01	0.27	99.22	33	905	225	103	133	25
		2109403k	GP	64.55	18.42	0.05	<0.01	0.07	2.26	13.01	0.01	0.12	98.53	21	887	156	58	24	17

Appendix E. *Element concentrations of K-feldspar determined by XRF. Continued.*

locality nr.	locality name	sample nr.	pegmatite type	major and minor elements (wt.%)										trace elements (ppm)					
				SiO_2	Al_2O3	Fe_2O_3	TiO_2	CaO	Na_2O	K_2O	P_2O_5	LOI	total	Sr	Rb	Pb	Cr	Ba	Ga
8	**Lille Kleivmyr**	2109404k	GP	64.09	18.26	0.09	<0.01	0.07	1.85	13.54	<0.01	0.10	98.05	22	929	151	74	39	23
		2109406k	GP	64.96	18.44	0.11	<0.01	0.16	1.08	13.59	<0.01	0.16	99.26	53	839	180	73	89	20
		2109408k	GP	64.95	18.55	0.11	<0.01	0.14	2.21	13.02	0.01	0.18	99.21	149	672	99	61	1118	14
		2109409k	GP	64.80	18.46	0.05	<0.01	0.07	2.12	13.25	0.01	0.07	98.89	85	705	163	67	402	21
		2109410k	GP	64.26	18.29	0.09	<0.01	0.15	1.99	13.39	0.01	0.19	98.38	98	688	116	52	519	13
		2209407k	GP	64.72	18.45	0.07	<0.01	0.07	1.94	13.60	0.01	0.13	99	45	861	134	42	174	28
		2109401p	GP	64.74	18.62	0.11	<0.01	0.08	2.00	13.31	0.02	0.14	99.05	227	430	83	81	2163	<10
9	**Våtåskammen**	1709401k	PGr	64.83	17.89	0.26	<0.01	0.07	1.68	13.45	0.01	0.36	98.57	81	598	92	228	120	11
10	**Vaselona**	2309404k	sheared ZoP	64.49	18.21	0.06	0.01	0.07	2.76	12.54	0.02	0.07	98.26	63	1342	141	38	353	28
11	**Fossheia, vest**	2309402k	sheared ZoP	65.16	18.46	0.11	<0.01	0.07	1.91	13.52	0.02	0.13	99.38	121	708	61	58	1326	19
12	**Fossheia, øst**	2309401k	HP	64.63	18.45	0.15	<0.01	0.12	1.79	13.73	<0.01	0.20	99.11	104	676	51	59	1026	26
14	**Metveit**	2309405k	HP	65.92	18.64	0.12	<0.01	0.22	2.64	12.25	0.02	0.10	99.94	198	522	56	44	873	20
15	**Heimdal**	1609409k	HP	65.30	17.82	0.62	0.02	0.21	1.95	12.34	0.01	0.29	98.62	507	309	47	260	3691	15

Appendix F. *Element concentrations of plagioclase determined by XRF.*

locality nr.	locality name	sample nr.	pegmatite type	major and minor elements (wt.%)										trace elements (ppm)					
				SiO_2	Al_2O_3	Fe_2O3	TiO_2	CaO	Na_2O	K_2O	P_2O_5	LOI	total	Sr	Rb	Pb	Cr	Ba	Ga
1	**Løvland**	2209401p	KP	65.42	22.14	0.23	<0.01	2.89	9.07	1.11	0.01	0.33	101.19	55	25	52	92	<10	43
		2209403p	KP	63.59	21.05	0.21	<0.01	2.30	9.46	1.16	0.01	0.33	98.06	44	55	61	73	27	44
		2209404p	KP	64.22	21.71	0.37	0.03	2.85	9.34	0.61	0.02	0.37	99.53	55	13	55	79	11	32
		2209405p	KP	63.73	21.14	0.16	<0.01	2.22	9.54	1.09	0.02	0.41	98.25	44	50	57	61	28	51
2	**Hellheia, midtre**	1809402p	NaP	64.27	22.13	0.20	<0.01	4.28	7.70	0.14	0.01	0.41	99.09	396	<5	27	149	44	22
		1809407p	NaP	63.42	22.63	0.13	<0.01	4.52	7.73	0.20	<0.01	0.30	98.95	384	<5	17	129	47	24
		1809408p	NaP	65.94	20.99	0.21	<0.01	4.42	6.94	0.16	0.01	0.33	98.99	393	6	22	207	45	30
		1809310p	NaP	64.83	21.78	0.14	<0.01	3.47	8.34	0.18	0.02	0.24	98.98	302	5	19	155	53	30
		1809411p	NaP	61.91	23.64	0.19	<0.01	4.64	8.11	0.14	<0.01	0.45	99.08	439	<5	29	128	47	27
3	**Hellheia, nordre**	2409401p	NaP	65.37	20.24	0.04	<0.01	1.45	10.15	0.88	0.02	0.23	98.28	37	29	36	43	41	54
4	**Bjortjørn**	2509401p	NaP	64.87	21.57	0.10	<0.01	2.68	9.56	0.65	0.01	0.44	99.81	95	13	80	55	19	31
6	**Skåremyr**	1909401p	ZoP	63.12	22.82	0.18	<0.01	3.79	8.51	0.41	<0.01	0.26	99.06	234	6	45	136	54	18
		1909404p	ZoP	63.39	22.96	0.12	<0.01	3.84	8.52	0.40	0.01	0.25	99.43	235	9	39	106	67	16
		1909406p	ZoP	64.75	21.30	0.09	<0.01	2.28	8.98	0.98	<0.01	0.33	98.66	63	27	33	85	55	26
		1909410p	ZoP	66.20	20.55	0.16	<0.01	1.33	9.20	1.39	0.01	0.31	99.09	28	46	28	112	52	32
7a	**Sønnristjern**	2009401p	ZoP	62.37	23.80	0.14	<0.01	5.01	8.50	0.48	<0.01	0.27	100.51	271	<5	30	73	35	21
		2009402p	ZoP	61.96	23.39	0.19	<0.01	4.74	8.65	0.54	0.01	0.24	99.66	201	10	40	108	23	28
		2009404p	ZoP	62.56	23.21	0.22	<0.01	4.53	8.06	0.63	<0.01	0.20	99.41	181	9	40	159	27	26
		2009405p	ZoP	62.12	22.95	0.26	<0.01	4.42	8.11	0.64	0.01	0.18	98.66	173	8	37	156	<10	26
		2009406p	ZoP	62.45	23.08	0.34	<0.01	4.41	8.08	0.58	<0.01	0.32	99.28	194	10	37	204	14	28
		2009407p	ZoP	63.51	22.34	0.13	<0.01	3.55	8.66	0.60	<0.01	0.26	99.00	55	5	84	114	14	38
		2009409p	ZoP	63.93	22.19	0.12	<0.01	3.31	8.64	0.67	0.01	0.28	99.10	40	13	83	131	<10	38
		2009411p	ZoP	63.36	22.21	0.16	<0.01	3.52	8.43	0.74	<0.01	0.42	98.81	49	11	77	101	<10	38
		2009412p	ZoP	62.76	22.90	0.29	<0.01	4.10	8.31	0.59	<0.01	0.32	99.23	121	5	44	160	<10	35

Appendix F. *Element concentrations of plagioclase determined by XRF. Continued.*

locality nr.	locality name	sample nr.	pegmatite type	major and minor elements (wt.%)										trace elements (ppm)					
				SiO_2	Al_2O_3	Fe_2O3	TiO_2	CaO	Na_2O	K_2O	P_2O_5	LOI	total	Sr	Rb	Pb	Cr	Ba	Ga
7b	**Sønnristjern**	2109411p	GP	62.62	23.47	0.13	<0.01	4.59	8.55	0.59	<0.01	0.28	100.22	205	9	33	70	27	23
7c	**Sønnristjern**	2109412p	GP	62.18	22.93	0.27	<0.01	4.55	7.86	1.42	<0.01	0.32	99.60	304	46	34	124	198	18
7d	**Sønnristjern**	2109413p	GP	61.87	23.42	0.18	<0.01	4.80	8.45	0.53	0.01	0.22	99.45	251	<5	36	80	33	24
7e	**Sønnristjern**	2109414p	GP	63.04	23.13	0.11	<0.01	4.19	8.70	0.49	0.01	0.33	99.98	167	8	52	59	30	30
7f	**Sønnristjern**	2109415k	GP	64.11	23.11	0.09	<0.01	4.00	8.80	0.68	0.01	0.28	101.02	95	17	64	56	23	30
8	**Lille Kleivmyr**	2109402p	GP	63.67	22.06	0.25	<0.01	3.59	8.19	0.76	<0.01	0.53	99.02	143	31	47	217	40	35
		2109403p	GP	63.87	21.85	0.12	<0.01	2.92	8.88	0.61	<0.01	0.30	98.48	32	14	74	102	<10	49
		2109404p	GP	63.79	21.56	0.14	<0.01	2.90	8.74	0.68	<0.01	0.34	98.15	42	20	77	113	<10	47
		2109406p	GP	63.01	22.63	0.24	<0.01	3.87	8.28	0.52	<0.01	0.54	99.10	114	12	37	177	16	27
		2109408p	GP	62.62	22.77	0.22	<0.01	4.25	8.20	0.48	0.01	0.19	98.72	159	7	45	139	10	30
		2109409p	GP	62.69	22.50	0.15	<0.01	3.93	8.31	0.54	<0.01	0.29	98.38	104	14	41	99	12	38
		2109410p	GP	63.27	22.03	0.23	<0.01	3.23	8.58	0.66	0.01	1.04	99.01	94	30	43	121	16	43
		2209407p	GP	61.86	23.32	0.17	<0.01	4.53	8.63	0.46	0.01	0.34	99.25	243	7	34	76	29	21
10	**Vaselona**	2309404p	sheared ZoP	66.19	21.03	0.12	<0.01	1.83	10.21	0.73	0.01	0.13	100.17	74	15	62	69	30	45
11	**Fossheia, vest**	2309402p	sheared ZoP	66.33	21.06	0.14	<0.01	2.92	10.00	0.72	0.01	0.19	101.31	45	22	40	62	29	53
12	**Fossheia, øst**	2309401p	HP	63.24	22.08	0.22	0.01	3.40	8.98	0.83	0.01	0.30	98.99	103	21	41	68	35	35
14	**Metveit, Herefoss pluton**	2309405p	HP	65.14	22.32	0.21	<0.01	3.13	9.32	0.84	0.02	0.28	101.21	202	11	23	74	40	22

Appendix G. *Major and minor element concentrations of mica determined by XRF.*

locality	**Hellheia, midtre**									**Hellheia, nordre**		**Bjortjørn**	**Skåremyr**	
sample nr.	1809401d	1809402d	1809404d	1809407d	1809408d	1809409d	1809410d	1809411d	1809415	2409401d	2409401e	2509401e	1909401d	1909403d
mica	Mg sideroph.	Fe phlog.	Mg sideroph.	Mg sideroph.	Mg sideroph.	Fe phlog.	Mg sideroph.	zinnwaldite	zinnwaldite	Mg sideroph.	zinnwaldite	zinnwaldite	Mg sideroph.	Mg sideroph.
SiO_2	34.54	35.5	35.65	35.23	36.07	35.09	34.69	44.52	44.32	35.75	45.13	45.71	35.15	34.43
TiO_2	1.78	1.92	2.10	1.52	1.92	1.77	2.21	0.13	0.13	2.67	0.21	0.27	2.65	2.73
Al_2O_3	17.11	15.66	16.83	17.44	16.2	15.95	16.99	31.57	31.40	15.77	31.55	30.58	15.88	16.93
Fe_2O_3	21.81	20.52	21.08	22.16	21.52	21.58	24.19	4.55	3.89	23.56	5.67	4.92	25.47	28.45
MnO	0.22	0.16	0.22	0.29	0.20	0.20	0.25	0.02	0.03	0.16	0.04	0.04	0.55	0.90
MgO	9.43	11.6	10.18	9.11	10.65	10.50	8.14	0.89	1.09	8.98	0.69	1.03	7.37	3.56
CaO	0.02	0.45	0.24	0.04	0.01	0.02	0.05	0.06	0.16	0.02	0.01	0.01	0.03	0.08
Li_2O	0.32	0.60	0.64	0.52	0.77	0.48	0.37	3.21	3.15	0.67	3.38	3.55	0.50	0.29
Na_2O	0.30	0.19	0.25	0.23	0.26	0.24	0.28	0.87	0.78	0.21	0.51	0.57	0.26	0.20
K_2O	8.94	9.10	8.96	9.21	8.94	8.67	8.90	9.60	9.75	8.73	10.12	9.95	9.02	8.44
RbO	0.20	0.20	n.d.	n.d.	0.21	0.16	0.20	0.29	0.30	0.19	0.29	0.25	0.17	n.d.
Cs_2O	0.08	0.07	n.d.	n.d.	0.07	0.06	0.07	0.04	0.05	0.09	0.04	0.05	0.04	n.d.
F	1.21	1.08	n.d.	n.d.	1.14	0.66	0.76	0.37	0.53	0.45	0.37	0.31	1.77	n.d.
Cl	<0.10	<0.10	n.d.	n.d.	<0.10	<0.10	<0.10	<0.10	<0.10	<0.10	<0.10	<0.10	<0.10	n.d.
sum	95.97	97.05	96.15	95.75	97.95	95.38	97.10	96.12	95.57	97.25	98.01	97.25	98.85	96.01
O = (F,Cl)	0.51	0.45	-	-	0.48	0.28	0.32	0.16	0.22	0.19	0.16	0.13	0.75	-
total	95.46	96.60	96.15	95.75	97.47	95.11	96.78	95.96	95.35	97.06	97.85	97.12	98.11	96.01

Appendix G. *Major and minor element concentrations of mica determined by XRF. Continued.*

locality	**Skåremyr**						**Sønnristjern**							
sample nr.	1909404d	1909406d	1909408d	1909410d	1909411d	1909416d	2009402d	2009404d	2009405d	2009406d	2009407d	2009409d	2009411d	2109413d
mica	Mg sideroph.	Mg sideroph.	Mg sideroph.	Mg sideroph.	Mg sideroph.	zinnwaldite	Mg sideroph.	Mg sideroph.	Mg sideroph.	Mg sideroph.	Mg sideroph.	Mg sideroph.	Mg sideroph.	Mg sideroph.
SiO_2	34.03	35.26	34.35	34.43	35.11	44.75	35.37	34.56	36.55	34.61	33.78	34.35	33.91	33.69
TiO_2	2.91	2.75	2.90	2.87	2.69	0.20	2.43	2.41	2.35	2.44	2.24	2.24	2.24	2.44
Al_2O_3	15.55	15.57	15.47	15.44	15.61	32.03	16.00	15.66	15.24	15.62	15.51	15.54	15.61	15.17
Fe_2O_3	24.90	25.59	25.28	25.05	25.04	5.47	24.79	25.25	24.37	25.68	25.63	25.5	26.16	25.71
MnO	0.45	0.46	0.53	0.53	0.50	0.08	0.65	0.67	0.61	0.69	0.80	0.68	0.78	0.64
MgO	8.11	7.78	8.00	7.91	7.70	0.82	7.59	7.58	7.55	7.76	7.50	7.50	7.79	7.41
CaO	0.05	0.08	0.02	0.01	0.06	0.05	0.16	0.25	0.17	0.28	0.22	0.07	0.14	<0.01
Li_2O	0.18	0.53	0.27	0.29	0.49	3.27	0.56	0.33	0.90	0.34	0.10	0.27	0.14	0.08
Na_2O	0.18	0.24	0.21	0.17	0.30	0.66	0.23	0.15	0.32	0.19	0.18	0.20	0.24	0.20
K_2O	8.84	8.86	8.91	8.98	8.88	10.09	8.91	8.86	8.62	8.43	8.34	8.74	8.43	9.04
RbO	0.10	0.12	0.11	0.13	0.11	n.d.	0.13	0.14	0.13	0.13	0.19	0.20	0.19	0.13
Cs_2O	0.02	0.03	0.02	0.02	0.02	n.d.	0.02	0.03	0.02	0.02	0.17	0.19	0.18	0.02
F	0.48	0.57	0.85	0.66	0.43	n.d.	1.13	1.01	1.28	0.96	1.12	1.09	0.97	1.22
Cl	<0.10	<0.10	<0.10	<0.10	<0.10	n.d.	<0.10	<0.10	<0.10	<0.10	<0.10	<0.10	<0.10	<0.10
sum	95.80	97.84	96.92	96.49	96.94	97.42	97.98	96.89	98.12	97.16	95.79	96.57	96.78	95.75
O = (F,Cl)	0.20	0.24	0.36	0.28	0.18	-	0.48	0.43	0.54	0.40	0.47	0.46	0.41	0.51
total	95.60	97.60	96.56	96.21	96.76	97.42	97.50	96.47	97.58	96.75	95.31	96.11	96.37	95.24

Appendix G. *Major and minor element concentrations of mica determined by XRF. Continued.*

locality	**Sønnristjern**	**Lille Kleivmyr**						**Vaselona**		**Fossheia, vest**	**Fossheia, øst**	**Heimdal**
sample nr.	2109414d	2109401d	2109402d	2109403d	2109409d	2109410d	2209407d	2309404d	2309404e	2309402d	2309401d	2309409d
mica	Mg sideroph.	Mg sideroph.	Mg sideroph.	Mg sideroph.	Mg sideroph.	Mg sideroph.	Mg sideroph.	Mg sideroph.	Li-Fe muscovite	Fe phlog.	Fe phlog.	Fe phlog.
SiO_2	33.80	34.4	33.48	33.58	34.95	34.15	33.98	35.23	44.37	33.21	35.06	37.75
TiO_2	2.31	2.19	1.89	1.55	2.21	2.33	2.38	2.61	0.84	2.54	2.76	1.88
Al_2O_3	15.07	16.32	16.81	17.25	16.76	16.53	15.82	14.79	28.47	14.34	13.72	13.02
Fe_2O_3	25.86	26.86	28.01	29.58	26.9	26.27	26.67	24.21	6.25	24.72	22.91	20.75
MnO	0.72	0.69	0.67	0.58	0.70	0.80	0.64	0.56	0.11	0.50	0.36	0.57
MgO	7.46	5.86	5.77	3.56	5.64	6.38	6.55	7.59	1.58	9.46	10.16	13.12
CaO	<0.01	0.03	0.07	0.09	0.03	0.22	0.11	0.22	0.08	1.39	0.30	0.04
Li_2O	0.11	0.28	0.02	0.05	0.44	0.21	0.16	0.52	3.16	<0.01	0.47	1.25
Na_2O	0.14	0.19	0.18	0.29	0.13	0.27	0.20	0.43	0.48	0.14	0.20	0.22
K_2O	8.96	8.97	8.08	8.38	9.05	7.38	8.31	8.70	9.93	5.06	8.19	9.31
RbO	0.20	0.19	0.25	0.24	0.20	0.16	0.11	0.34	0.29	0.14	0.20	0.10
Cs_2O	0.16	0.02	0.05	0.04	0.02	0.02	0.01	0.04	0.01	0.01	0.01	0.00
F	1.06	1.20	1.08	0.60	1.17	1.03	1.33	1.93	1.10	1.38	1.50	2.63
Cl	<0.10	<0.10	0.13	0.12	<0.10	<0.10	<0.10	0.15	<0.10	<0.10	0.15	0.20
sum	95.85	97.20	96.35	95.79	98.21	95.75	96.27	97.17	96.68	92.83	95.85	100.65
O = (F,Cl)	0.45	0.51	0.48	0.28	0.49	0.43	0.56	0.85	0.46	0.58	0.67	1.15
total	95.40	96.69	95.87	95.51	97.72	95.32	95.71	96.33	96.21	92.25	95.18	99.50

Appendix H. *Trace element concentrations of mica determined by XRF.*

locality	Hellheia, midtre							Hellheia, nordre		Bjortjørn	Skåremyr			
sample nr.	1809401d	1809402d	1809408d	1809409d	1809410d	1809411d	1809415	2409401d	2409401e	2509401e	1909401d	1909404d	1909406d	1909408d
mica	Mg sideroph.	Fe phlog.	Mg sideroph.	Fe phlog.	Mg sideroph.	zinnwaldite	zinnwaldite	Mg sideroph.	zinnwaldite	zinnwaldite	Mg sideroph.	Mg sideroph.	Mg sideroph.	Mg sideroph.
Mo	11	8	7	9	9	7	8	9	8	8	6	5	8	6
Nb	360	286	272	187	339	480	466	197	493	337	157	103	192	117
Zr	16	17	15	14	14	22	20	12	20	20	17	19	20	21
Y	<5	<5	<5	<5	<5	<5	<5	16	<5	<5	<5	<5	<5	<5
Sr	10	9	12	8	14	23	36	9	12	11	11	7	8	7
Rb	1720	1648	1732	1373	1699	2458	2503	1581	2426	2127	1395	866	997	929
U	<10	<10	<10	12	<10	<10	<10	10	12	<10	13	<10	<10	11
Th	8	7	5	6	6	10	10	<5	10	7	6	5	<5	7
Pb	<10	<10	<10	<10	12	16	19	<10	34	15	14	<10	<10	15
Cr	10	<10	<10	12	12	11	19	33	<10	14	63	74	89	80
V	170	199	211	223	191	18	21	349	19	46	438	498	462	505
Sc	59	74	69	72	39	50	31	126	62	18	80	36	55	41
Ba	532	601	547	520	651	188	348	473	49	50	491	704	560	641
Sn	54	18	25	25	47	143	110	17	179	60	39	27	42	43
Ga	75	56	61	57	78	265	269	63	283	188	38	40	49	37
Zn	262	200	269	276	203	31	35	183	53	55	538	440	447	495
Ni	143	149	154	130	134	37	38	76	32	30	43	46	50	51
Co	108	115	107	110	112	5	6	117	6	5	99	112	115	117
Cs	395	346	337	275	346	172	217	416	169	255	176	95	126	95
Ta	150	135	121	97	149	44	71	135	42	112	139	59	121	70

Appendix G. *Trace element concentrations of mica determined by XRF. Continued.*

locality	Skåremyr		Sønnristjern									Lille Kleivmyr	
sample nr.	1909410d	1909411d	2009402d	2009404d	2009405d	2009406d	2009407d	2009409d	2009411d	2109413d	2109414d	2109401d	2109402d
mica	Mg sideroph.	Mg sideroph.	Mg sideroph.	Mg sideroph.	Mg sideroph.	Mg sideroph.	Mg sideroph.	Mg sideroph.	Mg sideroph.	Mg sideroph.	Mg sideroph.	Mg sideroph.	Mg sideroph.
Mo	7	7	7	11	7	6	16	13	15	5	13	7	10
Nb	116	166	115	128	99	118	144	146	152	110	179	186	521
Zr	21	20	51	39	21	23	6	<5	5	35	6	27	22
Y	<5	<5	<5	<5	<5	<5	17	<5	25	<5	<5	<5	79
Sr	7	7	9	7	12	9	9	11	10	8	10	9	9
Rb	1098	910	1128	1142	1071	1070	1623	1692	1622	1103	1687	1577	2066
U	21	<10	10	213	13	<10	72	24	99	10	<10	26	70
Th	5	<5	6	7	5	<5	<5	<5	<5	<5	8	8	59
Pb	15	<10	20	20	17	17	23	27	27	<10	13	34	41
Cr	78	76	69	50	56	52	25	15	18	12	16	49	<10
V	503	455	326	314	306	323	283	289	290	319	295	251	224
Sc	40	41	44	49	39	49	55	52	52	62	71	127	142
Ba	650	560	173	140	119	125	117	121	116	305	315	225	77
Sn	36	33	79	85	71	85	114	116	114	81	98	135	180
Ga	36	47	72	78	63	74	98	80	93	73	79	107	108
Zn	517	422	530	477	436	534	641	665	701	530	538	1684	626
Ni	48	51	52	54	53	49	58	53	57	29	54	47	74
Co	122	112	92	98	84	100	96	101	112	100	99	79	84
Cs	95	109	99	133	115	113	799	914	843	96	754	84	231
Ta	68	90	49	38	47	44	69	52	63	55	103	45	114

Appendix G. *Trace element concentrations of mica determined by XRF. Continued.*

locality	**Lille Kleivmyr**					**Vaselona**		**Fossheia, vest**	**Fossheia, øst**	**Heimdal**
sample nr.	2109403d	2109409d	2109410d	2109411d	2209407d	2309404d	2309404e	2309402d	2309401d	2309409d
mica	Mg sideroph.	Mg sideroph.	Mg sideroph.	Mg sideroph.	Mg sideroph.	Mg sideroph.	Li-Fe muscovite	Fe phlog.	Fe phlog.	Fe phlog.
Mo	12	8	8	7	5	14	8	9	6	<5
Nb	777	258	250	121	102	192	273	99	179	30
Zr	210	22	20	56	21	16	22	18	31	21
Y	588	<5	5	8	10	10	<5	547	63	<5
Sr	9	9	10	10	10	19	11	12	12	11
Rb	2040	1724	1347	1151	906	2865	2459	1162	1713	882
U	291	14	10	15	19	27	<10	34	110	<10
Th	12	10	7	10	7	9	10	11	40	7
Pb	58	23	21	19	18	24	45	<10	72	<10
Cr	<10	30	16	55	20	19	<10	37	<10	<10
V	90	217	239	320	272	170	83	149	184	81
Sc	245	143	170	47	86	884	1092	213	128	31
Ba	38	85	91	197	375	299	152	235	267	1048
Sn	268	152	212	80	96	65	346	45	21	14
Ga	131	111	114	75	86	92	183	77	48	47
Zn	1636	1327	1257	485	1723	610	95	637	466	903
Ni	65	47	29	63	33	58	31	82	49	13
Co	60	74	63	107	93	91	6	119	113	77
Cs	173	110	98	139	43	180	49	44	46	13
Ta	131	52	49	53	37	48	15	32	33	35

Appendix I. *Variation diagrams for selected major and trace elements of mica.*